Department of Physics
Indian Institute of Technology Guwahati
Ph.D. Thesis

Quantum Correlations in Cavity Optomechanical Systems

Subhadeep Chakraborty

Thesis Supervisor: Prof. Amarendra Kumar Sarma
March 15, 2020.

Quantum Correlations in Cavity Optomechanical Systems

A Thesis submitted for the award of the degree of
Doctor of Philosophy in Physics
by

Subhadeep Chakraborty

Thesis Supervisor: **Prof. Amarendra Kumar Sarma**

Department of Physics
Indian Institute of Technology Guwahati
Guwahati - 781039, Assam, India

August, 2019

Statement

The work contained in the thesis entitled "**Quantum Correlations in Cavity Optomechanical Systems**" has been carried out at the Department of Physics, Indian Institute of Technology Guwahati, India by me under the supervision of Prof. Amarendra Kumar Sarma. The material of this thesis has not been submitted elsewhere for any other degree. Works presented in the thesis are all my own unless referenced to the contrary in the text.

(Subhadeep Chakraborty)
Department of Physics
Indian Institute of Technology Guwahati
Guwahati - 781039, India

March 15, 2020

Disclaimer

The bibliography included in this thesis is, by no means complete but contains the ones which are consulted thoroughly by me. I apologize for inadvertently missing out some of the research papers, review articles and other scientific documents pertaining to the focus of this thesis which should also have been cited. For illustration purpose some of the figures in this thesis are taken from other sources and properly cited.

Certificate

It is certified that the work contained in the thesis entitled "**Quantum Correlations in Cavity Optomechanical Systems**" by Subhadeep Chakraborty (Roll no.-146121016), a Ph.D. student of the Department of Physics, Indian Institute of Technology Guwahati is carried out under my supervision and has not been submitted elsewhere for the award of any other degree.

(Prof. Amarendra Kumar Sarma) March 15, 2020
Professor
Department of Physics
Indian Institute of Technology Guwahati
Guwahati - 781039, India

To

My beloved father...

Acknowledgement

First and foremost, I express my sincere gratitude to my thesis supervisor Prof. Amarendra Kumar Sarma for his constant guidance, continuous support and complete freedom to explore new scientific understandings during my Ph.D tenure. I have been always motivated by his expert supervision and dedication for work. I am also thankful to him for giving me the opportunity to be involved in different types of problems and collaborations that helped me a lot to increase my experience and knowledge about the subject.

I would like to acknowledge my doctoral committee members - Prof. Subhradip Ghosh, Prof. Aditya N. Panda and Dr. Gagan Kumar for their useful suggestions to improve my scientific understanding during the yearly assessments of my research work. I also thank all HODs (Prof. Saurabh Basu, Prof. Poulose Poulose and Prof. Subhradip Ghosh) for their various academic help during my Ph.D. I would like to thank all the technical assistants, academic and non-academic staff of the department who helped me in various ways during my research period. I specially thank Basab-da and Hemanta-da for their support in different computer related issues.

I am grateful to IIT Guwahati, and Ministry of Human Resource and Development, Government of India for the financial support. I would also like to acknowledge CSIR, Government of India for providing me an initial financial during my PhD. I am also thankful to Physics Department, IIT Guwahati for providing the necessary computation facilities.

I would like to thank my group members, Dr. Samit Kumar Gupta, Dr. Koushik Paul, Dr. Bijita Sarma, Dr. Jyoti Prasad Deka, Ms. Koijam Monica Devi, Ms. Dipti Kanika Mahato, and Mr. Sampreet Kalita for their continuous support and wonderful friendship. I have learned a lot from them about the various aspects of the fields.

I am fortunate enough to have a great friend circle here, seniors like Debopam-da, Abhisek-da, Anirban-da, Kallol-da, Ramiz-da, Sourav-da. I am extremely lucky

to have my friends like Sanghka, Shyam, Shamik, Ayan, Rony, Sanket. I had lot of great memories with them which I will never forget. I would like to thank my batchmates Ghanashyam, Indu, Joy, Jagan, Nawaz, Goutam and Gobinda. Most importantly, I would like to thank all my childhood friends like Sanat, Kuntal, Sasanka-da and Ankan-da for their wonderful friendship throughout the years.

Finally, I would like to thank all my family members, specially my parents for their unconditional love, support, freedom and sacrifices for me. Last but not the least, I am extremely grateful to my dearest friend, Camelia for always being there for me.

August, 2019 Subhadeep Chakraborty

Abstract

Understanding the quantum nature of macroscopic systems is a topic of intense research for quite some time now. Numerous efforts have been made to know the classical-to-quantum boundary in various platforms. In fact, it is still not clear exactly when to stop applying the so-called Newtons laws and switch over to the Schrodinger equation. Recently, a new field of research, namely cavity quantum optomechanics has emerged opening many doors to study these open ended fundamental questions, apart from numerous possible applications. A typical cavity optomechanical system consists of two mirrors, one fixed while the other one is movable. These systems may be of micrometer or nano-meter in dimensions. The electromagnetic radiation incident on the system may get coupled to the mechanical motion of the movable mirror. This opto-mechanical coupling is the heart of all phenomena such as quantum entanglement, state-transfer, squeezing and so on. In this thesis, we have explored various aspects of quantum correlations in cavity quantum optomechanical systems. We have proposed various schemes to improve the degree and robustness of quantum correlations. For example, our proposals show how one can achieve robust quantum entanglement even at high temperature. It should be noted that quantum entanglement is the key component of any quantum communication protocols and extremely vital for the realization of quantum computers. We have even come up with a scheme to delay the so-called entanglement sudden death (ESD), an issue considered to be an immediate stumbling block in the realization of various entanglement based quantum information and computing protocols. We have addressed this issue, in an optomechanical platform,by exploiting the phenomenon of exceptional points in binary and ternary mechanical $\mathcal{PT}$ symmetric architectures. Apart from quantum entanglement, we have explored other quantum correlations such as, quantum discord and quantum synchronization in our thesis.

List of Publications

1. **Subhadeep Chakraborty** and Amarendra K. Sarma, *Enhancing quantum correlations in an optomechanical system via cross-kerr nonlinearlity*, J. Opt. Soc. Am. B 34, 1503 (2017)

2. **Subhadeep Chakraborty** and Amarendra K. Sarma, *Entanglement dynamics of two coupled mechanical oscillators in modulated optomechanics* , Phys. Rev. A 97, 022336 (2018)

3. **Subhadeep Chakraborty** and Amarendra K. Sarma, *Qubit assisted enhancement of quantum correlations in an optomechanical system*, Ann. Phys. 392, 39 (2018)

4. **Subhadeep Chakraborty** and Amarendra K. Sarma, *Delayed sudden death of entanglement at exceptional points*, Phys. Rev. A 100, 063846 (2019)

5. **Subhadeep Chakraborty** and Amarendra K. Sarma, *Quantum synchronization and correlation in bidirectionally and unidirectionally coupled optomechanical oscillators*,arXiv:1908.07296

Conferences/Schools attended

1. ICTS program on "Open Quantum System", held in ICTS campus, Bangalore, India from 24 to 28 July, 2017 (poster presentation).

2. SERB school on "Frontiers in Quantum Optics", held in IIT Guwahati, Guwahati, India from 1 to 19 December, 2017 (participation).

3. International conference on *Recent Trends in Cold and Ultracold Matter*, (Ultracold 2018), held in IIT Guwahati, Guwahati, India from 27 to 29 March, 2018 (poster presentation).

4. International Symposium on Optics, *OSI-ISO 2018*, held at IIT Kanpur, Kanpur, India from 19 to 22 September 2018 (oral presentation).

5. International Conference on Fiber Optics and Photonics, *PHOTONICS 2018*, held at IIT Delhi, Delhi, India from 12 to 15 December 2018 (oral presentation).

Contents

List of Figures

Chapter 1

Introduction

Cavity quantum optomechanics turns out to be a universal tool for attaining quantum control of mechanical motion in recent years, owing to the rapid advances in micro- and nano-fabrication techniques and availability of very high quality (Q) cavities [1]. A typical cavity optomechanical system could be modelled by considering it as a Fabry-Perot cavity where one of the mirrors is fixed while the other one oscillates harmonically. The cavity could be driven by optical or microwave radiation depending on the size of the system. The coupling between the radiation and the movable mechanical mirror is caused by the so-called radiation-pressure interaction. The typical size of such systems may vary from nanometers to centimeters, with masses from femtograms to kilograms and with mechanical frequencies from a few Hz to GHz.

The first set of experiments with such prototype of cavity optomechanical systems could be traced back in the late 1970s, when Braginsky and co-workers were mainly motivated to build the early stage of gravitational wave-detectors. Such setup were basically large interferometer, with mirrors of kilogram in masses being separated by kilometer long arms formed by optical cavities. Capitalizing on the radiation-pressure interaction, Braginsky revealed the retarded nature of the force, that would lead to damping or antidamping in the mechanical motion, due to the finite cavity lifetime [2]. Later, in the late 1980s to early 90s, within such similar framework, the sensitivity limit as imposed by the fluctuation of radiation-pressure was addressed by Braginsky, Caves, and Walls [3–5]. It was the 1990s, when the quantum aspects of cavity optomechanical system started to be explored theoretically. This includes some of the following noteworthy studies on squeezing of light [6, 7], quantum nondemolition detection of light intensity [8], and, feedback cooling of mechanical oscillator [9]. Besides, exploiting strong optomechanical coupling, the possibility of generating nonclassical and entangled states of light field and mechanical motion was also pointed out [10]. On the experimental side, the first demonstration of optical feedback cooling of macroscopic mechanical end mirrors, based on radiation-pressure, came in 1999 [11]. This was followed by a series of works, with the goal to reach much lower temperature. In 2005, with the advent of both high-quality optical cavities and miniaturized mechanical mirrors, the optical microtoroid resonators came into the picture. This led to the demonstration of radiation-pressure-induced self-oscillations [12]. Around the same time, different groups achieved the radiation-pressure cavity cooling, for suspended micromirrors [13] and for microtoroids [14]. Among the other geometries where optomehanical coupling were observed include membrane, nanorods inside Fabry-Perot cavity, whispering gallery microdisks and microspheres and photonic crystals. In addition, cold atom clouds, and wave guides in photonic circuits and crystal were the other novel candidate to exhibit the optomechanical interactions. Also, there are other proposal for quadratically coupled [15, 16] and multiple membrane cavity optomechanical systems [17] and nonlinearly coupled optomechanical systems [18]. Current researches in this area mainly include cavity cooling of a mechanical oscillator [19–21], continuous-variable entangled state preparation [22–26], quantum squeezing of a mechanical mode [27–29], nonclassical state generation [30, 31], and quantum state transfer [32, 33] etc. Along with the above mentioned studies, it has also become a key tool for wide range of potential applications, such as: quantum information processing [116], ultra-high precision measurements [35], gravitational wave detection [36], and even biological measurements [37]. Hence, in recent years optomechanical devices are well rooted as a fertile light-matter interface to probe the the macroscopic massive mechanical resonators, in a way that would steer us to completely different worldview, far from our everyday classical intuitions.

In this thesis we are probing the quantumness of nano-mechanical oscillators in cavity optomechanical setup, owing to its technological relevance. We are proposing various practical schemes to enhance quantum correlations in such optomechanical systems. Entanglement, known as the "characteristic traits" quantum mechanics, lies at the heart of many applications, such as superdense coding, quantum teleportation and protocols of quantum cryptography. Besides Quantum entanglement, quantum discord is an additional measure of the quantum correlations which can not be captured by addressing entanglement only. Apart from these two standard measures, we also study the phenomena of quantum synchronization in a coupled cavity optomechanical systems.

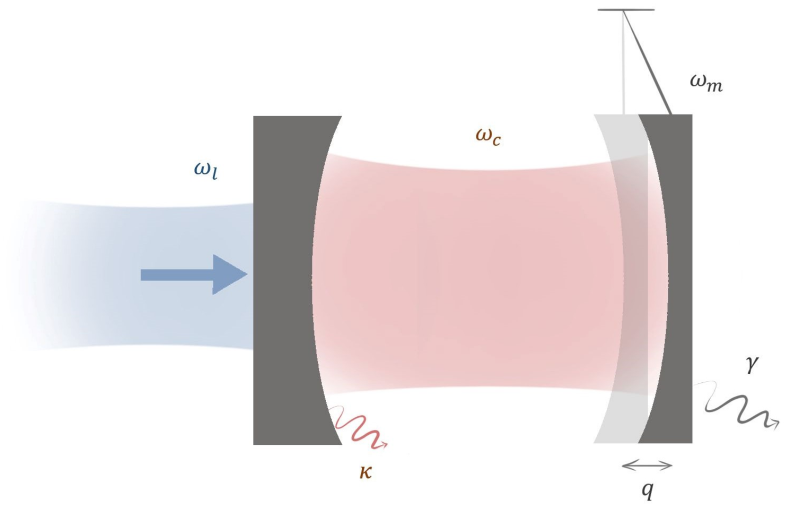

Figure 1.1: Schematic diagram of typical cavity optomechanical systems. A laser driven optical cavity gets coupled to a mechanical mirror via radiation pressure.

There are a number of excellent review articles and books covering various aspects of cavity quantum optomechanics [1, 38–40]. In the following, we are going to discuss briefly only those facets of cavity quantum optomechanics that are relevant to the present thesis.

1.1 Cavity optomechanics: Basic theory

1.1.1 The optomechanical Hamiltonian

Let us consider a prototypical cavity optomechanical system, i.e., a Fabry-Perot cavity where one of the end mirrors is fixed while the other one oscillates simple harmonically. The schematic of the system is depicted in Fig. 1.1.

As driven by an external laser, the photons inside the cavity exert a radiation-pressure force on the mechanical mirror. This in turn changes the length of the cavity, making the cavity resonance frequency modulated. Considering, l to be the equilibrium length of the cavity and q is the displacement made by the mechanical mirror, the (modified) cavity resonance frequency reads as $\omega_c(q) = \frac{N\pi c}{l+q}$, where N is the mode number and c is the speed of light in vacuum. As, we are typically interested in small mechanical displacement, i.e., $q \ll l$, we can Taylor expand the cavity frequency and write it as:

$$\omega_c(q) \approx \omega_c \left(1 - \frac{q}{L}\right), \tag{1.1}$$

where $\omega_c = \frac{N\pi c}{l}$ refers to the intrinsic cavity resonance frequency, in the absence of any optomechanical interaction.

Now, we proceed to construct the generic optomechanical Hamiltonian. A very basic assumption to start with, is that these optical and mechanical modes are quantum harmonic oscillators, respectively, with frequency ω_c and ω_m. The optomechanical Hamiltonian (in the unit of $\hbar = 1$) could then be written as

$$H_{OM} = \omega_c(q)a^\dagger a + \omega_m b^\dagger b, \tag{1.2}$$

where a is the annihilation operator of the cavity field and b is annihilation operator of the mechanical mirror. Substituting Eq. (1.1) in Eq. (1.2), we get

$$H_{OM} = \omega_c a^\dagger a + \omega_m b^\dagger b - g a^\dagger a(b^\dagger + b), \tag{1.3}$$

where

$$g = \frac{\omega_c}{l} q_{\text{zpf}}, \tag{1.4}$$

is the *single-photon* optomechanical coupling strength. Note that, while deriving in Eq. (1.3) we have introduced the quadrature operator $q = q_{\text{zpf}}\left(b + b^\dagger\right)$, where $q_{\text{zpf}} = \sqrt{\frac{\hbar}{2m\omega_m}}$ defines the zero-point fluctuation of the mechanical mirror (of mass m). A more rigorous derivation of this Hamiltonian could be found in Ref [38].

From this Hamiltonian (1.4), one must note the following points. Firstly, the interaction between then optical and mechanical mode is essentially nonlinear in nature, with the mechanical displacement being proportional to the cavity photon number or vice versa. Secondly, this optomechanical coupling is usually very small $g \ll \omega_m$ and, hence is not sufficient enough to show us the desired quantum effects. However, one can achieve a strong effective optomechanical coupling via strongly driving the cavity. To do so, we now include the coherent drive into the cavity and write the complete optomechanical Hamiltonian as:

$$H = \omega_c a^\dagger a + \omega_m b^\dagger b - g a^\dagger a(b^\dagger + b) + iE_0(a^\dagger e^{-i\omega_l t} - a e^{i\omega_l t}). \tag{1.5}$$

where E_0 and ω_l are, respectively, be the driving amplitude and frequency of the external laser. One may note that this driving amplitude can also be written as

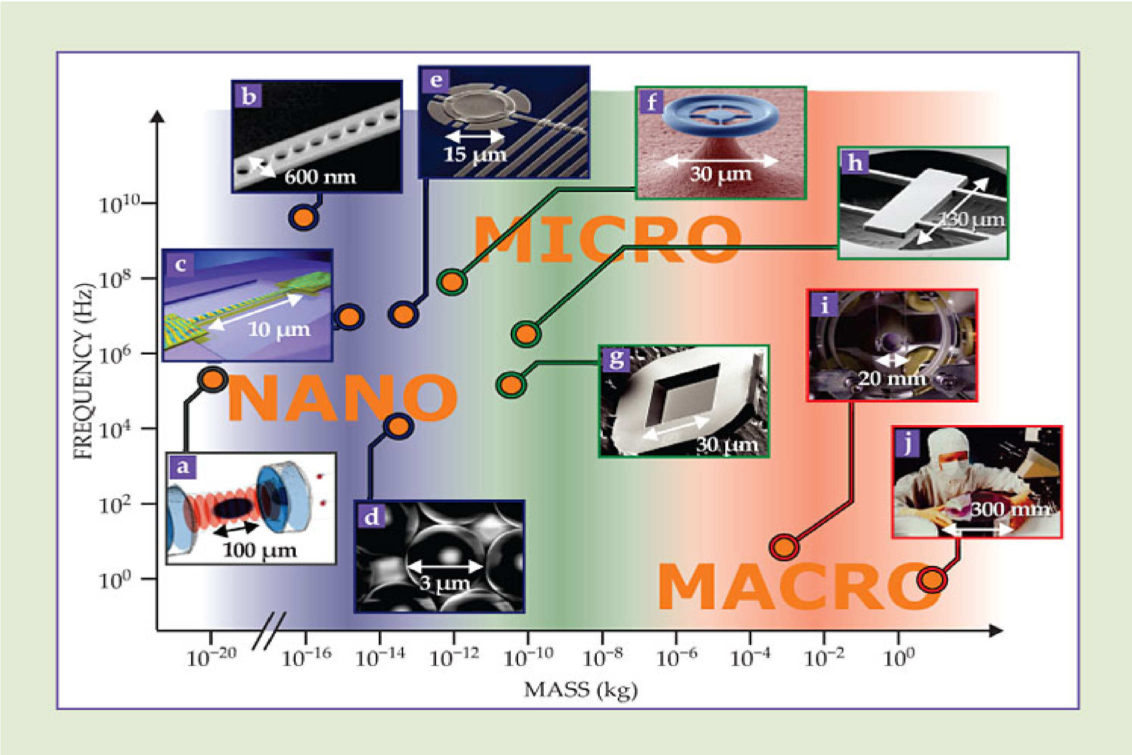

Figure 1.2: Gallery of cavity optomechanical devices: (a) ultracold atomic gasses, (d) microsphers and (g) micromembranes optomechanically coupled to light inside an optical cavity; (b,c) nanoscale waveguides, supporting both optical and mechanical resonances; (e) superconducting membranes, integrated into microwave cavities; (f) microtoroidal waveguides ranging from the microscopic (h) to macroscopic and which acts as a mechanical degrees of freedom to an optical cavity. Image taken from: *Quantum optomechanics* by M. Aspelmeyer, P. Meystre and K. Schwab, Physics Today **65**, 29 (2012), page 32, Figure 3.

$E_0 = \sqrt{\frac{P\kappa}{\hbar\omega_l}}$ where P is the power associated with the external laser and κ is the decay rate of the cavity field.

Next, to get rid of the explicit time dependence of the driving Hamiltonian, we switch to a frame rotating with the laser frequency ω_l and write the complete Hamiltonian (1.5) in a following manner:

$$H = \Delta_0 a^\dagger a + \omega_m b^\dagger b - g_0 a^\dagger a(b^\dagger + b) + iE_0(a^\dagger - a). \tag{1.6}$$

Here $\Delta_0 = \omega_c - \omega_l$ corresponds to the input cavity detuning. The Hamiltonian described by Eq. (1.6) serves as an excellent starting point to discuss the physics of cavity optomechanical systems. It is remarkable to note that this simple model is capable to describe the physics of a plethora of seemingly different optomechanical systems as depicted in Fig. 1.2.

1.1.2 Optomechanical equations of motion

In order to have a correct study of the phenomena related to an optomechanical system (OMS), it is extremely crucial to take into account the environmental effects on the OMS. The OMS is always surrounded by a thermal bath. the cavity photons and the phonons on the mechanical resonator decay due to the coupling to the environment. At the same time, thermal noise may also enter into the OMS owing to the coupling, as the mechanical resonator is in thermal equilibrium with the heat bath. The time evolution of the system operators can be described by using the Heisenberg equations of motion with the addition of the corresponding damping and noise terms as follows:

$$\frac{d}{dt}a = -i\left[a, H\right] - \frac{\kappa}{2}a - \sqrt{\kappa}a_{in}, \tag{1.7a}$$

$$\frac{d}{dt}b = -i\left[b, H\right] - \frac{\gamma}{2}a - \sqrt{\gamma}b_{in}. \tag{1.7b}$$

Here, the first term on the R.H.S describes the coherent evolution of the field operators, the second term takes the decay of the bosonic mode into account, while the last term refers to the noise entering into the system due its coupling to the environment. The cavity decay rate is denoted by κ, while the mechanical damping rate is denoted by γ. On the other hand, a_{in} and b_{in} refer to the input vacuum noise operators corresponding to the cavity mode and the mechanical mode, respectively. These noise operators are assumed to be Gaussian in nature, with the following non-zero correlation relations [41]:

$$\langle a_{in}\rangle = \langle b_{in}\rangle = 0, \tag{1.8a}$$

$$\langle a_{in}(t)a^{\dagger}_{in}(t')\rangle = \delta(t-t'), \tag{1.8b}$$

$$\langle b^{\dagger}_{in}(t)b_{in}(t')\rangle = n_{th}\delta(t-t'), \tag{1.8c}$$

$$\langle b_{in}(t)b^{\dagger}_{in}(t')\rangle = (n_{th}+1)\delta(t-t'). \tag{1.8d}$$

Here, $n_{th} = \left[\exp\left(\frac{\hbar\omega_m}{K_B T}\right) - 1\right]^{-1}$ is the average number of thermal quanta with K_B being the well-known Boltzmann constant and T is the temperature of the thermal bath.

1.2 Outline of the thesis

In the following, we present the outline of the thesis by including a description of the various problems that have been tackled in the form of different chapters of the thesis. There are a total of seven chapters. We present a brief description about the content of each chapter below.

Chapter 1: This chapter provides the introduction to the thesis, with a brief literature review of the recent developments in the cavity optomechanical systems. It is followed by a brief discussion of the basic theory of cavity optomechanical systems.

Chapter 2: In this brief chapter we discuss about various measures of quantum correlations in the context of continuous variable system. These measures are relevant to the problems discussed in the thesis.

Chapter 3: In this chapter, we report two schemes to generate and enhance the steady-state optomechanical entanglement at a considerably lower coupling strength or external laser driving. Both of these schemes offer some considerable advantages, for generating steady-state optomechanical entanglement, over the conventional systems. The proposed schemes may find its applications in realizing continuous-variable quantum information interfaces and networks.

Chapter 4: In this chapter, we study the entanglement dynamics of two coupled mechanical oscillators in a modulated optomechanical system. We find a strong connection between the entanglement dynamics and the stability of the normal modes. In particular, we have shown that with appropriate choice of mechanical coupling and modulation frequency, a significantly large degree of stationary entanglement could be achieved which is also extremely robust against the oscillator temperature.

Chapter 5: This chapter addresses the issue of entanglement sudden death in optomechanical systems. Almost a decade ago, physicists encountered a strange quantum phenomenon that predicts an unusual death of entanglement under the influence of local noisy environment, known as entanglement sudden death (ESD). This could be an immediate stumbling block in realizing all the entanglement based quantum information and computation protocols. In this chapter, we discuss a scheme to tackle such shortcoming by exploiting the phenomenon of exceptional points (EP). Starting with a binary mechanical $\mathcal{PT}$ symmetric system, realized over an optomechanical platform, we show that a substantial slowing down in ESD can be achieved via pushing the system towards an exceptional point. This finding has been further extended to higher (third) order exceptional point by considering a more complicated tripartite entanglement into account.

Chapter 6: Here, we present a systematic study on quantum synchronization between two dissimilar nanomechanical oscillators, placed within two optical cavities. The coupling between the optomechanical cells is considered to be purely optical in nature, with two different geometries: bidirectional and unidirectional. Based on these realizations, we first show that when synchronization builds up in the system, the two oscillators also become quantum mechanically correlated, with a finite degree of Gaussian quantum discord. Moreover, we find that for bidirectional configuration, both the synchronization and quantum discord exhibit a tongue, which is a quantum analogue of classic Arnold tongue like behavior. On the contrary, for an unidirectional configuration, we observe a completely anomalous behavior where the degree of synchronization peaks at a finite value of frequency detuning. This novel feature is recently observed in the context of anharmonic quantum oscillators and coined as quantum synchronization blockade. However, we also find that quantum discord is not able to capture such blockade like behavior.

Chapter 7: This chapter concludes the thesis with a summary of the major findings of the research works carried out, and a brief outline on the scope for future studies.

Chapter 2

Measures of quantum correlations

It is extremely crucial to quantify the quantumness of various correlations that may arise in an optomechanical systems. In this thesis, we are dealing with Gaussian states. Also, in this work, we are primarily interested in the following quantum correlations only: quantum entanglement, quantum discord and quantum synchronizations. In this chapter, we briefly discuss the measures related to quantum entanglement and quantum discord only. The measures related to quantum synchronisation is discussed in Ch. 6.3.

2.1 Gaussian states

In the context of continuous-variable (CV) quantum information, Gaussian states are of central importance. These are the states with Gaussian Wigner function and are completely characterized by its first and second moment of the field quadrature operators. For any n mode Gaussian state, the vector of the first moments reads $\bar{R} = \mathrm{Tr}\,(\rho R)$, while the second moments is denoted by the $2n \times 2n$ correlation matrix (CM) V of elements

$$V_{ij} = \frac{1}{2}\left(\langle R_i R_j + R_j R_i \rangle\right) - \langle R_i \rangle \langle R_j \rangle, \tag{2.1}$$

where R is a $2n$ dimensional vector of CV operators $R^T = (q_1, p_1, q_2, p_2, ..., q_n, p_n)$. The canonical commutation relations among these CV operators takes the following compact form

$$[R_k, R_l] = i\Omega_{kl} \tag{2.2}$$

where $\Omega_{kl} \equiv [\Omega]_{kl}$ are the elements of a $2n \times 2n$ symplectic matrix, given by

$$\Omega = \bigoplus_{k=1}^{n} \begin{pmatrix} 0 & 1 \\ -1 & 0 \end{pmatrix}, \tag{2.3}$$

Following a displacement operation in the phase space, the first moments could be arbitrarily adjusted to zero. Then, the Wigner function for a n mode Gaussian state can be written as [42–44]

$$W(R) = \frac{1}{(2\pi)^n \sqrt{\mathrm{Det}V}} e^{-\frac{1}{2}R^T V^{-1} R}. \tag{2.4}$$

Here, it is worth mentioning that in order to preserve the Gausianity of a Wigner function, the Hamiltonian should be linear or bilinear in the field operators. The most general form of such Hamiltonian could be written as [44, 45]

$$H = \sum_{k=1}^{n} g_k^{(1)} a_k^\dagger + \sum_{k \geq l=1}^{n} g_{kl}^{(2)} a_k^\dagger a_l + \sum_{k,l=1}^{n} g_{kl}^{(3)} a_k^\dagger a_l^\dagger + h.c., \tag{2.5}$$

where, the first block of this Hamiltonian corresponds to the displacement operation, the second block represent the beam-splitter kind of interaction, while the third one refers to two-mode squeezing type interaction. Since, in the linearized regime of optomechanical interaction, one is strictly restricted within such kind of interactions only, the Gaussian description along with CM formalism is of particular relevance here. Indeed, it is extensively used in all the following attached papers.

Now, given a CM V, it is always essential to ask whether there exist any constraint relation that has to be obeyed by any *bona fide* CM. For any density matrix operator ρ, it simply implies to the well-known positive-semidefiniteness requirement of ρ. In particular, to CV quantum systems, the Heisenberg relation among the canonical operators imposes a constraint on the CM, given by the following inequality [46, 47]

$$V + \frac{i\Omega}{2} \geq 0. \tag{2.6}$$

Note that such uncertainty relation applies to any CM, describing a physical state. For Gaussian state this is however not only the necessary but also the sufficient criteria to ensure the positive-semidefiniteness of ρ [47].

2.2 Two-mode Gaussian states

To discuss entanglement and the other relevant quantities, we consider the simplest scenario of two-mode Gaussian states. Such states can in general be written as:

$$V = \begin{pmatrix} A & C \\ C^T & B \end{pmatrix}, \tag{2.7}$$

where A, B and C are 2×2 block matrices. With this choices, one can then define the following four symplectic invariants:

$$I_1 = \det[A], \quad I_2 = \det[B], \quad I_3 = \det[C], \quad I_4 = \det[V]. \tag{2.8}$$

The two symplectic eigenvalues of a generic two-mode CM V can then be computed as [48]

$$\nu^{\pm} \equiv 2^{-1/2}\left[\Delta(V) \pm \sqrt{\Delta(V)^2 - 4I_4}\right]^{1/2}, \tag{2.9}$$

where $\Delta(V) \equiv I_1 + I_2 + 2I_3$. The uncertainty relation in Eq. (2.6), then leads to the following single inequality

$$\nu^- \geq 1/2, \tag{2.10}$$

which means that for any *bona fide* CM, the smallest symplectic eigenvalue must be greater than or equal to $1/2$.

2.2.1 Entanglement in two-mode Gaussian states

A standard measure to find whether a given quantum state is entangled or not is given by the PPT (positive partial transpose) criteria [49]. It states that a separable density operator under partial transposition necessarily goes over into a *bona fide* density operator. For CV quantum systems, such partial transposition is associated with the time reversal operation which maps a CV vector $R^{T(2)} = (q_1, p_1, q_2, p_2)$ to $R^{(2)} \to \Lambda R^{(2)}$ with $\Lambda = \mathrm{diag}\,(1, 1, 1, -1)$. Therefore, the PT (partial transpose) operation on the CM V leads to the following uncertainty relation [50]

$$\tilde{V} + \frac{i}{2}\Omega \geq 0 \tag{2.11}$$

where $\tilde{V} = \Lambda V \Lambda$. Recalling the four symplectic invariants 2.8, we find

$$\tilde{I}_1 = I_1, \quad \tilde{I}_2 = I_2, \quad \tilde{I}_3 = -I_3, \quad \tilde{I}_4 = I_4, \tag{2.12}$$

where $\tilde{I}_k$ are the the symplectic invariants of $\tilde{V}$. Then, under the PPT criteria, the uncertainty relation reads as

$$\tilde{\nu}^- \geq 1/2, \tag{2.13}$$

where $\tilde{\nu}^- \equiv 2^{-1/2}\left[\tilde{\Delta}(V) - \sqrt{\tilde{\Delta}(V)^2 - 4I_4}\right]^{1/2}$ is the smallest symplectic eigenvalue of $\tilde{V}$ with $\tilde{\Delta}(V) \equiv I_1 + I_2 - 2I_3$. This restriction (2.13) has to be obeyed by all separable correlation matrices. A quantitative measure for quantum entanglement can then be given by the degree of violation of Eq. (2.13). A standard practice here is to calculate for the *Logarithmic Negativity*, given by [51, 52]

$$E_N = \max\left[0, -\ln 2\tilde{\nu}^-\right], \tag{2.14}$$

Therefore, the Gaussian state is entangled if and only if $E_N > 0$, which is equivalent to $\tilde{\nu}^- < 1/2$ [50].

2.2.2 Gaussian quantum discord

Besides the quantum entanglement, quantum discord is another measure for the quantumness of the correlations present in a quantum state. In the seminal paper [53], Zurek introduced discord as the mismatch between the two classically equivalent descriptions of mutual information and showed that it can even exist for separable states (which are usually referred to have classical correlation). However, their study was limited in the finite dimensional system, which was further extended in the realm of continuous-variables (CV) in Refs. [54, 55]. In recent years, quantum discord has received much attention in optomechanical systems to study non-classical correlations in it [56]. In particular, it has been both theoretically and experimentally demonstrated that pre-availability of such non-classical correlation can activate entanglement, which is also more robust against temperature and thermal noise [57, 58]. By definition, quantum discord is given by the following difference (with respect to a measurement made on the mode B):

$$D_{G_{(A|B)}} = I_M(\rho_{AB}) - C_{(A|B)}(\rho_{AB}), \tag{2.15}$$

where, the first term $I_M(\rho_{AB})$ quantifies the amount of quantum mutual information, while the second term $C_{A|B)}(\rho_{AB})$ refers to the one-way classical correlation between the mode A and mode B.

For the considered Gaussian bipartite system characterized by the correlation matrix V, the quantum mutual information is written as [45]

$$I_M(\rho_{AB}) = f(\sqrt{I_1}) + f(\sqrt{I_2}) - f(\nu^+) - f(\nu^-), \tag{2.16}$$

where, the function f is defined as:

$$f(x) \equiv (x + \frac{1}{2}) \ln(x + \frac{1}{2}) - (x - \frac{1}{2}) \ln(x - \frac{1}{2}), \tag{2.17}$$

and, $\nu^{\pm}$ (2.9) are the two symplectic eigenvalues of V.

In particular to two-mode Gaussian states, Gaussian quantum discord is evaluated only by performing Gaussian measurement on the subsystems and expressed as [45, 54, 55]:

$$D_{G_{(A|B)}} = f(\sqrt{I_2}) - f(\nu^+) - f(\nu^-) + f(\sqrt{W}) \tag{2.18}$$

where, the function f is defined in Eq. (2.17) and

$$W = \begin{cases} \left[\frac{2|I_3| + \sqrt{4I_3^2 + (4I_2-1)(4I_4-I_1)}}{(4I_2-1)}\right]^2 & \text{if} \frac{4(I_1 I_2 - I_4)^2}{(I_1+4I_4)(1+4I_2)I_3^2} \leq 1, \\ \frac{I_1 I_2 + I_4 - I_3^2 - \sqrt{(I_1 I_2 + I_4 - I_3^2)^2 - 4I_1 I_2 I_4}}{2I_2} & \text{otherwise.} \end{cases} \tag{2.19}$$

These measures of quantum entanglement and Gaussian quantum discord will be frequently used in the following chapters.

Chapter 3

Enhancement of stationary optomechanical entanglement

In this chapter, we focus on the steady-state regime of the optomechanical correlations. A key challenge here is the stability condition which imposes a strong upper bound on the available entanglement. To circumvent such issues, we explore the possibilities of coupling a conventional optomechanical system to an additional two-level system or a nonlinear inductive element. It has been found that such interactions could lead to the inclusion of either an additional second order potential term q^2 (q be the position of the mechanical mirror) or an extra cross-Kerr type interaction between the optical and the mechanical field operators. We discuss the effect of these further added terms on the optomechanical entanglement generation. We also look for Gaussian quantum discord, as an additional measure of the quantum correlation.

3.1 Qubit assisted enhancement of quantum correlations in an optomechanical system

3.1.1 Brief overview

Entanglement [60, 61] is one of the most intriguing feature of quantum mechanics, having myriads of potential applications in quantum information and communication

The contents of this chapter are published in Subhadeep Chakraborty and Amarendra K. Sarma, Ann. Phys **392**, 39 (2018) and Subhadeep Chakraborty and Amarendra K. Sarma J. Opt. Soc. Am. B **34**, 1503 (2017).

[62]. So far, preparation and manipulation of entanglement has been successfully demonstrated in microscopic systems, such as atoms, photons, ions [63–65] etc. However, the validity of entanglement in the macroscopic realm is still a debatable fact. In this regard, optomechanical system [1, 38] where a macroscopic mechanical motion interacts with an optical field has emerged as a promising platform to realize entanglement at a macroscopic level. Several studies have been reported to generate entanglement between an optical and a mechanical mode or two optical modes [10, 22, 23, 66–79]. These studies mostly explore entanglement in the steady-state regime of the system where the strength of the entanglement is strictly limited by the stability conditions. In fact, in this regime entanglement becomes maximum only when the system is driven close to the instability threshold, which demands a strong many-photon optomechanical coupling or high external laser driving [66].

In typical cavity optomechanical system [1, 38], a laser driven optical cavity gets coupled to a harmonically oscillating end mirror. However, regarding the quantumness of the mechanical mirror, it should be noted that a pure quantum harmonic motion is dynamically analogous to its classical counterpart, as the expectation values of the canonical observables obey the same set of classical equation of motion [80]. Therefore, to fully explore the quantum nature of the mechanical mirror, it may be useful to introduce additional nonlinearity in the system. Here, it is worth mentioning that the intrinsic nonlinearity of a sub-gigahertz mechanical oscillator is usually very small (nonlinear amplitude smaller than $10^{-15}\omega_m$ [81]), and, therefore is relevant only in the regime of large oscillation amplitudes. Several studies have been reported to generate nonlinearities that are strong in the quantum regime [82–85]. In particular, recently, Rips et al. [86] have proposed a scheme to enhance the intrinsic geometrical nonlinearity via an inhomogeneous electrostatic field. This has been further exploited by Djorwé et al. in Ref. [87] to generate robust optomechanical entanglement. Along this line, in 2009 Jacobs et al. [88] have reported a theoretical study to engineer wide range of nonlinearities in a mesoscopic resonator by coupling it to a simple auxiliary system. Following [88], Lü et al. [89] engineered a Duffing nonlinearity to study mechanical squeezing in optomechanical system, and, Wang et al. [119] constructed a cubic nonlinearity to investigate steady state mechanical squeezing in a hybrid atom-optomechanical system. Furthermore, in Ref. [91] Jacobs. et al. showed that it is possible to engineer superposition states by coupling a qubit to the square of the resonator's position. A plethora of experimental studies on the coupling between the mechanics and a two-level system can also be found Refs. [92–97].

Motivated by these works, we first consider a hybrid optomechanical system in which the mechanical mirror is perturbatively coupled to a single auxiliary qubit. Following [88], we find that this coupling results in an additional second-order term q^2, in the Hamiltonian describing the system where q is the position of the mechanical mirror. All the higher order nonlinear terms are neglected, as we assume weak coupling between the mechanical mirror and the qubit. We discuss the effects of such inclusion of an additional q^2 term in various quantum correlations present in a cavity optomechanical system.

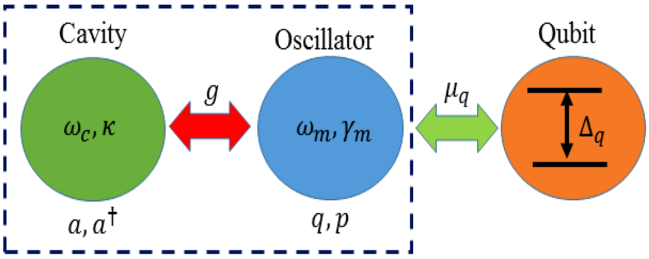

Figure 3.1: Schematic diagram of the cavity optomechanical system which consists of an optical cavity with frequency ω_c coupled to a mechanical mirror of frequency ω_m, via radiation pressure. Furthermore, we consider the mechanical mirror to be perturbatively coupled to an auxiliary qubit.

3.1.2 System dynamics

As depicted in Fig. 3.1, we consider a hybrid optomechanical system where the mirror is perturbatively coupled to an auxiliary qubit. The Hamiltonian of this system can be written as (in the unit of $\hbar = 1$):

$$H = H_0 + H_{mq}, \tag{3.1a}$$

$$H_0 = \omega_c a^\dagger a + \frac{\omega_m}{2}(p^2 + q^2) - g a^\dagger a q, \tag{3.1b}$$

$$H_{mq} = -\frac{\eta}{2} q^2, \tag{3.1c}$$

where a is the annihilation operator of the cavity field (with frequency ω_c), q (p) is the dimensionless position (momentum) operator of the mechanical mirror (with frequency ω_m), and g is the single-photon optomechanical coupling rate. In Eq. (3.1a), H_0 describes the Hamiltonian of the conventional optomechanical system, while H_{mq} refers to the Hamiltonian for the mirror-qubit interaction, with η being the coupling strength (see Appendix A. for a brief discussion on the generation of this term).

In addition, the system dynamics includes the fluctuation-dissipation processes affecting both the cavity field and mechanical mirror. Starting from Hamiltonian (3.1a), the time evolution of the system is given by the following set of nonlinear quantum Langevin equations (in a frame rotating with laser frequency ω_l):

$$\dot{q} = \omega_m p, \tag{3.2a}$$
$$\dot{p} = -\omega_m q + \eta q - \gamma_m p + g a^\dagger a + \xi, \tag{3.2b}$$
$$\dot{a} = -(\kappa + i\Delta_0)a + igaq - iE_0 + \sqrt{2\kappa_{ex}} a_{in} + \sqrt{2\kappa_0} f_{in}, \tag{3.2c}$$

where $\Delta_0 = \omega_c - \omega_l$ denotes the detuning of the cavity field from the laser frequency ω_l, $\kappa = \kappa_{ex} + \kappa_0$ is the total decay rate of the cavity field [1] and γ_m is the mechanical damping rate. We note that while defining Eq. (3.2c) the total cavity decay rate κ, we have considered two distinct contributions, one arising due to the losses at the input cavity mirror κ_{ex} and a second contribution from the internal losses of the cavity filed κ_0, associated with the scattering and absorption losses behind the first mirror. The input noises acting on the cavity field and mechanical mirror are characterized by the following set of non-zero correlation functions [41, 99], given by

$$\langle a_{in}(t) a_{in}^\dagger(t') \rangle = \delta(t - t'), \tag{3.3a}$$
$$\langle f_{in}(t) f_{in}^\dagger(t') \rangle = \delta(t - t'), \tag{3.3b}$$
$$\langle \xi(t)\xi(t') \rangle = \frac{\gamma_m}{\omega_m} \int \frac{d\omega}{2\pi} e^{-i\omega(t-t')} \omega \left[\coth\left(\frac{\hbar\omega}{2K_B T} \right) + 1 \right], \tag{3.3c}$$

where K_B is the Boltzmann constant and T is the mirror temperature. However, in the limit of large mechanical quality factor $Q = \omega_m/\gamma_m \gg 1$, one could well approximate the Brownian noise $\xi(t)$ to a Markovian delta-correlated relation, given by [100]:

$$\langle \xi(t)\xi(t') + \xi(t')\xi(t) \rangle / 2 \simeq \gamma_m \left(2n_{th} + 1 \right) \delta\left(t - t' \right), \tag{3.4}$$

with $n_{th} = \left[\exp\left(\frac{\hbar\omega_m}{K_B T} \right) - 1 \right]^{-1}$ being the mean thermal phonon number.

For an intensely driven cavity, we can further expand each of these Heisenberg operators as a sum of its c-number classical steady-state value plus an additional small fluctuation operator with zero mean value: $a = a_s + \delta a$, $q = q_s + \delta q$, $p = p_s + \delta p$.

The steady-state values are obtained by solving the following nonlinear algebraic equations:

$$p_s = 0, \tag{3.5a}$$
$$\omega_m q_s - \eta q_s - g|a_s|^2 = 0, \tag{3.5b}$$
$$(\kappa + i\Delta)a_s - \sqrt{2\kappa_{ex}}\alpha_{in} = 0, \tag{3.5c}$$

where $\alpha_{in} = \langle a_{in} \rangle$ is the driving amplitude and $\Delta = \Delta_0 - gq_s$ is the effective cavity detuning, modified owing to radiation pressure interaction. On the other hand, the dynamics of the quantum fluctuations are linearized in the limit $|a_s| \gg 1$ and written as:

$$\dot{\delta q} = \omega_m \delta p, \tag{3.6a}$$
$$\dot{\delta p} = -\left(\omega_m - \eta\right)\delta q - \gamma_m \delta p + \frac{G}{\sqrt{2}}\left(\delta a + \delta a^\dagger\right) + \xi, \tag{3.6b}$$
$$\dot{\delta a} = -(\kappa + i\Delta)\delta a + i\frac{G}{\sqrt{2}}\delta q + \sqrt{2\kappa_{ex}}a_{in} + \sqrt{2\kappa_0}f_{in}. \tag{3.6c}$$

Here a_s is considered to be real and $G = ga_s\sqrt{2}$ is the effective many-photon optomechanical coupling strength.

Next, we introduce the dimensionless quadrature operators, respectively, for the cavity field and the corresponding Hermitian input noise operators, as follows: $\delta X \equiv \frac{(\delta a + \delta a^\dagger)}{\sqrt{2}}$, $\delta Y \equiv \frac{(\delta a - \delta a^\dagger)}{i\sqrt{2}}$, and $X_{in} \equiv \frac{(a_{in} + a_{in}^\dagger)}{\sqrt{2}}$, $Y_{in} \equiv \frac{(a_{in} - a_{in}^\dagger)}{i\sqrt{2}}$, $F_{in} \equiv \frac{(f_{in} + f_{in}^\dagger)}{\sqrt{2}}$, $G_{in} \equiv \frac{(f_{in} - f_{in}^\dagger)}{i\sqrt{2}}$. With the above definitions, we express Eq. (3.6) in a matrix form:

$$\dot{u}(t) = Au(t) + n(t), \tag{3.7}$$

where $u^T(t) = (\delta q(t), \delta p(t), \delta X(t), \delta Y(t))$ is the vector of continuous-variable (CV) fluctuation operators, A is the drift matrix:

$$A = \begin{pmatrix} 0 & \omega_m & 0 & 0 \\ -\left(\omega_m - \eta\right) & -\gamma_m & G & 0 \\ 0 & 0 & -\kappa & \Delta \\ G & 0 & -\Delta & -\kappa \end{pmatrix}, \tag{3.8}$$

and $n^T(t) = \left(0, \xi(t), \sqrt{2\kappa_{ex}}X_{in}(t) + \sqrt{2\kappa_0}F_{in}(t), \sqrt{2\kappa_{ex}}Y_{in}(t) + \sqrt{2\kappa_0}G_{in}(t)\right)$ is the vector of corresponding noises. The solution of Eq. (3.7) reaches its steady state when all the eigenvalues of the drift matrix A have negative real parts. These stability conditions are checked via the Routh-Hurwitz criteria [101], which are given in terms of the system parameters, by the following two nontrivial equations:

$$2\gamma_m[\Delta^4 + \Delta^2(\gamma_m^2 + 2\gamma_m\kappa + 2\kappa^2 - 2\omega_m^2) + (\gamma_m\kappa + \kappa^2 + \omega_m^2)^2] + G^2\Delta\omega_m(\gamma_m + 2\kappa)^2 + 4\eta\gamma_m\kappa\omega_m(\Delta^2 - \gamma_m\kappa - \kappa^2 - \omega_m^2) + 2\eta^2\omega_m^2\gamma_m\kappa > 0, \quad (3.9a)$$

$$\left(\Delta^2 + \kappa^2\right)\omega_m^2 - \eta\left(\Delta^2 + \kappa^2\right)\omega_m - G^2\Delta\omega_m > 0. \quad (3.9b)$$

It should be noted that, strictly for red-detuned driving the first condition is always satisfied, only the second condition becomes relevant. Following a simplification of Eq. (3.9b), we obtain

$$G < G_{thres} = \sqrt{(\Delta^2 + \kappa^2)(\omega_m - \eta)/\Delta}. \quad (3.10)$$

where G_{thres} refers to the threshold optomechanical coupling, separating the stable and unstable phase of the system. We note that in contrast to standard optomechanical system [22], now the system's stability depends on the strength of the mirror-qubit coupling and one must have $\eta < \omega_m$. To numerically illustrate our result, we consider a set of experimentally accessible parameters as implemented in Refs. [13]. Figs. 3.2(a) and 3.2(b) depict the stable (yellow) and the unstable (green) phase of the optomechanical system in the $(G/\omega_m, \Delta/\omega_m)$ plane, respectively without $(\eta/\omega_m = 0)$ and with the mirror-qubit coupling $(\eta/\omega_m = 0.6)$. It is clear that in the former case the stability range is much wider than the later, i.e. the system remains stable from $G/\omega_m = 0.0$ to $G/\omega_m \approx 1.0$ (Fig. 3.2(a)). On the contrary, in the presence of the mirror-qubit coupling $\eta/\omega_m = 0.6$ (Fig. 3.2(b)), the stability region stretches from $G/\omega_m = 0.0$ to $G/\omega_m \approx 0.63$. Therefore, we can infer that the mirror-qubit coupling imposes a serious limitation on the maximum allowable effective optomechanical coupling strength. In the rest of this work, to operate safely within the stability range of the system, we will restrict ourselves to a coupling strength $G/\omega_m \leq 0.6$.

3.1.3 Optomechanical entanglement

Due to the above linearized dynamics and the zero-mean Gaussian nature of the quantum noises a_{in} (f_{in}) and ξ, the steady state for the quantum fluctuations is a

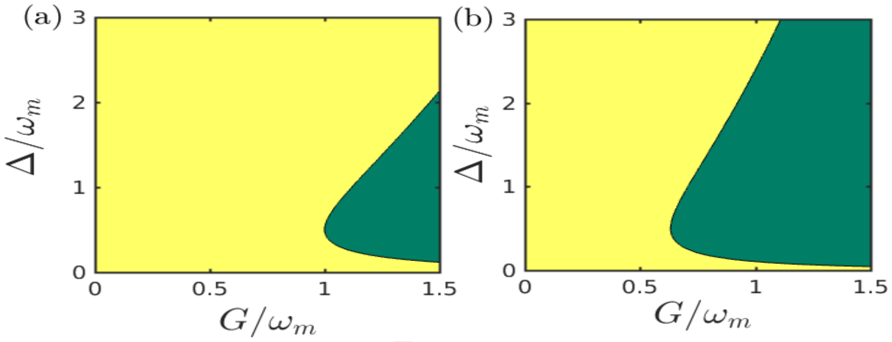

Figure 3.2: Stable (yellow) and unstable (green) region of the optomechanical system in the $(G/\omega_m, \Delta/\omega_m)$ plane, respectively for (a) $\eta/\omega_m = 0$ and (b) $\eta/\omega_m = 0.6$. The other parameters are chosen to be $\omega_m/(2\pi) = 10$ MHz, $Q = 10^5$, $\kappa/(2\pi) = 5$ MHz and $T_0 = 0.6$ K.

zero-mean Gaussian bipartite state, which is fully characterized by its 4×4 correlation matrix (CM):

$$V_{ij} = \left(\langle u_i(\infty)u_j(\infty) + u_j(\infty)u_i(\infty)\rangle\right)/2. \tag{3.11}$$

Here, $u^T(\infty) = (\delta q(\infty), \delta p(\infty), \delta X(\infty), \delta Y(\infty))$ is the vector of CV fluctuation operators in the steady-state ($t \to \infty$). When the system is stable, the steady-state CM satisfies the following Lyapunov equation [22]:

$$AV + VA^T = -D, \tag{3.12}$$

where D is a diagonal matrix of the noise correlations:

$$D = \text{Diag}\left[0, \gamma_m(2n_{th}+1), \kappa, \kappa\right]. \tag{3.13}$$

We now solve Eq. (3.12) to study various quantum correlations, present in a cavity optomechanical system.

In Fig. 3.3(a), we first plot logarithmic negativity E_N (2.14) versus the normalized detuning Δ/ω_m, for different mirror-qubit coupling strengths. It shows that for the chosen parameters, the usual system ($\eta = 0$) exhibits stationary optomechanical entanglement, which reaches its maximum $E_n^{max} = 0.18$ around $\Delta/\omega_m = 0.8$. However, the introduction of the mirror-qubit coupling enhances the degree of entanglement and shifts the position of the maxima towards a lower cavity detuning. In particular, we find a high degree of entanglement $E_n^{max} = 0.34$ at $\Delta/\omega_m = 0.51$

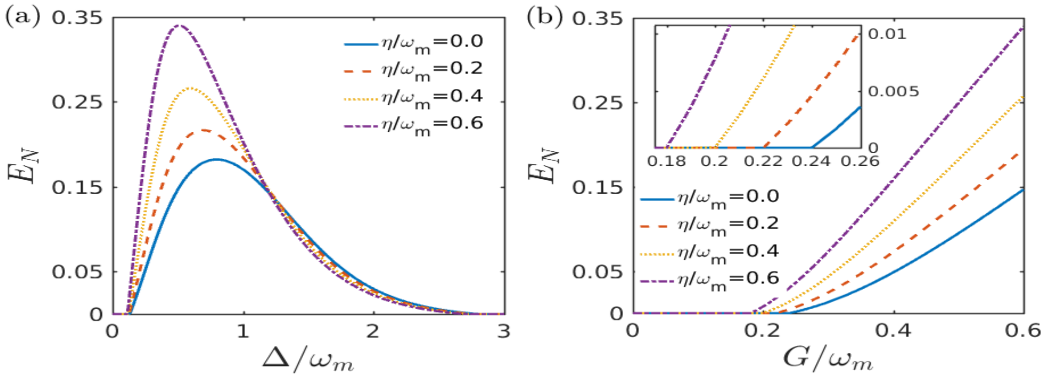

Figure 3.3: Plot of logarithmic negativity E_N as a function of (a) normalized detuning Δ/ω_m for a fixed coupling strength $G/\omega_m = 0.6$ and (b) dimensionless effective optomechanical coupling strength G/ω_m at a fixed detuning $\Delta/\omega_m = 0.5$, with all the other parameters same as in Fig. 2.

for $\eta/\omega_m = 0.6$. Here, it is also worth mentioning that for the chosen parameters, $(\Delta/\omega_m, \eta/\omega_m = 0.80, 0.0)$ and $(\Delta/\omega_m, \eta/\omega_m = 0.51, 0.6)$ respectively yield: $G_{thres} = 1.03\omega_m$ and $G_{thres} = 0.63\omega_m$. This implies that the maximum entanglement appears only when $G \to G_{thres}$ i.e. for the maximum possible optomechanical coupling strength. Therefore, we infer that this entanglement enhancement is achieved due to the additional mirror-qubit coupling, which brings the system close to the instability. Fig. 3.3(b) depicts the same logarithmic negativity E_N as a function of the dimensionless effective optomechanical coupling G/ω_m, for different mirror-qubit coupling strengths. As expected, after a critical coupling strength (G_c), entanglement appears and increases with increasing optomechanical coupling. We note that this enhancement becomes more profound with an increase in mirror-qubit coupling strength η/ω_m. More importantly, as illustrated in the inset of Fig. 3(b), we observe a lowering of this critical coupling strength G_c, with an increase in η/ω_m. For example, the usual system $(\eta = 0)$ starts exhibiting entanglement at $G_c/\omega_m = 0.24$, whereas, in presence of the mirror-qubit coupling $(\eta/\omega_m = 0.6)$ it shows entanglement at $G_c/\omega_m = 0.18$. Hence, the mirror-qubit coupling not only enhances the degree of entanglement but also generates it at a considerably lower optomechanical coupling strength.

Next, to study the robustness of our scheme, we plot in Fig. 3.4 logarithmic negativity E_N with respect to the mean thermal phonon number n_{th}, for various mirror-qubit coupling strengths. We observe that the degree of entanglement decreases monotonically with increasing thermal phonon number. However, the maximum number of thermal phonons up to which entanglement persists increases with

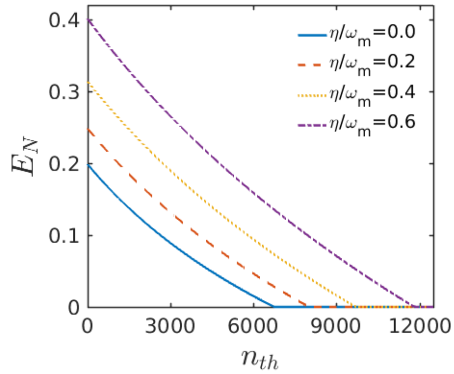

Figure 3.4: Plot of logarithmic negativity E_N as a function of the mean thermal phonon number n_{th}. Here, the effective cavity detuning and optomechanical coupling strength are respectively fixed at $\Delta/\omega_m = 0.5$ and $G/\omega_m = 0.6$, with all the other parameters same as in Fig. 2.

increasing mirror-qubit coupling strength. For example, in the generic case ($\eta = 0$) the entanglement is maintained up to $n_{th} = 6626$ ($T = 3.18$ K). In contrast, in presence of the mirror-qubit coupling $\eta = 0.6\omega_m$ the entanglement persists up to a relatively high $n_{th} = 11752$ ($T = 5.64$ K). Thus, the bipartite entanglement in presence of the mirror-qubit coupling becomes more robust against thermal phonon fluctuations.

3.1.4 Quantum mutual information and Gaussian quantum discord

In Figs. 3.5(a) and 3.5(b), we respectively plot the quantum mutual information I_M (2.16) and the Gaussian quantum discord D_G (2.18) as a function of the normalized detuning Δ/ω_m, for different mirror-qubit coupling strengths. In both these figures, we find that for the generic system ($\eta/\omega_m = 0$) I_M and D_G are maximum near $\Delta/\omega_m = 0$, and, then decrease monotonically with increasing Δ/ω_m [98]. However, with the introduction of mirror qubit coupling we observe a completely different behavior: Depending the strength of mirror-qubit coupling, both I_M and D_G enhance significantly at higher cavity detuning. In particular, for $\eta/\omega_m = 0.6$, we obtain the maximum $I_M = 1.29$ at $\Delta/\omega_m = 0.49$ and $D_G = 0.20$ at $\Delta/\omega_m = 0.80$. Therefore, this along with Fig. 3.3, confirms that invoking the mirror-qubit coupling to a generic optomechanical system is a promising mean to improve the quantum correlations between the cavity field and mechanical mirror.

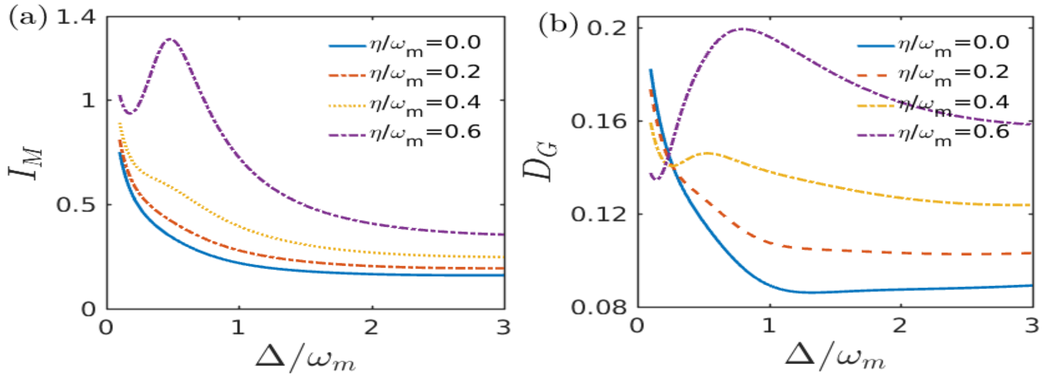

Figure 3.5: Plot of (a) quantum mutual information I_M and (b) Gaussian quantum discord D_G as a function of the normalized detuning Δ/ω_m, for different mirror-qubit coupling strengths η/ω_m, with all the other parameters same as in Fig. 2.

3.1.5 Conclusion

In conclusion, we reported a scheme to enhance the quantum correlation between a light field and a mechanical mirror. The system under consideration, consists of an optomechanical system where the mechanical mirror is perturbatively coupled to an auxiliary qubit. With in the standard linearized description, we found that due to the mirror-qubit coupling the system becomes unstable at a considerably lower optomechanical coupling strength, which leads to significant enhancement of steady-state entanglement near the instability threshold. We also reported that in presence of the mirror-qubit coupling, entanglement could be generated at lower optomechanical coupling strength which is extremely robust against the mirror temperature. Moreover, to investigate the correlations which can not be captured by studying entanglement only, we extended our calculation to quantum mutual information and Gaussian quantum discord. We found that unlike the generic system (without the mirror-qubit coupling), now both the mutual information and the quantum discord enhance significantly at a higher cavity detuning with an increase in mirror-qubit coupling strength. As all the chosen parameters are achievable within the current state-of-the-art experimental setups, our proposed scheme can be implemented to improve the quantum correlations in optomechanical platforms.

However, one should consider the following point as a drawback of our proposal. Due to the coupling to the cavity field, the mirror motion is driven by the external pump field. Here, it is worth mentioning that in order to maintain the perturbation approximation valid, the maximum eigenvalue of the mirror-qubit interaction should be significantly smaller than the separation energy of the auxiliary qubit. Therefore, while driving the cavity, one should focus at a lower driving amplitude, so that the qubit is not pushed into a nonlinear regime.

3.2 Enhancing quantum correlations in an optomechanical system via cross-Kerr nonlinearity

3.2.1 Brief overview

Very recently, optomechanical systems coupled to a two-level system or a nonlinear inductive element (single-Cooper pair transistor) have shown significant enhancement of the single-photon radiation-pressure coupling [102, 103]. More importantly, it has been theoretically deduced that such interaction induces an additional cross-Kerr type coupling between the optical and mechanical mode. In nonlinear optics, cross-Kerr effect describes the change in refractive index of one electromagnetic mode by the intensity of another. It has been extensively studied in the context of quantum information processing, such as non-demolition photon number detection [104], C-NOT gate [105] and, discrete [106] and continuous-variable entanglement concentration [107–109]. Concerning optomechanical system, the cross-Kerr coupling between the optical and mechanical mode, involves the change in the refractive index of the optical mode depending on the resonators phonon number [110, 111]. Recently, Ref. [112] has showed that this cross-Kerr coupling gives rise to a frequency shift in mechanical and optical mode, with the shift depending on the cavity photon number and mechanical phonon number. Furthermore, Ref. [113] studied the effect of cross-Kerr nonlinearity on the stability of the optomechanical system. Along this line, Ref. [114] showed that in presence of an additional cross-Kerr coupling, the steady-state response of the mechanical resonator becomes a nonmonotonous function of cavity photon number and the bistable behavior of the mean cavity photon can be turned into a tristable behavior. Motivated by these works, we study the combined effect of radiation pressure and cross-Kerr coupling on the quantum correlations present in an optomechanical system.

3.2.2 System and steady-state behavior

As depicted in Fig. 3.6, we consider an optomechanical system which consists of an optical and a mechanical mode, respectively, with frequency ω_a and ω_b. As usual,

The contents of this chapter are published in Subhadeep Chakraborty and Amarendra K. Sarma J. Opt. Soc. Am. B **34**, 1503 (2017) and Subhadeep Chakraborty and Amarendra K. Sarma, Ann. Phys **392**, 39 (2018).

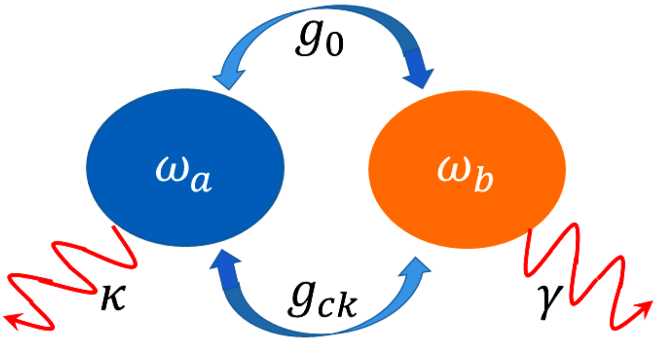

Figure 3.6: Schematic diagram of the considered optomechanical system. An optical mode (with frequency ω_a) couples the mechanical mode (with frequency ω_b) via the radiation-pressure coupling g_0 and an additional cross-Kerr coupling g_{ck}. Here, κ is the optical decay rate and γ is the mechanical damping rate.

these two modes are coupled via the generic radiation pressure coupling g_0. In addition, here we consider an extra cross-Kerr type coupling g_{ck} between the optical and the mechanical mode, generated by a two-level system or a superconducting charge qubit [102, 103]. Also, the whole system is driven by an external laser of frequency ω_l. With this consideration, the complete Hamiltonian of the optomechanical system in a rotating frame of the laser reads ($\hbar = 1$):

$$H = \Delta_0 a^\dagger a + \omega_b b^\dagger b - g_0 a^\dagger a(b^\dagger + b) - g_{ck} a^\dagger a b^\dagger b + iE_0(a^\dagger - a). \tag{3.14}$$

Here, a ($a^\dagger$) and b ($b^\dagger$) are, respectively, the annihilation (creation) operators of the optical and mechanical mode, $\Delta_0 = \omega_a - \omega_l$ is the optical detuning and E_0 is the driving amplitude, related to driving power P and optical decay rate κ by $|E_0| = \sqrt{2P\kappa/\hbar\omega_l}$.

In addition, the system dynamics also includes fluctuation-dissipation processes affecting both the optical and the mechanical mode. Starting from Hamiltonian (3.14), the time evolution of the optomechanical system is given by the following nonlinear quantum Langevin equations:

$$\dot{a} = -(i\Delta_0 + \kappa)a + ig_0 a(b^\dagger + b) + ig_{ck} a b^\dagger b + E_0 + \sqrt{2\kappa}a_{in}, \tag{3.15a}$$
$$\dot{b} = -(i\omega_b + \gamma)b + ig_0 a^\dagger a + ig_{ck} a^\dagger a b + \sqrt{2\gamma}b_{in}, \tag{3.15b}$$

where γ is the mechanical damping rate, and a_{in} and b_{in} are the corresponding zero-mean input Gaussian noises, with nonzero correlation functions [41], given by:

$$\langle a_{in}(t)a_{in}^{\dagger}(t')\rangle = \delta(t-t'), \tag{3.16a}$$
$$\langle b_{in}^{\dagger}(t)b_{in}(t')\rangle = n_{th}\delta(t-t'), \tag{3.16b}$$
$$\langle b_{in}(t)b_{in}^{\dagger}(t')\rangle = (n_{th}+1)\delta(t-t'). \tag{3.16c}$$

Here, n_{th} is the mean thermal phonon number, related to Boltzmann constant K_B and environmental temperature T by: $n_{th} = \left[\exp\left(\frac{\hbar\omega_b}{K_B T}\right) - 1\right]^{-1}$.

Under intense laser driving, we now expand each Heisenberg operators as a sum of its semi-classical steady-state value plus an additional small fluctuation operator with zero-mean value: $a = \alpha + \delta a$ and $b = \beta + \delta b$. The steady-state values are given by the following nonlinear equations:

$$(i\tilde{\Delta} + \kappa)\alpha - E_0 = 0, \tag{3.17a}$$
$$(i\tilde{\omega_b} + \gamma)\beta - ig_0|\alpha|^2 = 0, \tag{3.17b}$$

where $\tilde{\Delta} = \Delta_0 - g_0(\beta^* + \beta) - g_{ck}|\beta|^2$ is the effective optical detuning, modified owing to the both radiation pressure and cross-Kerr coupling, and, $\tilde{\omega_b} = \omega_b - g_{ck}|\alpha|^2$ is the effective mechanical frequency, modified owing to the cross-Kerr interaction. As for the fluctuations, their dynamics is given by the linearized quantum Langevin equations, written as:

$$\dot{\delta a} = -(i\tilde{\Delta} + \kappa)\delta a + i\frac{G}{2}(\delta b^{\dagger} + \delta b) + \sqrt{2\kappa}a_{in}, \tag{3.18a}$$
$$\dot{\delta b} = -(i\tilde{\omega_b} + \gamma)\delta b + i\frac{G}{2}(\delta a^{\dagger} + \delta a) + \sqrt{2\gamma}b_{in}, \tag{3.18b}$$

where $G = 2g|\alpha|$ is the effective optomechanical coupling strength with modified $g = g_0 + g_{ck}\beta$. Note that, in the above calculations the phase reference of the optical field is chosen such that α is real.

Next, we introduce the dimensionless quadrature operators, respectively, for the optical and the mechanical mode: $\delta X \equiv \frac{(\delta a + \delta a^{\dagger})}{\sqrt{2}}$, $\delta Y \equiv \frac{(\delta a - \delta a^{\dagger})}{i\sqrt{2}}$ and $\delta Q \equiv \frac{(\delta b + \delta b^{\dagger})}{\sqrt{2}}$, $\delta P \equiv \frac{(\delta b - \delta b^{\dagger})}{i\sqrt{2}}$, and, similarly for the corresponding Hermitian input noise operators: $X_{in} \equiv \frac{(a_{in} + a_{in}^{\dagger})}{\sqrt{2}}$, $Y_{in} \equiv \frac{(a_{in} - a_{in}^{\dagger})}{i\sqrt{2}}$ and $Q_{in} \equiv \frac{(b_{in} + b_{in}^{\dagger})}{\sqrt{2}}$, $P_{in} \equiv \frac{(b_{in} - b_{in}^{\dagger})}{i\sqrt{2}}$. With the above definitions, we express Eq. (3.18) in a more compact form:

$$\dot{u}(t) = Au(t) + n(t), \tag{3.19}$$

where $u^T(t) = (\delta Q(t), \delta P(t), \delta X(t), \delta Y(t))$ is the vector of continuous variable (CV) fluctuation operators, A is the drift matrix:

$$A = \begin{pmatrix} -\gamma & \tilde{\omega_b} & 0 & 0 \\ -\tilde{\omega_b} & -\gamma & G & 0 \\ 0 & 0 & -\kappa & \tilde{\Delta} \\ G & 0 & -\tilde{\Delta} & -\kappa \end{pmatrix}, \tag{3.20}$$

and $n^T(t) = \left(\sqrt{2\gamma}Q_{in}(t), \sqrt{2\gamma}P_{in}(t), \sqrt{2\kappa}X_{in}(t), \sqrt{2\kappa}Y_{in}(t)\right)$ is the vector of corresponding noises. A formal solution of Eq. (3.19) is given by:

$$u(t) = M(t)u(0) + \int_0^t dsM(s)n(t-s), \tag{3.21}$$

where $M(t) = e^{AT}$. The system is stable and reaches its steady-state when all the eigenvalues of the drift matrix A have negative real parts. These stability conditions are derived by applying the Routh-Hurwitz criteria [101], which is given in terms of the system parameters by the following two nontrivial equations:

$$4\gamma\kappa[\tilde{\Delta}^4 + 2\tilde{\Delta}^2(\gamma^2 + \kappa^2 - \tilde{\omega_b}^2) + (\gamma^2 + \kappa^2 + \tilde{\omega_b}^2)^2 \tag{3.22a}$$
$$+4\gamma\kappa(\tilde{\Delta} + \kappa + \gamma^2 + \kappa^2 + \tilde{\omega_b}^2)] + 4G^2\tilde{\Delta}\tilde{\omega_b}(\gamma+\kappa)^2 > 0,$$
$$(\tilde{\Delta}^2 + \kappa^2)(\tilde{\omega_b}^2 + \gamma^2) - G^2\tilde{\Delta}\tilde{\omega_b} > 0. \tag{3.22b}$$

Note that, in the following work we will strictly restrict to red-detuned driving ($\tilde{\Delta} > 0$), for which the first condition is always satisfied, only the second condition is relevant.

To numerically illustrate the effect of the cross-Kerr coupling on the steady-state behavior of the optomechanical system, we consider a set of experimentally accessible parameters: $\omega_a/2\pi = 370$ THz, $\omega_b/2\pi = 10$ MHz, $g_0 = 1.347$ KHz, $\gamma/2\pi = 100$ Hz, $P_0 = 0.1$ mW and $n_{th} = 100$. In Fig. 3.7(a), we plot the steady-state amplitudes of the optical and mechanical mode along with the stability range of the system (with $g_{ck} = 10^{-3}g_0$), as a function of the driving power. It is clear that for the chosen value of the parameters, both these amplitudes satisfy $|\alpha|, |\beta| \gg 1$ which ensures the validity of our linearization assumption. We also note that unlike pure radiation-pressure coupling, now $|\beta|$ changes drastically with increasing power, as could be explained from Eq. (3.17b). In Fig. 3.6(b) we plot $\tilde{\omega_b}$ and g against the driving power. We can see that with increasing power $\tilde{\omega_b}$ decreases and g increases.

In particular, at a driving power $P = 2.23P_0$ (just before the instability), we get $\tilde{\omega_b} \approx 0.4\omega_b$ and $g \approx 2.5g_0$. Therefore, in presence of the cross-Kerr coupling, owing to this significant change in the effective mechanical frequency and (single photon) coupling strength, the system becomes unstable at a considerably lower driving power. It is worthwhile to note that in Ref. [112], Raphael et al. have shown that the frequency of the mechanical resonator gets shifted owing to the cross-Kerr effect and the shift depends on the number of photons in the cavity. On the other hand, in Ref. [114], Wei et al. have shown that the mean phonon number, which increases monotonically with increase in the photon number in presence of the radiation-pressure coupling, changes drastically with the introduction of the cross-Kerr coupling. Our analysis, as could be seen from Eq. (3.17) and Fig. 3.7 agrees well with these observations. However, in this work, the parameter regime where the system becomes unstable is of prime concern to us owing to its significance in attaining high entanglement.

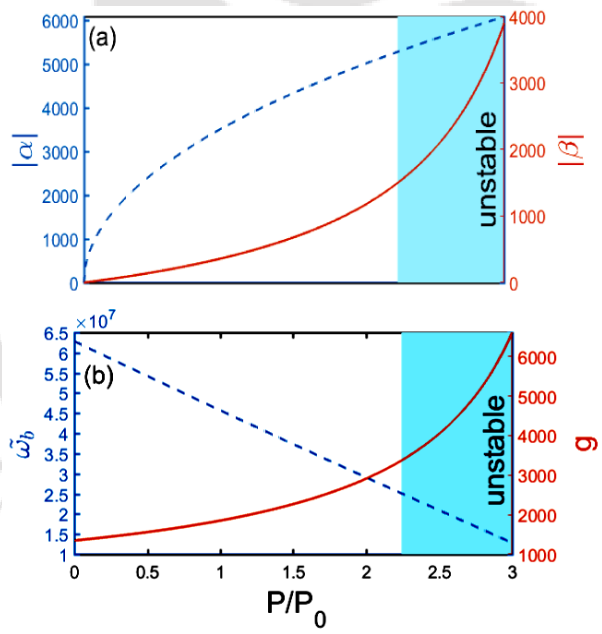

Figure 3.7: (a) The steady-state amplitudes $|\alpha|$ (blue dashed) and $|\beta|$ (red solid), and, (b) the modified mechanical frequency $\tilde{\omega_b}$ (blue dashed) and coupling strength g (red solid) versus the normalized driving power P/P_0. The shaded (cyan) region corresponds to the unstable phase of the optomechanical system. The other parameters are fixed at: $g_{ck} = 10^{-3}g_0$, $\kappa/\omega_b = 0.4$ and $\Delta_0/\omega_b = 0.5$.

3.2.3 Optomechanical entanglement

Due to the above linearized dynamics and zero-mean Gaussian nature of the quantum noises, the steady-state for the quantum fluctuations is simply a Gaussian bipartite state, which is fully characterized by its 4×4 correlation matrix (CM):

$$V_{ij} = \left(\langle u_i(\infty) u_j(\infty) + u_j(\infty) u_i(\infty) \rangle \right) / 2. \tag{3.23}$$

Here, $u^T(\infty) = (\delta Q(\infty), \delta P(\infty), \delta X(\infty), \delta Y(\infty))$ is the vector of CV fluctuation operators in the steady-state ($t \to \infty$). When the system is stable, performing a substitution of Eq. (3.21) in the definition of CM, we get

$$V_{ij} = \sum_{k,l} \int_0^\infty ds \int_0^\infty ds' M_{ik}(s) M_{jl}(s') \Phi_{kl}(s - s'), \tag{3.24}$$

where $\Phi_{kl}(s - s') = (\langle n_k(s) n_l(s') + n_l(s') n_k(s) \rangle)/2$ is the matrix of the stationary noise correlations. Using Eq. (3.16), $\Phi_{kl}(s - s')$ further simplifies to $\Phi_{kl}(s - s') = D_{kl} \delta(s - s')$, where D is a diagonal matrix, given by:

$$D = \mathrm{Diag}\left[\gamma(2n_{th} + 1), \gamma(2n_{th} + 1), \kappa, \kappa \right]. \tag{3.25}$$

Therefore, (3.24) becomes $V = \int_0^\infty ds M(s) D M(s)^T$, which, when the stability conditions are satisfied ($M(\infty) = 0$) is equivalent to the following Lyapunov equation for V:

$$AV + VA^T = -D. \tag{3.26}$$

Following a numerical solution of Eq. (3.26), one can assess the degree of quantum entanglement (2.14) and Gaussian quantum discord (2.18) between the optical and mechanical mode.

First, we focus on the steady-state optomechanical entanglement and the influence of cross-Kerr coupling on it. In Fig. 3.8, we plot E_N as a function of the normalized cross-Kerr coupling strength g_{ck}/g_0, for a fixed driving power and optical detuning. We can see that with increase in the cross-Kerr coupling, the degree of entanglement increases monotonically and becomes maximum just before the instability. In particular, for the pure radiation-pressure coupling case ($g_{ck} = 0$) we have $E_N = 0.025$. On the other hand, in the presence of cross-Kerr coupling, with coupling strength $g_{ck} = 10^{-3} g_0$, we obtain $E_N = 0.27$. Therefore, by invoking cross-

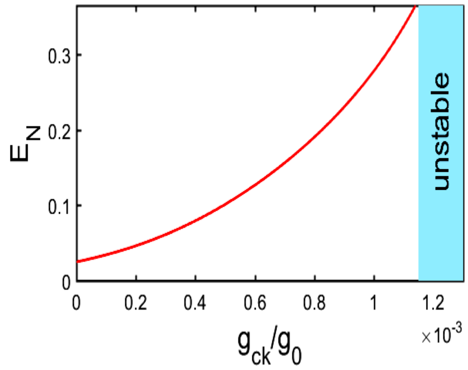

Figure 3.8: E_N as a function of the normalized cross-Kerr coupling strength g_{ck}/g_0, at a fixed $P/P_0 = 2.0$, $\Delta_0/\omega_b = 0.5$ and $\kappa/\omega_b = 0.4$.

Kerr coupling on a generic optomechanical system, we can significantly enhance the degree of the steady-state optomechanical entanglement.

To further probe into entanglement properties and its dependence on the system parameters, we plot in Fig. 3.9, E_N as a function of the normalized detuning Δ_0/ω_b and the normalized driving power P/P_0, for $g_{ck} = 0$ (a) (no cross-Kerr coupling), $g_{ck} = 0.5 \times 10^{-3} g_0$ (b), and $g_{ck} = 1.0 \times 10^{-3} g_0$ (c). We observe that with increase in the cross-Kerr coupling strength, the degree of entanglement increases, however, the parameter region in which the steady-state is entangled significantly narrows. In fact, with increasing cross-Kerr coupling strength, as discussed in earlier section, the system becomes unstable at a lower driving power, which leads to the significant enhancement of steady-state optomechanical entanglement near the instability threshold.

Fig. 3.10, depicts the same E_N as a function of the normalized optical decay rate κ/ω_b and normalized driving power P/P_0, for $g_{ck} = 0$ (a) (no cross-Kerr coupling), $g_{ck} = 0.5 \times 10^{-3} g_0$ (b), and $g_{ck} = 1.0 \times 10^{-3} g_0$ (c). Here also, we find the enhancement of the steady-state optomechanical with increasing cross-Kerr coupling strength. However, now the maximum entanglement only occurs for $g_{ck} = 1 \times 10^{-3} g_0$ (Fig. 3.10(c)) at higher driving power and lower optical decay rate. It is also important to note that even in the presence of cross-Kerr coupling, we find significant entanglement only in the resolved sideband region, i.e. for $\kappa/\omega_b < 1$.

Finally, in Fig. 3.11, we plot E_N as a function of the mean thermal phonon number n_{th}. We observe that the degree of entanglement monotonically decreases with increase in the thermal phonon number. However, the maximum number of thermal phonons up to which the entanglement persists increases with increasing

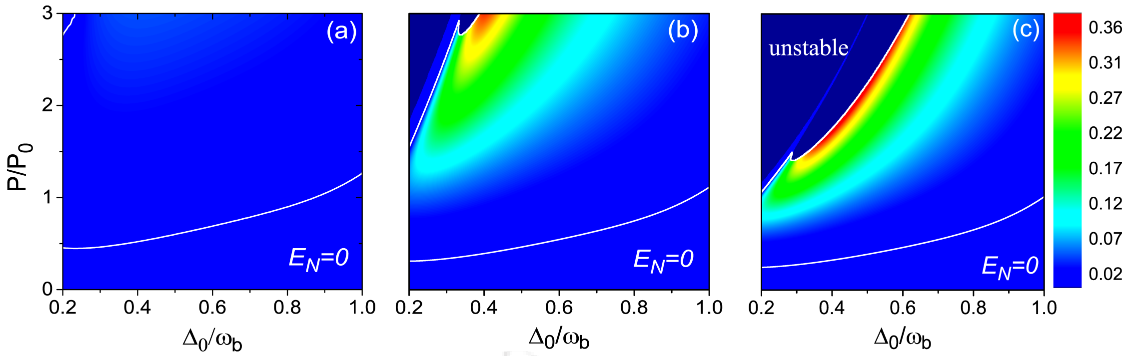

Figure 3.9: Contour plot of E_N versus the normalized detuning Δ_0/ω_b and driving power P/P_0, for $g_{ck} = 0$ (a) (no cross-Kerr coupling), $g_{ck} = 0.5 \times 10^{-3} g_0$ (b), and $g_{ck} = 1.0 \times 10^{-3} g_0$ (c). The optical decay rate is fixed at $\kappa/\omega_b = 0.4$. The white thick line separates the entangled and the non-entangled phase of the system.

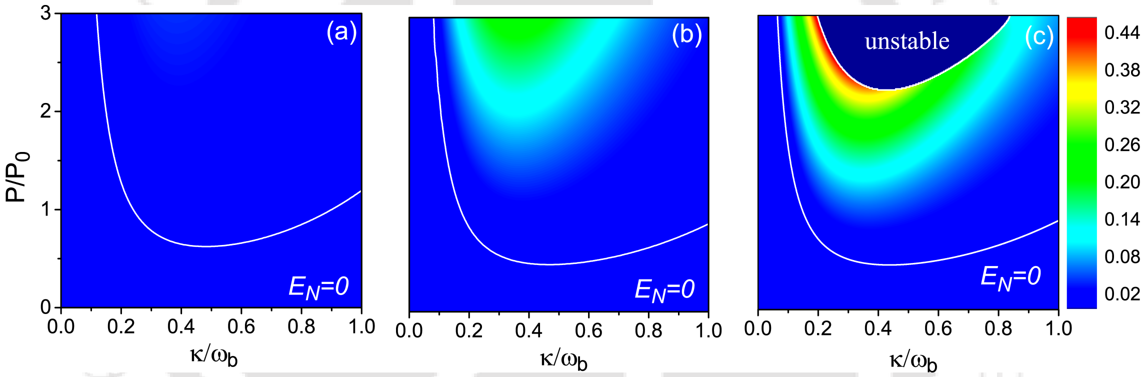

Figure 3.10: Contour plot of E_N versus the normalized optical decay rate κ/ω_b and normalized driving power P/P_0, for $g_{ck} = 0$ (a) (no cross-Kerr coupling), $g_{ck} = 0.5 \times 10^{-3} g_0$ (b), and $g_{ck} = 1.0 \times 10^{-3} g_0$ (c). The optical detuning is fixed at $\Delta_0/\omega_b = 0.5$.

cross-Kerr coupling. For example, for the pure radiation-pressure coupling case the entanglement persists up to $n_{th} \approx 460$. In contrast, in presence of an additional cross-Kerr coupling, with coupling strength $g_{ck} = 10^{-3} g_0$, we have entanglement up to $n_{th} \approx 4970$. This shows that with the introduction of cross-Kerr coupling, the bipartite entanglement becomes more robust against the fluctuation of the bath temperature.

It is worthwhile to mention that similar conclusions could be drawn for a different set of parameters as well. For example, we find that the proposed scheme works well for the following set of parameters, recently used in an experiment [20]: $\omega_a/2\pi = 195$

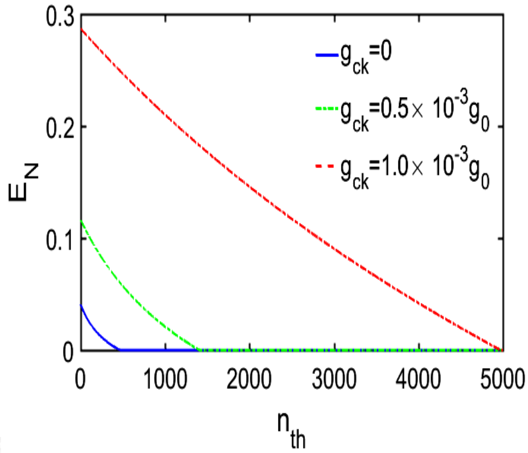

Figure 3.11: E_N versus the mean thermal phonon number for different cross-Kerr coupling strengths. The other parameters are fixed at $\Delta_0/\omega_b = 0.5$, $\kappa/\omega_b = 0.4$ and $P/P_0 = 2.0$.

THz, $\omega_b/2\pi = 3.68$ GHz, $g_0/2\pi = 910$ KHz, $\gamma/2\pi = 35$ KHz, $P_0 = 0.5$ mW and $n_{th} = 100$. We further note that though with increase in the thermal phonon numbers entanglement gradually decreases, quantum correlation can persist up to to a much higher number of thermal phonons as quantified by the parameter, Gaussian quantum discord. This issue is addressed in the following section.

3.2.4 Gaussian quantum discord

To study the effect of cross-Kerr nonlinearity on the Gaussian quantum discord, we first plot in Fig. 3.12, discord as a function of the normalized cross-Kerr coupling strength g_{ck}/g_0. We find that like optomechanical entanglement discord increases monotonically with increasing cross-Kerr coupling and becomes maximum just before the instability. For example, initially for the pure radiation-pressure coupling ($g_{ck} = 0$) we have $D_G \approx 0.01$, on the other hand, in presence of an additional cross-Kerr coupling of coupling strength $g_{ck} = 10^{-3}g_0$ we obtain $D_G \approx 0.1$. Therefore, this result along with Fig. 3.8 confirm that incorporating cross-Kerr nonlinearity on a generic optomechanical system can considerably enhance the quantum correlation between the optical and the mechanical mode.

Next, in Fig. 3.13 we plot the same Gaussian quantum discord against the mean thermal phonon number, for increasing cross-Kerr coupling strengths. We observe that unlike optomechanical entanglement discord is a nonmonotonous function of

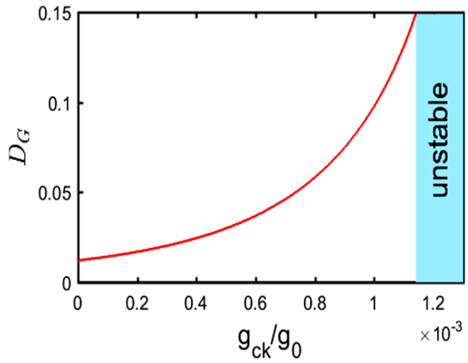

Figure 3.12: D_G as a function of the normalized cross-Kerr coupling strength g_{ck}/g_0. The other parameters are fixed at $\Delta_0/\omega_b = 0.5$, $\kappa/\omega_b = 0.4$ and $P/P_0 = 2.0$.

the mean thermal phonon number. Initially, for smaller number of thermal phonons it increases. But then, at higher number of thermal phonons it decreases. A similar kind of nonmonotonous behavior of the Gaussian QD against the thermal phonon number has recently been reported in Ref. [115]. It is also worth mentioning that as compared to optomechanical entanglement, discord survives up to a significantly higher number of thermal phonons. We further note that at higher number of thermal phonons, with the increase in cross-Kerr coupling the degree of quantum discord enhances significantly over the conventional system ($g_{ck} = 0$). Therefore, we infer that in the presence of an additional cross-Kerr coupling the quantum correlation present in the system becomes more robust against the variation of thermal phonon fluctuation.

3.2.5 Conclusion

In conclusion, we present a scheme to enhance the steady-state quantum correlations in an optomechanical system by incorporating an additional cross-Kerr type coupling between the optical and mechanical mode. We first consider logarithmic negativity to quantify the degree of stationary entanglement between the optical and mechanical mode, and then, we focus on Gaussian quantum discord to investigate the quantumness of the correlation beyond entanglement. We found that owing to the cross-Kerr nonlinearity the system becomes unstable at a considerably lower driving power, which leads to significant enhancement of both entanglement and discord near the instability threshold. Moreover, we showed that in presence of the cross-Kerr nonlinearity the generated entanglement becomes more robust against the

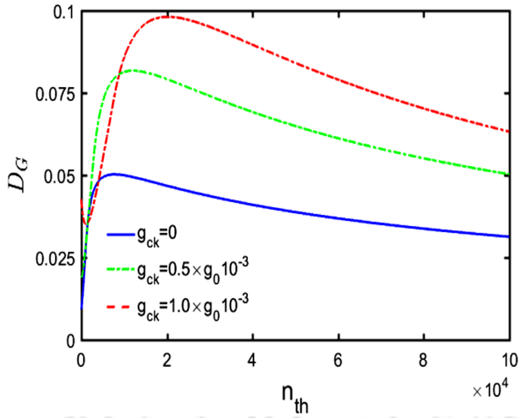

Figure 3.13: D_G against mean thermal phonon number n_{th}. The other parameters are fixed at $\Delta_0/\omega_b = 0.5$, $\kappa/\omega_b = 0.4$ and $P/P_0 = 1.5$.

variation of system parameters and thermal phonon fluctuations. Furthermore, we found that unlike optomechanical entanglement, quantum correlation between the optical and mechanical mode as quantified by the parameter called, Gaussian quantum discord, could persists up to a much higher bath temperature in the presence of cross-Kerr coupling. Therefore, this work paves the way for exploring cross-Kerr nonlinearity as a promising way to optimize both the quantum entanglement and quantum discord in a generic optomechanical system.

Chapter 4

Entanglement dynamics of two coupled mechanical oscillators in modulated optomechanics

In this chapter, we aim to entangle two massive macroscopic mechanical oscillators in an optomechanical setup. To do so, we consider a periodically modulated external driving and mechanical coupling. We show that how depending on the mechanical coupling strength, one can observe either a stationary or a dynamical behavior of the mechanical entanglement. Remarkably, both these entanglements are extremely robust against the oscillator's temperature. An analytical expression for the critical mechanical coupling strength is also derived.

4.1 Brief overview

Relying on the generic radiation-pressure coupling, much studies have already been reported on the entanglement generation between a cavity field and a mechanical oscillator [22, 66, 78, 116–120]. Besides, based on similar architecture, a lot of emphasis has been currently put forward to create entanglement between two macroscopic mechanical oscillators. These studies mostly include light-to-matter entanglement transfer [7, 129], driving the optical cavity with a two-tone field [130, 131], dissipation induced optomechanical entanglement [132, 133] and the reservoir engineered based schemes [134–138]. We also note that, recently, an experimental demonstra-

---

The contents of this chapter are published in Subhadeep Chakaborty and Amarendra K. Sarma, Phys. Rev. A **97**, 022336 (2018).

tion of entangling two massive macroscopic mechanical oscillators has been reported in Ref. [139–141]. However, in most of the cases, the possibility of observing such a nonclassical state is seriously hindered by the presence of the environmental noise. Hence a lot of emphasis has currently been put in realizing quantum entanglement at higher bath temperature.

While the search for robust and *hot entanglement* [121] in optomechanical systems is on, it occurs that modulating an optomechanical system may be a very rewarding proposition in achieving a more robust nonclassicality. For example, in 2009, Mari et al. [122] first showed that by gently modulating an optomechanical system, one could not only enhance the degree of squeezing in mechanical quadratures but also improve the stationary entanglement between the cavity field and the nanomechanical resonator. Following Ref. [122], Farace et al. [123] studied the effect of both the amplitude modulation and frequency modulation in an optomechanical system. They showed that there exists an optimal modulation regime where the desired quantum effects can either be enhanced or suppressed. Along this line, Schmidt et al [124] implemented a suitable amplitude modulation scheme in optomechanical circuits for continuous variable (CV) quantum state processing. More recently, Chen et al. [125] has exploited the same amplitude modulation to improve the stationary mechanical entanglement in a double cavity optomechanical system.

In parallel to the developments in optomechanical systems, one modulation scheme of particular interest is the so-called periodic modulation of the coupling strength. It is now well established that by periodically driving the coupling strength with a frequency twice that of the oscillator frequency, one can squeeze the collective quadratures, leading to entanglement generation between the two harmonic oscillators. In 2010, within a similar framework, two identical harmonic oscillators in contact with two independent thermal baths and coupled via a time periodic driving, Galve et al. [126] first demonstrated the existence of stationary entanglement at a relatively high temperature. Following Ref. [126], Roque et al. [127] reported the dynamics of quantum correlations between two coupled harmonic oscillators in contact with a common heat bath. They found that it is not the bath temperature, rather the system parameters to which the entanglement dynamics is more sensitive. However, it should be noted that in their study they could not find any steady-state behavior of the generated entanglement. On the other hand, recently, Chen et al. [128] considered a system of two coupled harmonic oscillators connected via a weak time-dependent coupling. In the absence of any environmental decoherence, they re-

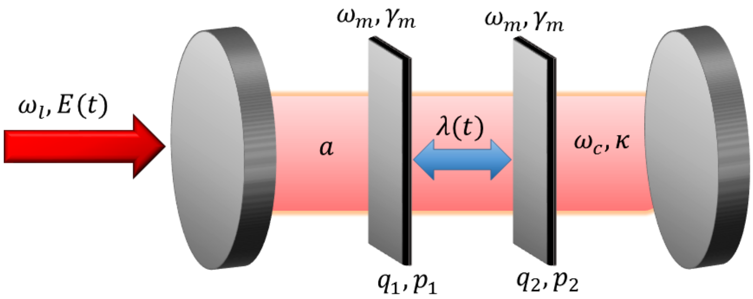

Figure 4.1: Schematic diagram of the considered optomechanical system. The cavity is driven by an amplitude modulated laser $E(t)$, and, the two mechanical oscillators are coupled via a periodically modulated coupling strength $\lambda(t)$.

ported that a transition from bounded to unbounded entanglement dynamics occurs when the modulation strength crosses a critical value.

Here, we discuss the effects of both these periodically modulated external driving and mechanical coupling on the entanglement generation between two macroscopic mechanical oscillators.

4.2 Model and dynamics

The system under consideration, consists of two identical mechanical oscillators placed within an optical cavity. An external laser with a time-dependent amplitude $E(t)$ and frequency ω_l drives the cavity which makes the two oscillators couple indirectly via the radiation-pressure interaction. Besides, there is a direct mechanical coupling between the two oscillators, with a periodically modulated coupling strength $\lambda(t)$. The schematic of our system is depicted in Fig. 4.1, and, the Hamiltonian (in a frame rotating with the laser frequency) is written as follows (in the unit of $\hbar = 1$):

$$H = \Delta_0 a^\dagger a + \sum_{j=1}^{2} \frac{\omega_m}{2}(q_j^2 + p_j^2) + g a^\dagger a \sum_{j=1}^{2} q_j + \lambda(t) q_1 q_2 + i\left(E(t)a^\dagger - E^*(t)a\right). \tag{4.1}$$

Here, a ($a^\dagger$) refers to the annihilation (creation) operator of the cavity field (with frequency ω_c and decay rate κ), q_j (p_j) is the dimensionless position (momentum) operator of the j-th mechanical oscillator (with frequency ω_m and damping rate γ_m). g refers to the strength of the single photon radiation-pressure coupling. In

Hamiltonian Eq. (4.1), the first and the second terms correspond to the Hamiltonian of the driven cavity and the mechanical oscillators, respectively, with $\Delta_0 = \omega_c - \omega_l$ being the optical detuning. The third term describes the optomechanical interaction between the cavity field and the mechanical oscillators, while the fourth term refers to the bilinear coupling between the two oscillators. Finally, the last term gives the external laser driving.

In addition to this, the system dynamics is unavoidably subjected to the fluctuation-dissipation processes affecting both the cavity field and the mechanical oscillators. Taking all the damping and noise terms into account, the dynamics of the system is fully described by the following set of nonlinear quantum Langevin equations (QLEs):

$$\dot{q_j} = \omega_m p_j, \tag{4.2a}$$

$$\dot{p_j} = -\omega_m q_j - g a^\dagger a - \lambda(t) q_{3-j} - \gamma_m p_j + \xi_j(t), \tag{4.2b}$$

$$\dot{a} = -\{i(\Delta_0 + g\sum_{j=1}^{2} q_j) + \kappa\}a + E(t) + \sqrt{2\kappa}a_{in}, \tag{4.2c}$$

where a_{in} is the vacuum input noise operator, with the only nonzero correlation function [41]:

$$\langle a_{in}(t) a_{in}^\dagger(t')\rangle = \delta(t-t'). \tag{4.3}$$

$\xi_j(t)$ are the stochastic Hermitian Brownian noise operator, with the non-Markovian correlation function given by [99]

$$\langle \xi_j(t)\xi_k(t')\rangle = \frac{\delta_{jk}}{2\pi}\frac{\gamma_m}{\omega_m}\int \omega e^{-i\omega(t-t')}\left[\coth\left(\frac{\hbar\omega}{2K_BT}\right)+1\right]d\omega, \tag{4.4}$$

(k_B being the Boltzmann constant and T being the temperature of the mechanical oscillators). However, in the limit of large mechanical quality factor $Q = \omega_m/\gamma_m \gg 1$, one could well approximate this Brownian noise to a Markovian delta-correlated relation [100]:

$$\langle \xi_j(t)\xi_j(t') + \xi_j(t')\xi_j(t)\rangle/2 \simeq \gamma_m\left(2n_{th}+1\right)\delta\left(t-t'\right), \tag{4.5}$$

with $n_{th} = \left[\exp\left(\frac{\hbar\omega_m}{K_BT}\right)-1\right]^{-1}$ being the number of mean thermal phonons.

Next, when the system is strongly driven to a large classical mean value, we can adopt the standard linearization technique and rewrite each Heisenberg operator as follows: $o(t) = \langle o(t)\rangle + \delta o(t)$ $(o = q_j, p_j, a)$. Here, $\langle o(t)\rangle$ refers to the classical

c-number mean value and $\delta o(t)$ is the zero-mean quantum fluctuation around the classical mean value. The equation of motion corresponding to the classical mean values is given by the following set of nonlinear differential equations:

$$\langle \dot{q}_j(t)\rangle = \omega_m \langle p_j(t)\rangle, \tag{4.6a}$$

$$\langle \dot{p}_j(t)\rangle = -\omega_m \langle q_j(t)\rangle - g|\langle a(t)\rangle|^2 - \lambda(t)\langle q_{3-j}(t)\rangle - \gamma_m \langle p_j(t)\rangle, \tag{4.6b}$$

$$\langle \dot{a}(t)\rangle = -\{i(\Delta_0 + g\sum_{j=1}^{2}\langle q_j(t)\rangle) + \kappa\}\langle a(t)\rangle + E(t). \tag{4.6c}$$

On the other hand, the dynamics of the quantum fluctuations is governed by the following linearized QLEs, written in a matrix form:

$$\dot{u(t)} = A(t)u(t) + n(t). \tag{4.7}$$

Here, $u^T(t) = (\delta q_1(t), \delta p_1(t), \delta q_2(t), \delta p_2(t), \delta X(t), \delta Y(t))$ is the vector of quadrature fluctuation operators, $n^T(t) = \left(0, \xi_1(t), 0, \xi_2(t), \sqrt{2\kappa}X_{in}(t), \sqrt{2\kappa}Y_{in}(t)\right)$ is the vector of corresponding noises and

$$A(t) = \begin{pmatrix} 0 & \omega_m & 0 & 0 & 0 & 0 \\ -\omega_m & -\gamma_m & -\lambda(t) & 0 & G_x(t) & G_y(t) \\ 0 & 0 & 0 & \omega_m & 0 & 0 \\ -\lambda(t) & 0 & -\omega_m & -\gamma_m & G_x(t) & G_y(t) \\ -G_y(t) & 0 & -G_y(t) & 0 & -\kappa & \Delta(t) \\ G_x(t) & 0 & G_x(t) & 0 & -\Delta(t) & -\kappa \end{pmatrix}, \tag{4.8}$$

is the drift matrix. The time-dependent coupling and the detuning terms are, respectively, defined as follows:

$$G(t) = -\sqrt{2}g\langle a(t)\rangle, \tag{4.9a}$$

$$G(t) = G_x(t) + iG_y(t), \tag{4.9b}$$

$$\Delta(t) = \Delta_0 + g\sum_{j=1}^{2}\langle q_j(t)\rangle, \tag{4.9c}$$

It should be noted that in Eq. (4.7) we have used the quadrature operators for the cavity field with the corresponding Hermitian input noise operators, respectively defined as: $\delta X \equiv \frac{(\delta a + \delta a^\dagger)}{\sqrt{2}}$, $\delta Y \equiv \frac{(\delta a - \delta a^\dagger)}{i\sqrt{2}}$, and $X_{in} \equiv \frac{(a_{in} + a_{in}^\dagger)}{\sqrt{2}}$, $Y_{in} \equiv \frac{(a_{in} - a_{in}^\dagger)}{i\sqrt{2}}$.

Due to the above linearized dynamics and the zero-mean Gaussian nature of the quantum noises, the quantum fluctuations in the stable regime evolve to an asymptotic Gaussian state which is completely characterized by its 6×6 correlation matrix, given by:

$$V_{ij} = \left(\langle u_i(t)u_j(t) + u_j(t)u_i(t)\rangle\right)/2. \tag{4.10}$$

The equation of motion corresponding to the correlation matrix, using Eq. (4.7) and Eq. (4.10), can be written as follows:

$$\dot{V}(t) = A(t)V(t) + V(t)A^T(t) + D, \tag{4.11}$$

where $D = \mathrm{Diag}\left[0, \gamma_m(2n_{th}+1), 0, \gamma_m(2n_{th}+1), \kappa, \kappa\right]$ is the matrix of noise-correlation. Note that, Eq. (4.11) is an inhomogeneous first-order differential equation with 21 elements which could be numerically solved with the initial condition $V(0) = \mathrm{Diag}\left[n_{th}+1/2, n_{th}+1/2, n_{th}+1/2, n_{th}+1/2, 1/2, 1/2\right]$. Here, we have assumed that each mechanical oscillators are prepared in their thermal states at temperature T and the cavity field is in it's vacuum state.

4.3 Results and discussions

Before proceeding to a direct numerical investigation of the mechanical entanglement, we first specify the exact form of time modulation for both the external driving and the mechanical coupling strength, as follows:

$$E(t) = E_0 + E_1\cos\left(\Omega t\right), \quad \lambda(t) = \lambda_0\cos\left(\Omega t\right). \tag{4.12}$$

Moreover, we choose the following set of parameters for our numerical simulations: $\Delta_0/\omega_m = 1.0$, $\kappa/\omega_m = 0.1$, $\gamma_m/\omega_m = 5\times 10^{-4}$, $g/\omega_m = 1\times 10^{-5}$, $E_0/\omega_m = 1\times 10^4$, $E_1/\omega_m = 1\times 10^3$, $T_0/\omega_m = \hbar/k_B$, $\Omega/\omega_m = 2.003$ (this particular choice will be justified later) and $\tau = 2\pi/\Omega$.

In Fig. 4.2, we plot the time evolution of the mechanical entanglement E_N for multiple values of λ_0/ω_m. It can be observed that in absence of the mechanical coupling ($\lambda_0/\omega_m = 0$), the two oscillators exhibit a very small degree of stationary entanglement. However, as soon as the mechanical coupling is introduced, there is a sudden but significant enhancement in E_N at initial time, which finally converges to an asymptotic steady-state value. We note that this enhancement becomes more profound with an increase in coupling strength λ_0/ω_m. Moreover, in the asymptotic

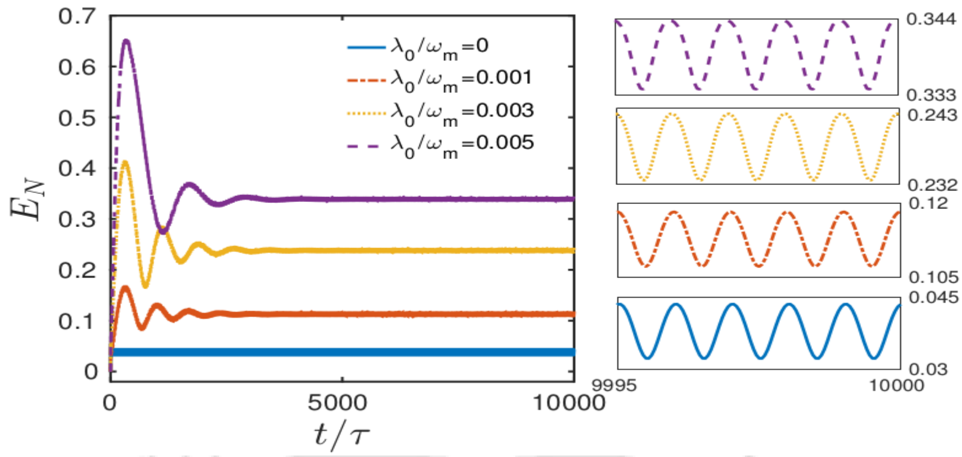

Figure 4.2: Entanglement dynamics of the two coupled mechanical oscillators for $\lambda_0/\omega_m = [0, 0.005]$ (from bottom to top) at $T = 0$. The left hand panel shows the asymptotic nature of the mechanical entanglement.

regime, we find that the entanglement acquires the same period of modulation (see the right hand panel of Fig. 4.2). Hence one can identify the degree of the entanglement as the maximum over one period $\tau = 2\pi/\Omega$ of modulation, defined as follows [123]:

$$E_N = \max_{t \in [\mathcal{T}, \mathcal{T}+\tau]} E_N(t), \tag{4.13}$$

after a long enough time $\mathcal{T} \gg 1/\kappa, 1/\gamma_m$. It is worth mentioning that, with the application of periodically modulated mechanical coupling, $\lambda_0/\omega_m = 0.005$ we obtain a remarkable degree of stationary entanglement, $E_N = 0.34$, as opposed to $E_N = 0.04$, which is achieved with no direct mechanical coupling.

The dependence of the stationary mechanical entanglement on the oscillator temperature is exhibited in Fig. 4.3. As expected, it could be seen that the degree of entanglement decreases monotonically with increase in temperature T. However, one should note the improved robustness for the same mechanical entanglement with an increase in the coupling strength λ_0. For example, it is shown that in presence of the mechanical coupling $\lambda_0/\omega_m = 0.005$, the degree of entanglement survives up to a relatively high temperature $T/T_0 \approx 0.9$, in sharp contrast to the case where entanglement is found to persist upto temperature $T/T_0 \approx 0.3$ in absence of the mechanical coupling.

Next, in Fig. 4.4(a), we once again depict the time evolution of E_N, similar to Fig. 4.2 but with a set of higher values of λ_0/ω_m. Now one could observe that, with increase in λ_0, the entanglement not only grows much faster in time but also decays

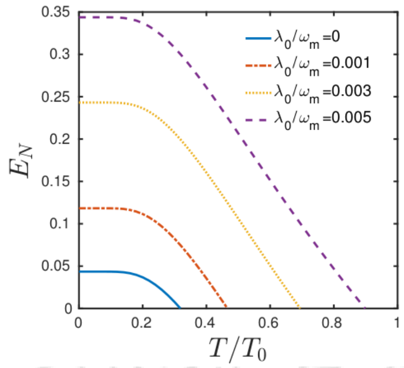

Figure 4.3: Dependence of stationary mechanical entanglement on the oscillator temperature for $\lambda_0/\omega_m = [0, 0.005]$ (from bottom to top). The other parameters are fixed as Fig. 4.2.

quickly to zero. Thus, it is evident that depending on the strength of the mechanical coupling, one could achieve a completely different dynamical behaviour of the mechanical entanglement. In order to investigate the role of oscillator temperature on the entanglement dynamics, we have redone the calculations for $T = 3T_0$ and depicted it in Fig. 4.4(b). It exhibits that with the increase in temperature, E_N decreases and there is a delay in the entanglement formation as well as reduction in survival time for entanglement, compared with its $T = 0$ counterpart. It should be noted that this feature is also reported in Ref. [127]. However, if one compares Fig. 4.3 and Fig. 4.4(b), it is clear that a significant degree of entanglement could be attained at a relatively high temperature, with higher mechanical coupling strength.

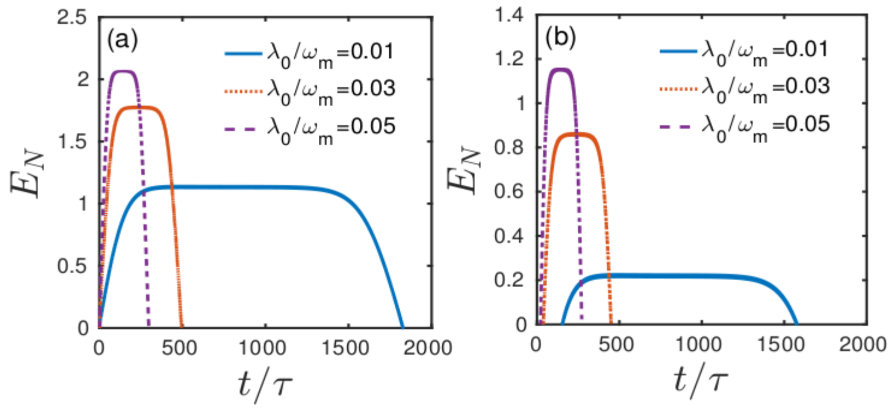

Figure 4.4: (Color online) Entanglement dynamics of the two coupled mechanical oscillators for $\lambda_0/\omega_m = [0.01, 0.05]$ (from bottom to top) at (a) $T/T_0 = 0$ and (b) $T/T_0 = 3$. The other parameters are fixed as Fig. 4.2.

Now, to further probe into the entanglement dynamics and the role of the mechanical coupling on it, we introduce the normal modes for the mechanical oscillators as follows: $\delta q_\pm = (\delta q_1 \pm \delta q_2)/\sqrt{2}$, $\delta p_\pm = (\delta p_1 \pm \delta p_2)/\sqrt{2}$, and, rewrite the linearized optomechanical Hamiltonian in the following way:

$$H^{\text{lin}} = H_+ + H_-, \tag{4.14}$$

where, $H_\pm$ is given by

$$\begin{aligned} H_+ &= \frac{\Delta}{2}\left(\delta X^2 + \delta Y^2\right) + \frac{1}{2}\left(\omega_m \delta p_+^2 + (\omega_m + \lambda(t))\,\delta q_+^2\right) & \text{(4.15a)} \\ &\quad - \sqrt{2}\left(G_x \delta X + G_y \delta G_y\right)\delta q_+, \\ H_- &= \frac{1}{2}\left(\omega_m \delta p_-^2 + (\omega_m - \lambda(t))\,\delta q_-^2\right). & \text{(4.15b)} \end{aligned}$$

The above Hamiltonian Eq. (4.14) describes two independent parametric oscillators, one of which ("+" mode) is coupled to the cavity field via the usual optomechanical interaction, while the other ("−" mode) one is completely free. Following a similar procedure, used to obtain Eq. (4.11), we construct the correlation matrix corresponding to the normal modes and the cavity field.

In order to illustrate the dynamics of the normal modes in the so-called phase-space, in Figs. 4.5 and 4.6 we depict the respective Wigner functions (Eq. (2.4)) at some specific times, for two different mechanical coupling strengths $\lambda_0/\omega_m = 0.005$ and $\lambda_0/\omega_m = 0.01$. We note that the value of the coupling strengths are so chosen to yield two different kinds of entanglement dynamics. The localization of the Wigner function in phase space, for "+" mode, could be clearly seen in Fig. 4.5(a)-(c) and 4.6(a)-(c), and, this localization is independent of the mechanical coupling strengths. On the contrary, the "−" mode exhibits both the localization and delocalization phenomena depending on the strength of the mechanical coupling. Fig. 4.5(d)-(f) show localization of the "−" mode when we have, $\lambda_0/\omega_m = 0.005$, which is maintained even for a sufficiently long time $t/\tau = 5000$. However, as could be seen from Fig. 4.6(d)-(f), with increase in λ_0/ω_m, the delocalization occurs quickly in time: The Wigner function stretches along the dynamical rotating axis along with a contraction in the perpendicular direction. This feature becomes quite prominent if one observe the dynamics at a time $t/\tau = 300.45$. This clearly signifies a dynamical instability corresponding to the "−" mode. Therefore, we can infer that the asymptotic nature of the mechanical entanglement is directly related to the instability in the "−" mode.

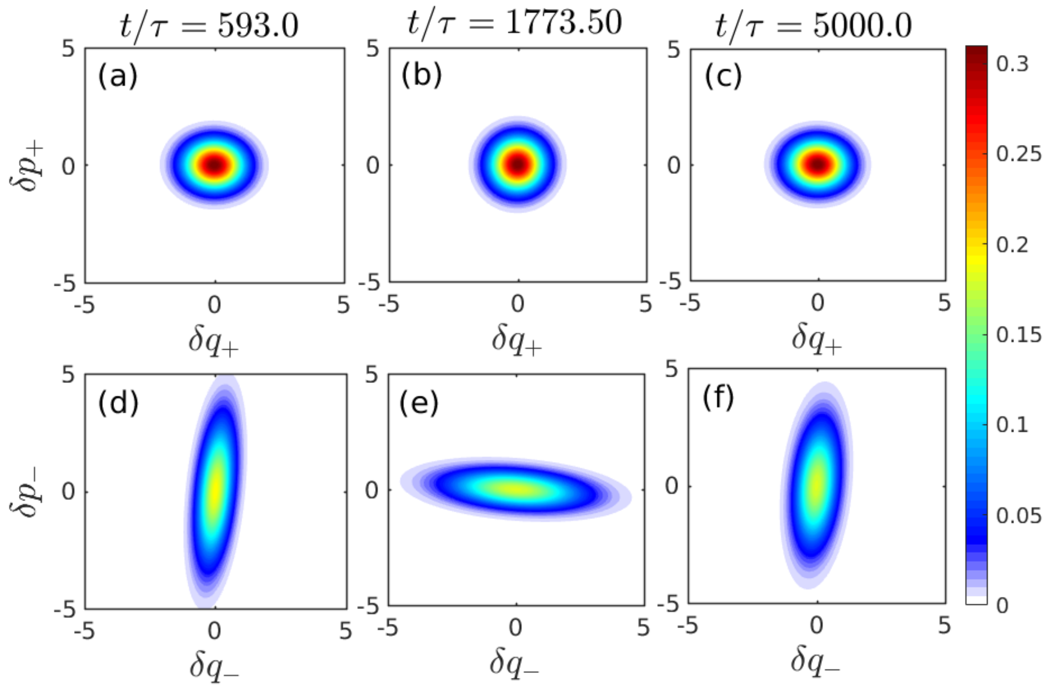

Figure 4.5: The wigner function for "+" and "−" mode at differetnt times, for the mechanical coupling stregth $\lambda_0/\omega_m = 0.005$.

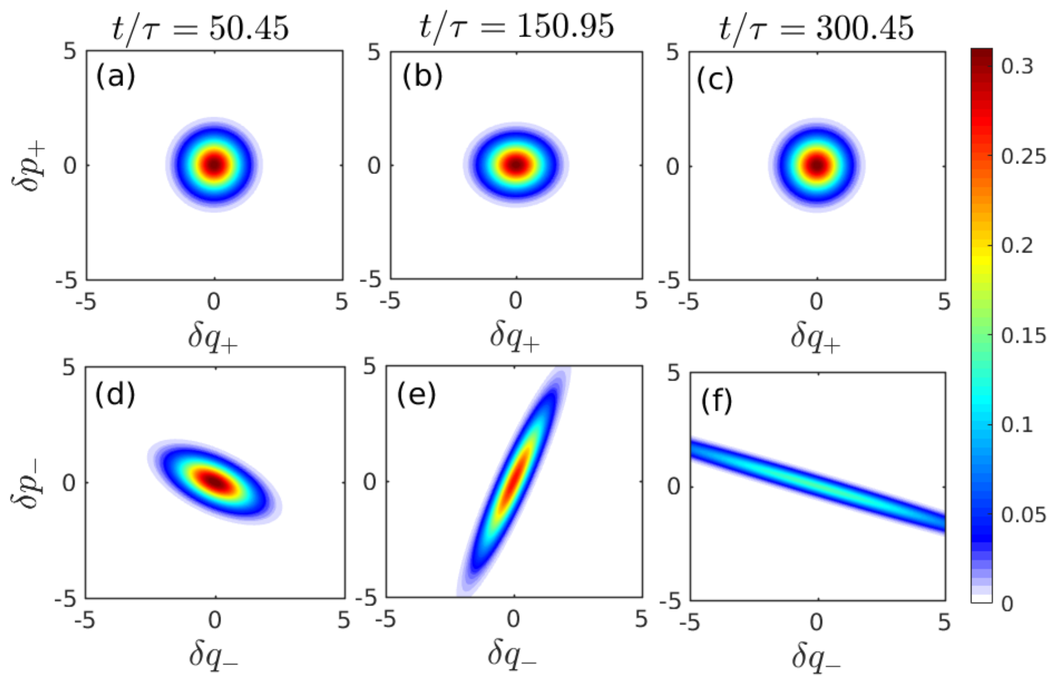

Figure 4.6: The wigner function for "+" and "−" mode at differetnt times, for the mechanical coupling strength $\lambda_0/\omega_m = 0.01$.

Now, to explicitly derive the relationship between the entanglement dynamics and the strength of the mechanical coupling, we focus on the stability of the "−" mode. Starting form the Hamiltonian Eq. (4.15b), we derive the equation of motion corresponding to the "−" mode, as given below:

$$\ddot{\delta q}_- + \left(\omega_m^2 - \omega_m \lambda_0 \cos \Omega t\right) \delta q_- + \gamma_m \dot{\delta q}_- = 0. \tag{4.16}$$

The above equation corresponds to a dissipative classical parametric oscillator, with a time modulated mechanical frequency $\omega_m^2(t) = \omega_m^2 - \omega_m \lambda_0 \cos(\Omega t)$. Following a substitution $\tilde{t} = \frac{\Omega t}{2}$, we can rewrite the Eq. (4.16), in the following form:

$$\ddot{\delta q}_- + \left(\tilde{\omega}_m - 2\tilde{\lambda}_0 \cos 2\tilde{t}\right) \delta q_- + \tilde{\gamma}_m \dot{\delta q}_- = 0, \tag{4.17}$$

where the dimensionless parameters are defined as follows:

$$\tilde{\omega}_m = \frac{4\omega_m^2}{\Omega^2},\ \tilde{\lambda}_0 = \frac{2\omega_m \lambda_0}{\Omega_2},\ \tilde{\gamma}_m = \frac{2\gamma_m}{\Omega}. \tag{4.18}$$

Now, defining $\delta q_- = \tilde{\delta q}_- e^{-\tilde{\gamma}_m \tilde{t}/2}$ and substituting in Eq. (4.17), we get the standard form of the canonical Mathieu equation

$$\ddot{\tilde{\delta q}}_- + \left(\delta - 2\epsilon \cos(2\tilde{t})\right) \tilde{\delta q}_- = 0, \tag{4.19}$$

where δ and ϵ are respectively given by $\delta = \frac{4\omega_m^2 - \gamma_m^2}{\Omega^2}$ and $\epsilon = \frac{2\omega_m \lambda_0}{\Omega^2}$. It is clear that, for a modulation frequency $\Omega^2 \approx 4\omega_m^2$, we have $\delta \approx 1$ and $\epsilon \ll 1$. In this limit, one can neglect all the higher-order terms in the eigenvalues of the Mathieu's equation Eq. (4.19) (see Appendix B. for a better discussion) and obtain:

$$\alpha_1(\epsilon) \approx 1 + \epsilon, \tag{4.20a}$$

$$\beta_1(\epsilon) \approx 1 - \epsilon. \tag{4.20b}$$

The stability of the "−" mode in the ϵ-δ plane, is depicted in Fig. 4.7. One can observe that, for the "−" mode to be stable the following stability criteria must be satisfied:

$$\beta_1(\epsilon) = 1 - \epsilon \leq \delta \leq \alpha_1(\epsilon) = 1 + \epsilon. \tag{4.21}$$

Solving Eq. (4.21) in terms of the Ω, ω_m and γ_m, we can obtain an analytical expression for the critical mechanical coupling strength λ_{0c}, given as follows:

$$\frac{\lambda_0}{\omega_m} \leq \frac{\lambda_{0c}}{\omega_m} = \frac{\Omega^2 - 4\omega_m^2 + \gamma_m^2}{2\omega_m^2}. \tag{4.22}$$

It should be noted that for the modulation frequency $\Omega_m = 2.003\omega_m$, one gets the following critical mechanical coupling strength $\lambda_{0c}/\omega_m = 0.006$. This situation is further illustrated in Fig. 4.7, respectively, for the three distinct mechanical coupling strengths $\lambda_0/\omega_m = 0.005$ (green circle), $\lambda_0/\omega_m = 0.006$ (blue diamond), and $\lambda_0/\omega_m = 0.007$ (red square). We can see that the points corresponding to the aforementioned coupling strengths, respectively, locate in the stable, on the boundary and in the unstable zone of the "−" mode. This well justifies our previously obtained entanglement dynamics, corresponding to the different sets of the mechanical coupling strengths.

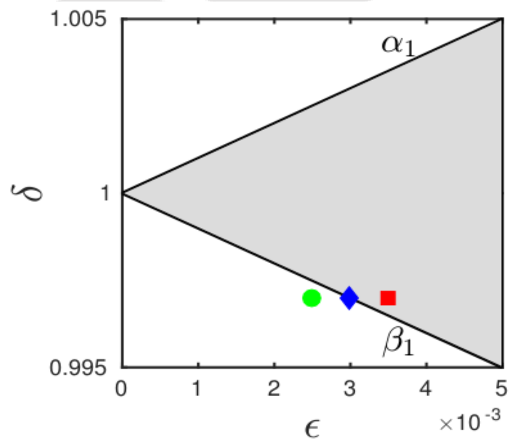

Figure 4.7: Stable (white) and unstable (grey) phase of the "−" mode, for $\epsilon \ll 1$. Here, the circle (green), diamond (blue) and square (red) respectively corresponds to the $\lambda_0/\omega_m = 0.005, 0.006$ and 0.007.

Finally, in Fig. 4.8 we depict the dependence of the stationary mechanical entanglement on the modulation frequency. It can be seen that the entanglement E_N is quite sensitive to the variation in the modulation frequency, which can be attributed directly to the instability in the "−" mode. Furthermore, one can observe that the peak of the stationary entanglement is obtained exactly at $\Omega/\omega_m = 2.003$, which justifies our initial choice of the modulation frequency.

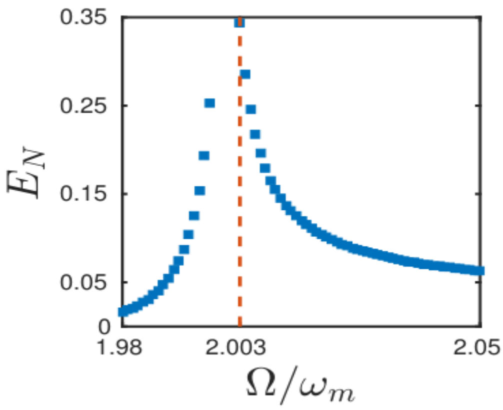

Figure 4.8: (Color online) Dependence of stationary mechanical entanglement E_N on the modulation frequency.

4.4 Conclusion

In conclusion, we have proposed a scheme to entangle two directly coupled mechanical oscillators, in an optomechanical system. Our scheme exploits the periodic modulation technique, in both the external driving and mechanical coupling strengths. We observe that an abrupt transition from stationary to dynamical mechanical entanglement occurs when the "−" mode becomes unstable. More importantly, it is shown that in the presence of the mechanical coupling, a significant improvement in the robustness of the generated entanglement could be achieved with respect to the oscillators temperature. Finally, based on the eigenvalues of the Mathieu's equations, we give an analytical estimations corresponding to the the critical mechanical coupling strength, where the transition occurs. The feasibility of the chosen parameters, makes our proposed scheme a promising mean to realize macroscopic quantum entanglement within current state-of-the-art experimental setups.

Chapter 5

Delayed sudden death of entanglement at exceptional points

Almost a decade ago, physicists encountered a strange quantum phenomenon that predicts an unusual death of entanglement, under the influence of local noisy environment. Known as entanglement sudden death (ESD), This could be an immediate stumbling block in realizing all the entanglement based quantum information and computation protocols. In this chapter, we propose a scheme to tackle such shortcomings by exploiting the phenomenon of exceptional points (EP). We consider binary and ternary mechanical $\mathcal{PT}$ symmetric architectures, realized over an optomechanical platform. We show that a substantial delay in ESD can be achieved in the $\mathcal{PT}$ symmetric binary system by pushing the system towards an exceptional point. This finding has been further extended to higher (third) order exceptional point by considering a more complicated tripartite entanglement into account.

5.1 Brief overview

$\mathcal{PT}$ symmetric quantum mechanics, as an extension of standard quantum theory into the complex domain, was introduced by Carl Bender and Stefan Boettcher in 1998. Followed by their seminal papers [142, 143], this whole new class of non-Hermitian Hamiltonians was established that could exhibit a spectrum of entirely real eigenvalues under the only restriction $[H, \mathcal{PT}] = 0$ [144]. Here, $\mathcal{P}$ refers to the parity operator that simply interchanges two of the constituent modes of the

The contents of this chapter are published in Subhadeep Chakaborty and Amarendra K. Sarma, Phys. Rev. A **100**, 063846 (2019).

system, while $\mathcal{T}$ is the time-reversal operator that takes $i \rightarrow -i$. A more striking feature of such Hamiltonians is the breaking of $\mathcal{PT}$ symmetry, in which the eigenspectra switches from being entirely real to completely imaginary. Such abrupt $\mathcal{PT}$ phase transition is marked by the presence of an exceptional point [145, 149] where two (or more) eigenvalues and their corresponding eigenvectors coalesce and become degenerate.

While the search for $\mathcal{PT}$ symmetric devices is on, it occurs that one can easily implement such notions by judiciously providing gain and loss to an optical system. This leads to a remarkable exploration of $\mathcal{PT}$ phase transitions in particular to photonic systems, such as optical waveguides [146–149], lattices and resonators [150–153]. Moreover, based on such realizations, the existence of EP has further triggered many exotic phenomena which include nonreciprocal light propagation [151], laser mode control [152–155], unidirectional invisibility [150, 156–158], optical sensing [159–161], light stopping [162] and structuring [163].

At this point, one must note that most of these studies explored so far are confined in the so-called classical regime, as the involved components are essentially macroscopic in nature. Therefore, any $\mathcal{PT}$ symmetric device whose dynamics is governed by an intrinsic quantum mechanical equation of motion would provide a better insight into this theory. Along this direction, researchers have a proposed few architectures that include cold atoms [164, 165], Bose-Einstein condensates [166], optomechanical devices [167–169], and recent circuit QED systems [170]. These quantum $\mathcal{PT}$ symmetric devices facilitate us to explore many intrinsic quantum properties, such as critical phenomena [171], entanglement [172], chiral population transfer [173, 174], decoherence dynamics [175], and, information retrieval and criticality [176]. However, the true quantumness of a $\mathcal{PT}$ symmetric device still remains questionable, as while dealing with such gain (amplifying) and cooling (dampening) mechanisms one often abandons the associated quantum noises which rather must exist to preserve the proper commutation relation. So far, $\mathcal{PT}$ symmetry including quantum noises has been attempted in a very few studies [177–180], which indicate a drastic difference from the usual (without considering quantum noises) predictions. Notably, in Ref. [181], it has been shown the continuous variable (CV) entanglement, generated in a system of two coupled waveguides is seriously affected owing to the presence of quantum noises. Recently, incorporating gain saturation, it is proposed to reduce the influence of quantum noise [182] on entanglement.

Entanglement [61], being a form of correlation that is inherent to quantum systems, has become an invaluable resource for futuristic quantum computation and communication protocols. However, for a real-world implementation of such schemes, the longevity of the available entanglement is what experimentalists mostly concerned about. As, it is now well understood that any unavoidable interaction with external environment brings noise to the system which is substantially detrimental to the generated entanglement. One of such destructive manifestations, is the entanglement sudden death (ESD) [183] where the system losses entanglement in finite time. This unfortunate fate of entanglement has been both theoretically predicted and experimentally verified in a wide variety of entangled pairs involving atoms [184], photons [185], spin chains [186] and continuous Gaussian states [187, 188]. Therefore, any manipulation that either avoids or delays ESD will help in executing various quantum information processing (QIP) protocols, that would otherwise be spoiled by the short entanglement lifetime. To overcome such shortcomings, a number of distinctive proposals have been put forward, such as quantum error correction [189, 190], local unitary operation [191, 192] dynamical decoupling [193, 194], decoherence free subspace [195, 196], the quantum Zeno effect [197, 198], delayed choice of decoherence suppression [199], and quantum measurement reversal [200–202].

In this chapter, we investigate such phenomenon of death of entanglement under the $\mathcal{PT}$ symmetric scenario. To the best of our knowledge, entanglement in $\mathcal{PT}$ symmetric geometries has been mostly dealt with optical binary systems, around the canonical $\mathcal{PT}$ phase transition point (EP). Therefore, it is intriguing ask: what happens to the entanglement evolution if one goes beyond the standard bipartite model to a more involved multipartite configuration, possessing higher-order exceptional point? To answer this question, we respectively consider a binary and a ternary mechanical $\mathcal{PT}$ symmetric system within an optomechanical setup. In order to engineer the mechanical gain/loss into the system, we exercise the similar approach [168, 203] of first tuning the cavity to the Stokes/Anti-Stokes sidebands, followed by an adiabatic elimination of the cavity field. However, unlike the previous reports, here we take the full quantum noises into account.

5.2 Cavity optomechanics based architecture to realize the gain (loss) in a mechanical system

In this section, we outline the derivation of the equations describing the effective dynamics of the mechanical resonator in the presence of optomechanically induced gain and loss. To begin with, we first consider a generic cavity optomechanical system [1], consisting of a single cavity mode of frequency ω_c and a mechanical mode of frequency ω_m. Following a rotating frame transformation at a (laser) frequency ω_l, the Hamiltonian of this system reads ($\hbar = 1$):

$$H = \Delta_0 a^\dagger a + \omega_m b^\dagger b - g a^\dagger a(b^\dagger + b) + E_0\left(a^\dagger + a\right), \tag{5.1}$$

where a ($a^\dagger$) and b ($b^\dagger$) are, respectively, the annihilation (creation) operators of the cavity field and the mechanical resonator. g is the strength of the single-photon optomechanical coupling, and, E_0 is the driving amplitude with $\Delta_0 = \omega_c - \omega_l$ being the cavity detuning. Taking the fluctuation-dissipation processes into account, the dynamics of the system is then fully described by the following set of nonlinear quantum Langevin equations (QLEs),

$$\dot{a} = -(i\Delta_0 + \kappa/2)a + iga(b^\dagger + b) - iE_0 + \sqrt{\kappa}a^{in}, \tag{5.2a}$$
$$\dot{b} = -(i\omega_m + \gamma/2)b + iga^\dagger a + \sqrt{\gamma}b^{in}. \tag{5.2b}$$

Here κ (γ) is the cavity decay (mechanical damping) rate. a^{in} is the zero-mean vacuum input noise operator, satisfying the only non-zero correlation function: $\langle a_{in}(t)a^\dagger_{in}(t')\rangle = \delta(t-t')$, and b^{in} refers to the random Brownian noise operator, with zero-mean value and Markovian correlation functions [41], given by: $\langle b^{in^\dagger}(t)b^{in}(t')\rangle = n_{th}\delta(t-t')$, $\langle b^{in}(t)b^{in^\dagger}(t')\rangle = (n_{th}+1)\delta(t-t')$. The parameter $n_{th} = \left[\exp\left(\frac{\hbar\omega_m}{k_B T}\right) - 1\right]^{-1}$ denotes the mean thermal phonon number at temperature T (k_B being the Boltzmann constant).

For a strongly driven cavity, we now adopt the standard linearization technique and expand each operators as a sum of its c-number classical steady-state value plus a time-dependent zero-mean quantum fluctuation operator, i.e., $a(t) \to \alpha + a(t)$ and $b(t) \to \beta + b(t)$. These steady states values could then be obtained by solving the following nonlinear algebraic equations:

$$(i\Delta + \kappa/2)\alpha + iE_0 = 0, \tag{5.3a}$$
$$(i\omega_m + \gamma_m/2)\beta - ig|\alpha|^2 = 0, \tag{5.3b}$$

where $\Delta = \Delta_0 - 2g\mathrm{Re}(\beta)$ is the effective cavity detuning. On the other hand, the dynamics of the quantum fluctuations are given by the linearized QLEs (valid in the limit of $|\alpha| \gg 1$), written as:

$$\dot{a} = -(i\Delta + \kappa/2)a + iG(b^\dagger + b) + \sqrt{\kappa}a^{in}, \tag{5.4a}$$
$$\dot{b} = -(i\omega_m + \gamma/2)b + iG(a^\dagger + a) + \sqrt{\gamma}b^{in}, \tag{5.4b}$$

with $G = g|\alpha|$ being the effective many-photon optomechanical coupling strength.

Next, we introduce two slowly varying operators: $\tilde{a} = ae^{i\Delta t}$ and $\tilde{b} = be^{i\omega_m t}$, and, rewrite Eq. (5.4) in the following way:

$$\dot{\tilde{a}} = -\frac{\kappa}{2}\tilde{a} + iG\left(\tilde{b}^\dagger e^{i(\Delta+\omega_m)t} + \tilde{b}e^{i(\Delta-\omega_m)t}\right) + \sqrt{\kappa}\tilde{a}^{in}, \tag{5.5a}$$
$$\dot{\tilde{b}} = -\frac{\gamma}{2}\tilde{b} + iG\left(\tilde{a}^\dagger e^{i(\omega_m+\Delta)t} + \tilde{a}e^{i(\omega_m-\Delta)t}\right) + \sqrt{\gamma}\tilde{b}^{in}. \tag{5.5b}$$

Note that in the above equations, we have also defined the new noise operators $\tilde{a}^{in} = a^{in}e^{i\Delta t}$ and $\tilde{b}^{in} = b^{in}e^{i\omega_m t}$ which possess the same correlation functions.

We now proceed to discuss how to realize gain (damping) in the mechanical resonator, in a pure quantum mechanical way. To do so, we first assume that the cavity is resonant with the Stokes sideband of the driving laser, $\Delta = -\omega_m$, and invoke the rotating wave approximation (RWA) (which is justified in the limit of $\omega_m \gg \{G, \kappa, \gamma\}$) to obtain:

$$\dot{\tilde{a}} = -\frac{\kappa}{2}\tilde{a} + iG\tilde{b}^\dagger + \sqrt{\kappa}\tilde{a}^{in}, \tag{5.6a}$$
$$\dot{\tilde{b}} = -\frac{\gamma_m}{2}\tilde{b} + iG\tilde{a}^\dagger + \sqrt{\gamma}\tilde{b}^{in}. \tag{5.6b}$$

Under the condition that the cavity decay rate is much larger than the effective optomechanical coupling strength, $\kappa \gg \{G, \gamma_m\}$, one can adiabatically eliminate the cavity field and gets

$$\tilde{a} = i\frac{2G}{\kappa}\tilde{b}^\dagger + \frac{2}{\sqrt{\kappa}}\tilde{a}^{in}. \tag{5.7}$$

Following a substitution of Eq. (5.7) in Eq. (5.6b), we end up with the following equation describing effective the dynamics of the mechanical resonator:

$$\dot{\tilde{b}} = \left(\frac{\Gamma}{2} - \frac{\gamma}{2}\right)\tilde{b} + i\sqrt{\Gamma}\tilde{a}^{in^\dagger} + \sqrt{\gamma}\tilde{b}^{in}. \tag{5.8}$$

Here, one should note the inclusion of the following two terms: $\Gamma = \frac{4G^2}{\kappa}$ which quantifies the amount of optomechanically induced gain in the mechanical resonator, and, the cavity induced noise term $\sqrt{\Gamma}a^{in^\dagger}$ which helps to preserve the right commutation relation.

On the other hand, when the cavity is resonant with the Anti-Stoke sideband of the driving laser, $\Delta = \omega_m$, following a similar procedure, one obtains:

$$\dot{\tilde{b}} = -\left(\frac{\Gamma}{2} + \frac{\gamma}{2}\right)\tilde{b} + i\sqrt{\Gamma}\tilde{a}^{in} + \sqrt{\gamma}\tilde{b}^{in}, \tag{5.9}$$

where the same $\Gamma = \frac{4G^2}{\kappa}$ corresponds to the optomechanically induced loss in the mechanical resonator.

The physics behind optomechanically induced gain/loss could perhaps be understood in the following manner. Let us first assume that the cavity is detuned to the Stokes sideband, i.e., $\Delta = -\omega_m$. Here, following the RWA, one can easily infer that the interaction Hamiltonian is of the form, $H_I = -G\left(a^\dagger b^\dagger + ab\right)$ (see Eq. (5.6)). Such an interaction leads to a transition of any arbitrary state $|m, n\rangle$ (m, n represents the photon and phonon numbers respectively) to $|m+1, n+1\rangle$. Further, when subjected to a strong optical dissipation, this state $|m+1, n+1\rangle$ irreversibly looses a single photon and becomes $|m, n+1\rangle$. After eliminating the cavity filed, this whole process is now equivalent to a transition from $|n\rangle$ to $|n+1\rangle$, with an effective gain rate Γ. On the other hand, when the cavity is detuned to the Anti-Stoke sideband, i.e., $\Delta = \omega_m$, one ends up with an interaction of the form, $H_I = -G\left(a^\dagger b + ab^\dagger\right)$. This interaction couples a state $|m, n\rangle$ to $|m+1, n-1\rangle$. Then, following an elimination of the cavity field, one eventually gets a transition from $|n\rangle$ to $|n-1\rangle$, with a same damping rate Γ.

5.3 Entanglement in $\mathcal{PT}$ symmetric binary systems

We now couple two such identical mechanical resonators, each characterized by a frequency (damping rate) ω_m (γ_m), via a mechanical coupling of strength J. A schematic of such mechanical $\mathcal{PT}$ symmetric system and its optomechanical realization have been illustrated, respectively, in Fig. 5.1(a) and Fig 5.1(b). Then, following the prescription as derived in Sec. 5.2, one can write the effective dynamical equations corresponding to each mechanical resonators, as follows:

$$\dot{b_1} = \left(\frac{\Gamma}{2} - \frac{\gamma}{2}\right) b_1 + iJb_2 + i\sqrt{\Gamma}a_1^{in^\dagger} + \sqrt{\gamma}b_1^{in}, \tag{5.10a}$$

$$\dot{b_2} = -\left(\frac{\Gamma}{2} + \frac{\gamma}{2}\right) b_2 + iJb_1 + i\sqrt{\Gamma}a_2^{in} + \sqrt{\gamma}b_2^{in}. \tag{5.10b}$$

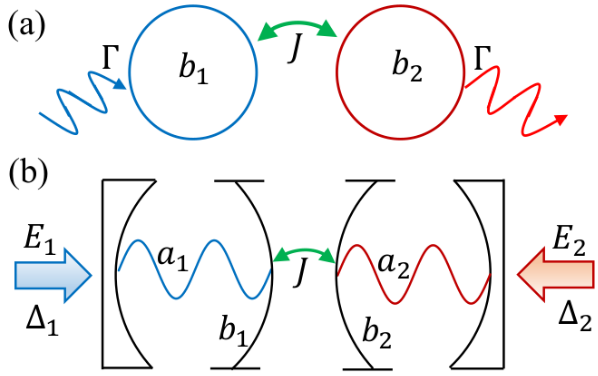

Figure 5.1: (a) Schematic diagram of binary mechanical $\mathcal{PT}$ symmetric resonators, with optomechanically induced gain-loss. (b) Scheme for engineering mechanical gain/loss in an optomechanical platform. Here, two optomechanical cavities, respectively, driven at Stokes and Anti-Stokes of the driving lasers, are coupled mutually via a mechanical interaction.

Here, b_1, b_2 ($b_1^\dagger, b_2^\dagger$) be the annihilation (creation) operators of the gain and the lossy resonators, respectively. Γ is the effective optomechanically induced gain/loss rate. Notably, here the interaction Hamiltonian between these two mechanical resonators is assumed to be $H_{int} = -J(b_1^\dagger b_2 + b_1 b_2^\dagger)$. Such an interaction could be generated from the common X-X type interactions as achieved in Refs [204, 205] under a RWA. The remaining parameters a_j^{in} and b_j^{in} ($j = 1, 2$), respectively, corresponds to the vacuum input noises, acting on the cavity fields and the mechanical resonators. In the parameter regime, where the effective optomechanical coupling is strong enough, one can further discard the intrinsic mechanical damping as $\Gamma \gg \gamma$. However, to simulate the actual physical condition, we retain a finite damping $\gamma > 0$ throughout our calculations.

By ignoring the quantum noises, one can recast the above equation as $\dot{u}(t) = -iH_2 u(t)$. Here, $u^T(t) = (q_1(t), p_1(t), q_2(t), p_2(t))$ is the state vector, written in terms of the dimensionless CV quadrature operators $q_j \equiv \left(b_j + b_j^\dagger\right)/\sqrt{2}$ and $p_j \equiv \left(b_j - b_j^\dagger\right)/i\sqrt{2}$ (with $j = 1, 2$), while H_2 be the non-Hermitian Hamiltonian, given by

$$H_2 = i \begin{pmatrix} \frac{\Gamma}{2} & 0 & 0 & -J \\ 0 & \frac{\Gamma}{2} & J & 0 \\ 0 & -J & -\frac{\Gamma}{2} & 0 \\ J & 0 & 0 & -\frac{\Gamma}{2} \end{pmatrix}. \tag{5.11}$$

One can then easily verify that under the simultaneous $\mathcal{PT}$ operation, the Hamil-

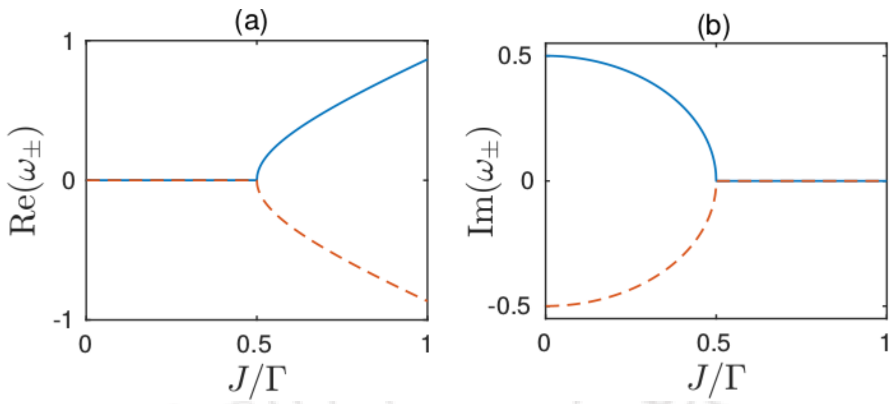

Figure 5.2: (a) The real, and, (b) the imaginary parts of $\omega_\pm$ *vs.* the normalized coupling coefficient J/Γ. The system exhibits an exceptional point (of order 2) at $J = \frac{\Gamma}{2}$.

tonian remains invariant, i.e., $[\mathcal{PT}, H_2] = 0$.

Now, in order to study the $\mathcal{PT}$ phase transition, we first diagonalize the Hamiltonian and find the eigenfrequencies:

$$\omega_\pm = \pm\sqrt{J^2 - \left(\frac{\Gamma}{2}\right)^2}, \tag{5.12}$$

It is evident that respectively for $J > \Gamma/2$ and $J < \Gamma/2$ there exist two distinct phases: one that includes all the real eigenvalues, namely a $\mathcal{PT}$ symmetric phase, while the other possesses purely imaginary eigenvalues, namely a broken $\mathcal{PT}$ symmetric phase. The critical coupling strength which separates these two phases is located at $J_{c_2} = \Gamma/2$. An exact situation can be found in Fig. 5.2, where we depict the eigenfrequencies as a function of the normalized coupling strength J/Γ. Also, we observe that this same J_{c_2} marks the exceptional point (of order 2) of this system where the two eigenvalues coalesce. It should be noted that in order to obtain a closed expression for the $\mathcal{PT}$ symmetric condition, we have not included the mechanical damping γ as justified by the fact, $\Gamma \gg \gamma$. However, in all our numerical calculations, we do consider a finite degree of mechanical damping γ.

Physically, the emergence of EP refers to the situation where the mechanical coupling rate J gets exactly balanced with the respective mechanical heating/cooling rates Γ. Then, for all $J > \frac{\Gamma}{2}$ there is an coherent exchange of energy between these two resonators which corresponds to the $\mathcal{PT}$ symmetric phase. However, as soon as the coupling becomes weak to support the energy exchange, i.e. for any $J < \frac{\Gamma}{2}$ there is an localization of energy in the the passive resonator which in turn leads to the breaking of the $\mathcal{PT}$ symmetry.

Next, we take the full quantum noises into the account and rewrite Eq. (5.10) in a more compact from: $\dot{u}(t) = Au(t) + n(t)$. Here, $u(t)$ be the same CV state vector, $A = -iH_2$ is the drift matrix, and, $n^T(t) = \left(\sqrt{\Gamma}Y_1^{in} + \sqrt{\gamma}Q_1^{in}, \sqrt{\Gamma}X_1^{in} + \sqrt{\gamma}P_1^{in}, \sqrt{\Gamma}Y_2^{in} + \sqrt{\gamma}Q_2^{in}, \sqrt{\Gamma}X_2^{in} + \sqrt{\gamma}P_2^{in}\right)$ is the matrix of corresponding noises. The input noise quadratures, as used in $n^T(t)$, are respectively defined as follows: $X_c^{in} \equiv \left(a_c^{in} + a_c^{in^\dagger}\right)/\sqrt{2}$, $Y_c^{in} \equiv \left(a_c^{in} - a_c^{in^\dagger}\right)/i\sqrt{2}$, and, $Q_c^{in} \equiv \left(b_c^{in} + b_c^{in^\dagger}\right)/\sqrt{2}, P_c^{in} \equiv \left(b_c^{in} - b_c^{in^\dagger}\right)/i\sqrt{2}$ where $c = 1, 2$. A stable solution of this equation requires all the eigenvalues with negative real parts. In what follows, we find that one can have such solutions only when the system remains in the $\mathcal{PT}$ symmetric phase.

We further note that owing to the above linearized dynamics and zero-mean Gaussian nature of the quantum noises, the system retains its Gaussian characteristics. In turn, one can adopt the standard covariance matrix (CM) formalism to fully describe the system [42]. Let $V(t)$ be the CM with each elements defined as $V_{ij}(t) = \langle u_i(t)u_j(t) + u_j(t)u_i(t)\rangle/2$. Then, one has the following equation of motion as satisfied by the CM

$$\dot{V}(t) = AV(t) + V(t)A^T + D. \tag{5.13}$$

Here, $D = \left(\frac{\Gamma}{2} + \gamma\left(n_{th} + \frac{1}{2}\right)\right) \mathrm{diag}\,(1, 1, 1, 1)$ is the matrix of the noise correlations, obtained under the Markovian assumption and $\langle n_i(t)n_j(t') + n_j(t')n_i(t)\rangle/2 = \delta\,(t-t')\,D_{ij}$.

The above Eq. (5.13) is an inhomogeneous first order differential equation which can be solved numerically with a proper initial condition. As studying the quantum correlation is of our prime concern, here, we consider this input state to be a generic CV entangled state, i.e., a two mode squeezed state $|z\rangle = e^{r\left(b_1^\dagger b_2^\dagger - b_1 b_2\right)}|0, 0\rangle$ with r being the squeezing parameter. Here, one may look into various striking proposals for entanglement generation using optomechanical setups in Ref. [139–141].

In Fig. 5.3(a) we first show the time evolution of the quantum entanglement (2.14) in the absence of any noises. One can see that when the system is in the $\mathcal{PT}$ symmetric phase, the entanglement oscillates periodically. This oscillations could be attributed to the nature of the eigenvalues $\pm i\sqrt{J^2 - J_{c_2}^2}$ of A, as obtained for $J > J_{c_2}$. However, as we approach the EP, we notice a lesser oscillation with a longer time period. Finally, in the close vicinity of EP ($J \to J_{c_2}$), the entanglement dynamics almost "freezes out", i.e., it takes a longer time to complete one oscillation. In Fig. 5.3(b), we show the same entanglement evolution, but, now taking the quantum noises taking into the account. One can see that as soon as noise is introduced into the system, the entanglement quickly decays to zero, a typical ESD like behavior. However, a more notable feature of this figure is the delayed death of entanglement, as achieved via pushing the system towards the exceptional point (EP).

To further support this conclusion, in Fig. 5.4 we compare the two-mode Wigner functions (2.4) for two different coupling strengths, at two different times. One can see that at $\Gamma t = 0.5$ both these $W(q_1, q_2)^{p_1=0}_{p_2=0}$ exhibit a squeezing like behavior which is sufficient to ensure the presence of entanglement between these two-modes. However, at a subsequent time $\Gamma t = 0.75$, one finds the $W(q_1, q_2)^{p_1=0}_{p_2=0}$ corresponding $J = \Gamma$ almost losses its squeezing characteristic, while the other still retains it with a finite degree. Moreover, it is also important to note that for both these coupling strengths the Wigner functions remain localized in the phase-space, i.e., there is no abrupt stretching associated with $W(q_1, q_2)^{p_1=0}_{p_2=0}$ that could push the system towards instability.

5.4 Entanglement in $\mathcal{PT}$ symmetric ternary systems

Motivated by these results, we now extend this same strategy to the higher-order exceptional points. A possible realization that supports a EP3 (exceptional point of order 3) would be a ternary mechanical system where the gain and lossy resonators are being separated by a neutral one (see Fig. 5.5). Then, proceeding in a similar manner, one can write the following equation of motion, as satisfied by the each

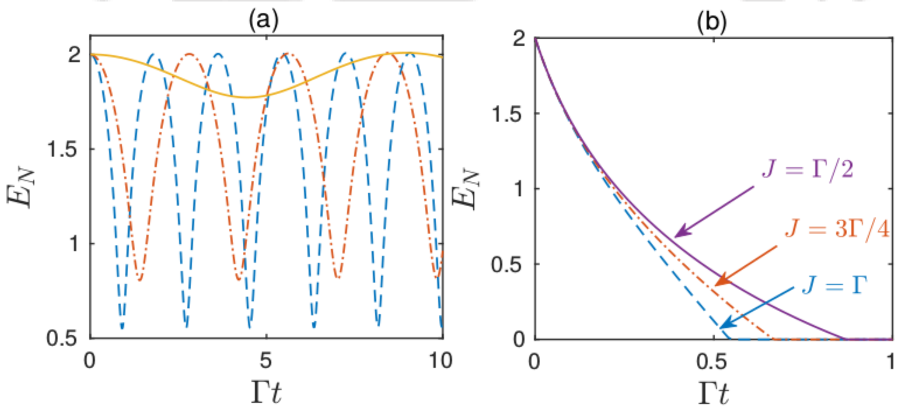

Figure 5.3: Entanglement evolution between the gain-loss resonators, (a) in the absence and (b) in the presence of noises. The parameters used are $\Gamma = 1$ and $\gamma = 10^{-3}$. In panel (a) the blue (dashed), red (dash-dotted) and yellow (solid) lines respectively corresponds to the $J = \Gamma$, $J = 0.75\Gamma$ and $J = 0.53\Gamma$.

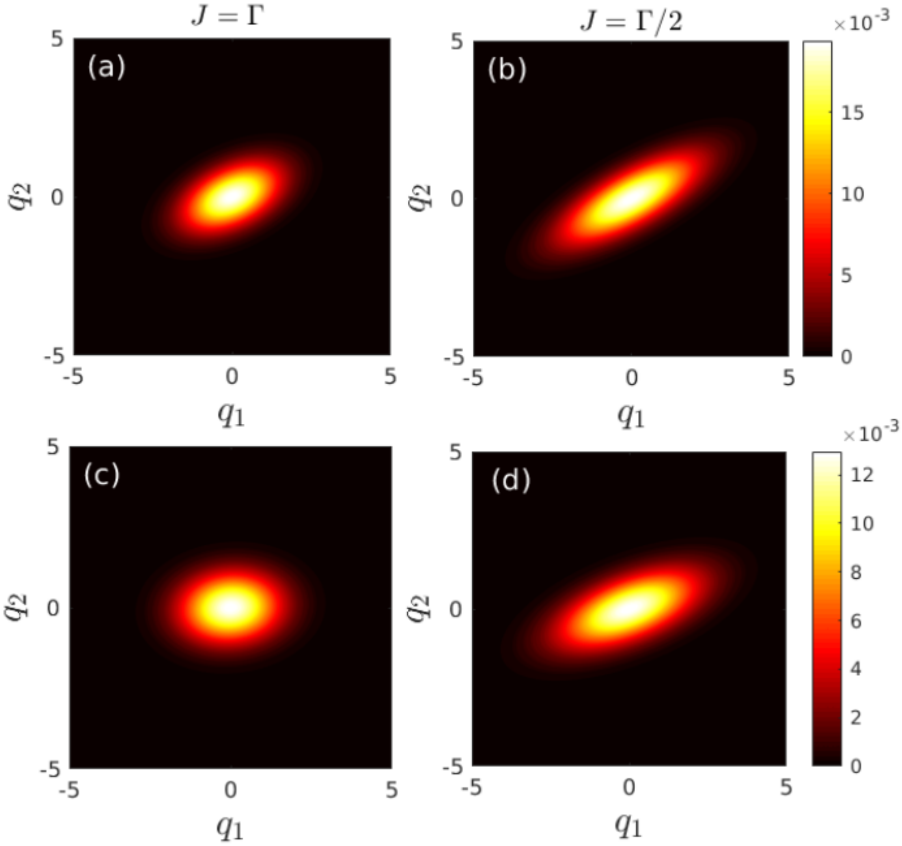

Figure 5.4: Time evolution of Wigner functions $W(q_1, q_2)^{p_1=0}_{p_2=0}$, respectively, at $\Gamma t = 0.5$ (upper two panels), and $\Gamma t = 0.75$ (bottom two panels).

mechanical resonators

$$\dot{b_1} = \left(\frac{\Gamma}{2} - \frac{\gamma}{2}\right) b_1 + iJb_2 + i\sqrt{\Gamma} a_1^{in\dagger} + \sqrt{\gamma} b_1^{in}, \tag{5.14a}$$

$$\dot{b_2} = -\frac{\gamma}{2} b_2 + iJb_1 + iJb_3 + \sqrt{\gamma} b_2^{in}, \tag{5.14b}$$

$$\dot{b_3} = -\left(\frac{\Gamma}{2} + \frac{\gamma}{2}\right) b_3 + iJb_2 + i\sqrt{\Gamma} a_2^{in} + \sqrt{\gamma} b_3^{in}. \tag{5.14c}$$

Here, b_1, b_2, b_3 $(b_1^\dagger, b_2^\dagger, b_3^\dagger)$, refer to the annihilation (creation) operators of the gain, neutral and lossy resonators, respectively, while the other parameters remain unchanged with the previous descriptions. Then in the absence of any noises, one can have the following cubic algebraic equation as obeyed by each of these eigenfrequencies ω_n $(n \in \{-1, 0, 1\})$

$$\omega_n \left(\omega_n^2 + \frac{\Gamma^2}{4} - 2J^2\right) = 0. \tag{5.15}$$

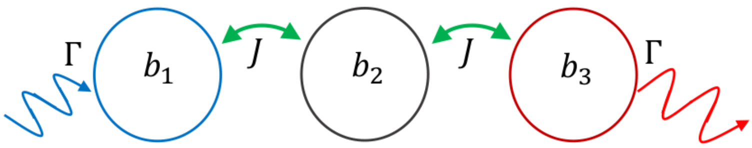

Figure 5.5: Schematic illustration of $\mathcal{PT}$ symmetric ternary mechanical setup. Here, the side resonators are subjected to equivalent gain and loss, while the middle one is neutral.

It is evident that for a critical coupling strength $J_{c_3} = \frac{\Gamma}{2\sqrt{2}}$, all the three eigenfrequencies merge at $\omega_n = 0$. This characteristic feature of EP3 has been pictorially demonstrated in Fig. 5.6, where we show the dependence of the eigenfrequencies on the normalized coupling strength J/Γ.

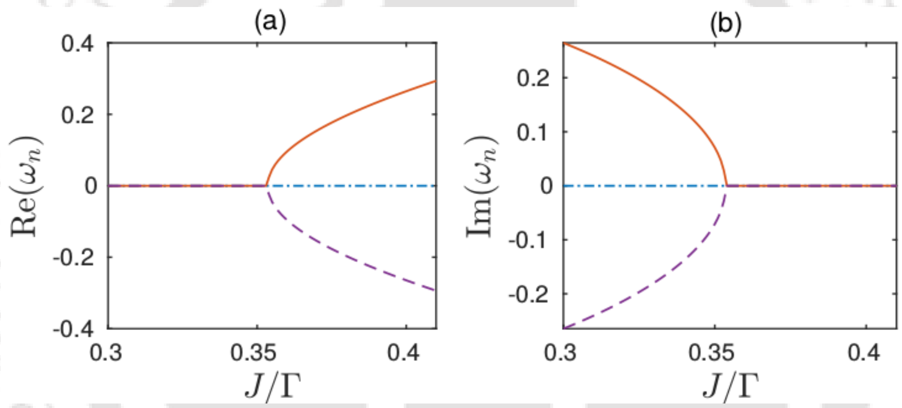

Figure 5.6: (a) The real and (b) the imaginary parts of ω_n as a function of the normalized coupling coefficient J/Γ. The three eigenfrequencies merge at $J = \frac{\Gamma}{2\sqrt{2}}$, exhibiting a third-order exceptional point

Now, to take this discussion further ahead, we consider the case of tripartite entanglement between theses three mechanical resonators, under the $\mathcal{PT}$ symmetric scenario. The measurement of such complicated multipartite entanglement goes as follows. Let us first define the following linear combinations of the quadrature variances:

$$x \equiv h_1 q_1 + h_2 q_2 + h_3 q_3, \tag{5.16a}$$

$$y \equiv g_1 p_1 + g_2 p_2 + g_3 p_3, \tag{5.16b}$$

where q_1, q_2, q_3 (p_1, p_2, p_3) be the position (momentum) operators of the gain, neutral and lossy resonators, respectively, while h_k and g_k are being any arbitrary real parameters. Then, following the prescription as proposed in Refs. [206–208], we employ the nonseparability measurement

$$S = \langle(\Delta x)^2\rangle + \langle(\Delta y)^2\rangle. \tag{5.17}$$

The three-party state is then said to be *genuinely tripartite entangled* iff it negates the following single inequality

$$\begin{aligned} S \quad & \geq \min\{|h_3 g_3| + |h_1 g_1 + h_2 g_2|, \\ & |h_2 g_2| + |h_1 g_1 + h_3 g_3|, |h_1 g_1| + |h_2 g_2 + h_3 g_3|\}, \end{aligned} \tag{5.18}$$

whereas, only the violation of any of theses inequalities

$$S \geq (|h_k g_k| + |h_l g_l + h_m g_m|)\,, \tag{5.19}$$

for a given permutation of $\{k, l, m\}$ of $\{1, 2, 3\}$, guarantees a *full tripartite inseparability*. These classes of nonseparabilities may sound equivalent, but as pointed out by Teh and Reid [207] they remain indistinguishable only for pure quantum states, while for mixed states meeting the full inseparability criteria does not suffice to claim multipartite entanglement.

In order to numerically evaluate the bounds of Eq. (5.18) and (5.19), we now consider the following set of the parameters $h_1 = g_1 = 1$ and $g_2 = g_3 = -h_2 = -h_3 = 1/\sqrt{2}$. The reason behind such particular combination is $\left[q_1 - (q_2 + q_3)/\sqrt{2},\right.$ $\left.p_1 + (p_2 + p_3)/\sqrt{2}\right] = 0$, which allows to have an arbitrary good degree of violation of Eq. (5.18). Then, one has to fulfill $S < 1$ to ensure the emergence of genuine tripartite entanglement, while $S < 2$ will suffice to confirm at least full tripartite inseparability.

Fig. 5.7 depicts the time evolution of S, starting from a CV GHZ state with the squeezing parameters r_1, r_2 being equal to 1 [206]. It is observed that, with the inclusion of quantum noise, the tripartite state quickly suffers a sudden death of (genuine tripartite) entanglement, followed by a fully tripartite inseparable state. However, it is remarkable to note that at EP3, such three-party state losses entanglement more slowly as compared to any other points in unbroken the $\mathcal{PT}$ symmetric phase. One may also notice that by operating near the EP3, it is possible to prolongate the time pertaining to a full tripartite inseparable state.

Finally, in Fig. 5.8 we examine the effect of thermal noise on the bipartite (Fig. 5.8(a)) and tripartite entanglement (Fig. 5.8(b)) evolution. As expected, the degradation of quantum entanglement with increasing thermal phonon is observed.

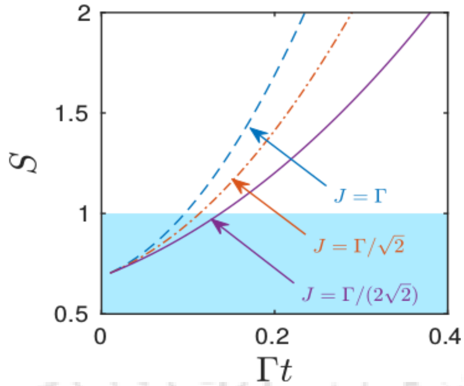

Figure 5.7: Time evolution of the nonseparability criteria S, for three different coupling strengths. The shaded area guarantees the presence of genuine tripartite entanglement. The parameters used are same with Fig. 5.3.

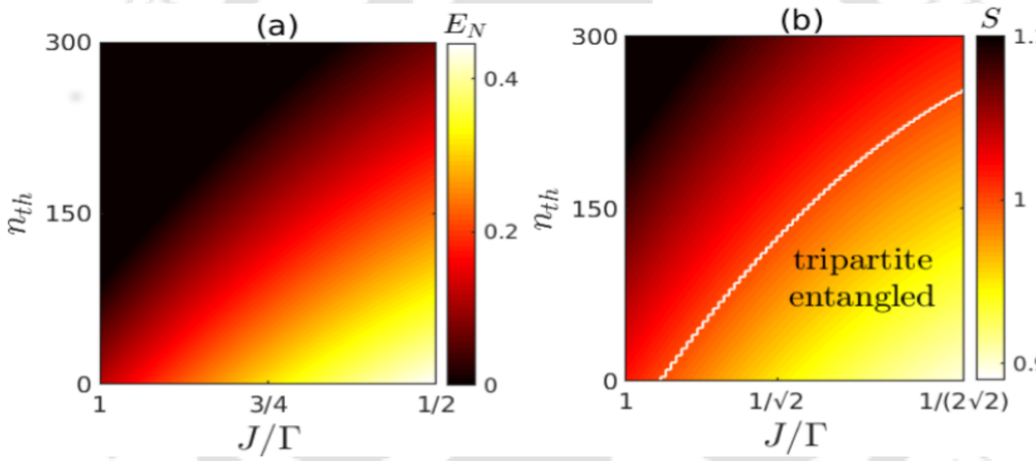

Figure 5.8: (a) Bipartite and (b) tripartite entanglement measures, as a function of the normalized coupling J/Γ and the number of thermal phonons n_{th}. The time corresponding to each snapshots are, respectively, (a) $\Gamma t = 0.5$ and (b) $\Gamma t = 0.1$. In Fig. 5.8(b), the white line separates between two distinct regimes of genuine tripartite entanglement and full tripartite inseparability.

However, it is worthwhile to note that, the available bipartite (tripartite) entanglement achieved in the close vicinity of the EPs (EP3) is fairly robust. This makes our proposed scheme a viable means to improve the entanglement sustainability with the aid of exceptional points. Also, it may be useful to note that, though we assume that the frequencies of both mechanical oscillators as well as their coupling rates to the cavity field are exactly the same, we find that slight deviations from these conditions do not change the overall conclusion of the obtained results. This makes the work experimentally relevant

5.5 Conclusion

In conclusion, we have performed a systematic study to unravel the relation between death of entanglement and the phenomenon of exceptional points. The architectures that we have specifically focused on, are essentially, binary and ternary mechanical $\mathcal{PT}$ symmetric systems with optomechanically induced gain-loss. Our study shows that a substantial delay in sudden death of entanglement is possible at exceptional points, respectively, of orders two and three. It is also shown that near the EPs, the available entanglement survives to a much higher degree of thermal phonons. These findings may pave the ways for exploiting $\mathcal{PT}$ symmetric devices as novel means to control the entanglement dynamics in different QIP protocols. It is also worthwhile to note that our approach could in principle, be applied in various photonic and phononic $\mathcal{PT}$ symmetric systems, with engineered gain-loss mechanisms. Further efforts along this directions include the investigation of quantum entanglement in the broken $\mathcal{PT}$ symmetric regime, where the effect gain saturation must be treated with care.

Chapter 6

Quantum synchronization and correlation in bidirectionally and unidirectionally coupled optomechanical oscillators

Spontaneous synchronization, in particular to the quantum domain, has been found to share a very strong connection with the onset quantum correlations. In this chapter, we explore such possibilities for the onset of quantum synchronization and the generation of quantum correlation in two optically coupled optomechanical oscillators. We show that Gaussian quantum discord, despite its strong connection with synchronization generation, fails to provide a conclusive map for quantum phase synchronization.

6.1 Brief overview

The phenomenon of synchronization essentially describes the ability of group of self-oscillators to spontaneously adjust their intrinsic rhythms, to oscillate in unison [209]. The very first observation of synchronization could be traced back to the earliest 17th century when Huygens described the antisynchronous motion in two maritime pendulum clocks [210]. Since then, synchronization has been commonly observed in wide varieties of physical, biological, chemical and social systems [211–216]. Spontaneous synchronization is also great technological importance, as it finds its applications in high precision clocks [217], sensing [218], information processing [219] and communications [220].

While the classical nonlinear dynamical systems stand as an excellent paradigm for synchronization, recently, there has been a quest to observe analogous phenomenon in quantum counterparts. Josephson junctions [221, 222], van der Pol (vdP) [223–225], Kerr-anharmonic oscillators [226], atomic ensembles [227], ions [228] and spin systems [229, 230] are to name a few of those quantum models where synchronization has been thoroughly observed. Optomechanical systems [231] is another such example, best suited to study synchronization in micro- and nano-mechanical oscillators. A key advantage of such systems is the ability to couple high frequency mechanical oscillators to one or more electromagnetic fields inside a resonant cavity. As this coupling is inherently nonlinear in nature, the resultant classical dynamics could undergo a limit-cycle oscillation, often referred to as optomechanical self-oscillation. The theoretical studies on optomechanical synchronization has initially been focused only on the classical realm of such self-oscillators, where Kuramoto model is a paradigmatic [232, 233]. Besides the theoretical investigations, synchronization has also been experimentally demonstrated, using optomechanical system with coupled micro-disks [234] and optical racetrack cavity with integrated mechanical oscillators [235]. Only recently, optomechanical array synchronization has been achieved, using seven such micro-disks oscillators sharing a common optical field.

Apart from these classically inspired investigations, there has been a growing interest to explore synchronization deep into the quantum regime. For instance, in particular to optomechanical systems, it has already been pointed out that quantum noise can give rise to an unsynchronous motion even for identical mechanical oscillators at different sites, under weak intercellular interaction [237]. Also, taking thermal noise into account, Ref [238]. predicts a quantum noise driven bistable regime in optomechanical synchronization. Remarkably, a proposal for producing stronger degree quantum synchronization by invoking a squeezing drive in quantum vDP oscillator is reported in Ref [239]. However, one must note that measuring quantum synchronization is still challenging enough and has been afforded in Refs. [228, 240]. Besides, there has been numerous efforts devoted to connect the onset of quantum synchronization and the generation of quantum correlations [225, 229, 241–243]. Notably, mutual information as a purely information-theoretic measure of quantum synchronization has been suggested in Ref. [244]. Very recently the connection between classical synchronization and persistent entanglement in aisolated quantum system has been demonstrated in Ref [245]. Although, arguably the most fascinating outcome of such quantum synchronizations would be the observation *synchronization blockade* where identical self-oscillator are peculiarly blocked for attaining maximum synchronization. This phenomenon was first observed in Kerr-anharmonic oscillators [246] and later realized in circuit QED [247], spin-1 [230] systems and recent optomechanical systems [248].

In this chapter, we systematically investigate the phenomenon of quantum phase synchronization in optically coupled optomechanical oscillators. This specific choice of exploiting the optical coupling as opposed to the mechanical one is primarily motivated by the recent theoretical investigation [237, 249, 250], as well as the experimental demonstrations [234, 251] of synchronization in coupled optomechanical oscillators. In fact, here we focus on two distinct topologies in which these optomechanical oscillators interact. The first being the bidirectional configuration where photons are exchanged in a reversible manner between both the optical cavities, while in the second one, namely the unidirectional configuration, photons are exchanged in an unidirectional way, i.e., only one of the cavities is receiving photons from the other one.

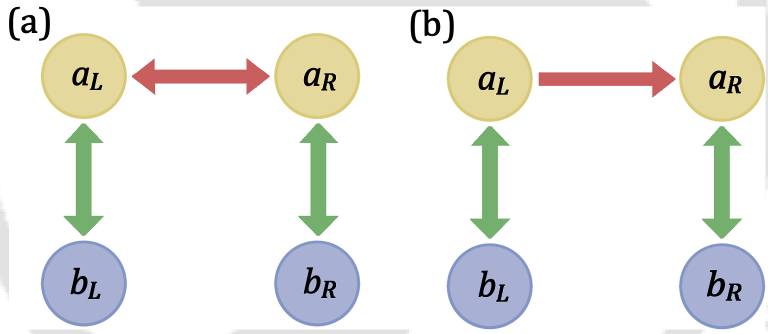

Figure 6.1: Schematic diagram of, respectively, the bidirectionally (a) and unidirectionally (b) coupled optomechanical oscillators. These couplings are considered to be purely optical in nature, as could be generated via optical fiber.

6.2 Model and dynamics

Let us first consider two optomechanical oscillators ($j = L($ left$)$, R (Right)), each of which contains one optical mode of frequency ω_{cj} and one mechanical mode of frequency ω_{mj}. The generic Hamiltonian ($\hbar = 1$) that describes these individual oscillators [1] is given by $H_j = \omega_{cj} a_j^\dagger a_j + \omega_{mj} b_j^\dagger b_j - g_j a_j^\dagger a_j (b_j^\dagger + b_j)$, where a_j, b_j be the annihilation operators of the optical and mechanical modes, respectively, and g_j is the usual radiation-pressure coupling rate.

Now, as shown in Fig. 6.1, we consider two distinct topologies in which these two optomechanical oscillators interact. To begin with, we first consider the bidirectional configuration (see Fig. 6.1(a)) where both these optomechanical cavities are allowed to exchange photons in a reversible manner. Such an interaction could be mimicked by a Hamiltonian of the form $H_c = -\lambda(a_1^\dagger a_2 + a_1 a_2^\dagger)$, where λ being any arbitrary coupling strength. Also, to drive these optical cavities, we use two separate laser sources, each characterized by an amplitude E_l and frequency ω_l. Taking the dissipative effects into account, we can write the following quantum Langevin equations (in a frame rotating at ω_l):

$$\begin{aligned}
\dot{a_L} &= \left(-\kappa_L + i\Delta_L^0 + ig_L(b_L^\dagger + b_L)\right) a_L + i\lambda a_R + E_l + \sqrt{2\kappa_L} a_L^{in}, \\
\dot{b_L} &= (-\gamma_L - i\omega_{mL})\, b_L + ig_L a_L^\dagger a_l + \sqrt{2\gamma_L} b_L^{in} \qquad (6.1a) \\
\dot{a_R} &= \left(-\kappa_R + i\Delta_R^0 + ig_R(b_R^\dagger + b_R)\right) a_R + i\lambda a_L + E_l + \sqrt{2\kappa_R} a_R^{in}, \\
\dot{b_R} &= (-\gamma_R - i\omega_{mR})\, b_R + ig_R a_R^\dagger a_R + \sqrt{2\gamma_R} b_R^{in}, \qquad (6.1b)
\end{aligned}$$

where Δ_j^0 is the input optical detuning, κ_j and γ_j are, respectively, the optical and mechanical damping rates, and a_j^{in} and b_j^{in} are the corresponding input bath operators. These operators are considered to be zero-mean Gaussian fields, satisfying the standard correlation relations [41] $\langle a_j^{in}(t)^\dagger a_{j'}^{in}(t') + a_{j'}^{in}(t') a_j^{in}(t)^\dagger \rangle = \delta_{jj'}\delta(t-t')$ and $\langle b_j^{in}(t)^\dagger b_{j'}^{in}(t') + b_{j'}^{in}(t') b_j^{in}(t)^\dagger \rangle = (2n_{th}+1)\delta_{jj'}\delta(t-t')$, where $n_{th} = \left[\exp\left(\frac{\hbar\omega_{mj}}{K_B T}\right) - 1\right]^{-1}$ defines the mean thermal occupation number, at a temperature T. (As we are only interested in $\omega_{mL} \approx \omega_{mR}$, the thermal phonon numbers corresponding to each oscillators can safely be taken to be equivalent.)

We next consider the unidirectional configuration (see Fig. 6.1(b)) where these optomechanical oscillators are arranged in a forward feed manner. This topology is quite different from the above described reversible one. As, it allows only the photons leaving from left cavity to enter the right one, and, thereby restricting any photons, traveling from right to reach the left cavity. Such cascaded geometry can be modeled using [252–254]: $a_R^{in}(t) = \sqrt{\eta} a_L^{out}(t-\tau)$, where $a_R^{in}(t)$ ($a_L^{out}(t)$) is the input (output) optical field entering to (leaving from) the right (left) cavity, η ($\eta \leq 1$) is the transmission loss between these optical cavities and τ is the time required for light transmitting from left to right oscillator. However, for theoretical simplification, we will consider $\tau = 0$ in the rest of this manuscript. As for driving these optical cavities, here, we use only a single laser source (with same amplitude E_l and frequency ω_l) and shine it on the left cavity. The full dissipative dynamics can then be described by the following set of quantum Langevin equations (in a frame rotating at ω_l):

$$\begin{aligned} \dot{a_L} &= \left(-\kappa_L + i\Delta_L^0 + ig_L(b_L^\dagger + b_L)\right) a_L + E_l + \sqrt{2\kappa_L} a_L^{in}, \\ \dot{b_L} &= (-\gamma_L - i\omega_{mL})\, b_L + ig_L a_L^\dagger a_l + \sqrt{2\gamma_L} b_L^{in} \end{aligned} \tag{6.2a}$$

$$\begin{aligned} \dot{a_R} &= \left(-\kappa_R + i\Delta_R^0 + ig_R(b_R^\dagger + b_R)\right) a_R + \sqrt{2\kappa_R}\sqrt{\eta}(a_L^{in} - \sqrt{2\kappa_L} a_L), \\ \dot{b_R} &= (-\gamma_R - i\omega_{mR})\, b_R + ig_R a_R^\dagger a_R + \sqrt{2\gamma_R} b_R^{in}, \end{aligned} \tag{6.2b}$$

where denotations of the parameters Δ_j^0, κ_j, γ_j, a_j^{in} and b_j^{in} remain unaltered, with the previous description.

We now expand these operators $\mathcal{O}(t)$ as sums of classical expectations values $\langle \mathcal{O}(t) \rangle$ plus quantum fluctuation operators $\delta\mathcal{O}(t)$, i.e., we write $\mathcal{O}(t) = \langle \mathcal{O}(t) \rangle + \delta\mathcal{O}(t)$. Then, following a substitution, we get a set of nonlinear differential equations as satisfied by the classical expectations. Now, while solving these equations, we set $\Delta_j^0 = \omega_{mj}$ and choose the laser amplitude E_l to be large enough, so that each solution yield a limit-cycle in the classical steady-state regime. As these solutions also acquire large coherent amplitudes, we can safely linearize the quantum Langevin equations for the fluctuation operators $\delta\mathcal{O}(t)$. Then, for the bidirectional configuration, we have the following set of linearized quantum Langevin equations

$$\delta\dot{a_L}(t) = (-\kappa_L + i\Delta_L)\delta a_L + ig_L\langle a_L(t)\rangle(\delta b_L^\dagger + \delta b_L) + i\lambda\delta a_R + \sqrt{2\kappa_L} a_L^{in} \tag{6.3a}$$

$$\delta\dot{b_L}(t) = (-\gamma_L - i\omega_{mL})\delta b_L + ig_L(\langle a_L(t)\rangle^*\delta a_L + \delta a_L^\dagger\langle a_L(t)\rangle) + \sqrt{2\gamma_L} b_L^{in}, \tag{6.3b}$$

$$\delta\dot{a_R}(t) = (-\kappa_R + i\Delta_R)\delta a_R + ig_R\langle a_R(t)\rangle(\delta b_R^\dagger + \delta b_R) + i\lambda\delta a_L + \sqrt{2\kappa_R} a_R^{in}, \tag{6.3c}$$

$$\delta\dot{b_R}(t) = (-\gamma_R - i\omega_{mR})\delta b_R + ig_R(\langle a_R(t)\rangle^*\delta a_R + \delta a_R^\dagger\langle a_R(t)\rangle) + \sqrt{2\gamma_R} b_R^{in}, \tag{6.3d}$$

while for the unidirectional configuration, the same reads as follows:

$$\delta\dot{a_L}(t) = (-\kappa_L + i\Delta_L)\delta a_L + ig_L\langle a_L(t)\rangle(\delta b_L^\dagger + \delta b_L) + \sqrt{2\kappa_L} a_L^{in} \tag{6.4a}$$

$$\delta\dot{b_L}(t) = (-\gamma_L - i\omega_{mL})\delta b_L + ig_L(\langle a_L(t)\rangle^*\delta a_L + \delta a_L^\dagger\langle a_L(t)\rangle) + \sqrt{2\gamma_L} b_L^{in}, \tag{6.4b}$$

$$\begin{aligned} \delta\dot{a_R}(t) = {}&(-\kappa_R + i\Delta_R)\delta a_R + ig_R\langle a_R(t)\rangle(\delta b_R^\dagger + \delta b_R) - 2\sqrt{\eta\kappa_L\kappa_R}\delta a_L \\ &+ \sqrt{2\eta\kappa_R} a_L^{in}, \end{aligned} \tag{6.4c}$$

$$\delta\dot{b_R}(t) = (-\gamma_R - i\omega_{mR})\delta b_R + ig_R(\langle a_R(t)\rangle^*\delta a_R + \delta a_R^\dagger\langle a_R(t)\rangle) + \sqrt{2\gamma_R} b_R^{in}. \tag{6.4d}$$

6.3 Quantum synchronization measure

With these quantum dynamical equations in hand, we now proceed to measure the degree of quantum phase synchronization. To do so, we follow the prescription, suggested by Mari in Ref [240]. At first, let us express the classical expectation values as $\langle \mathcal{O}_j(t)\rangle = r_j(t)e^{i\phi_j(t)}$ where $r_j(t)$ and $\phi_j(t)$ are, respectively, the the amplitude and phase of $\langle \mathcal{O}_j(t)\rangle$. Then, we have the fluctuation operator as $\mathcal{O}_j(t) - \langle \mathcal{O}_j(t)\rangle =: \delta\mathcal{O}_j(t)e^{i\phi_j(t)}$. In particular to CV (continuous variable) quantum systems, a convenient way to express this fluctuation operators $\delta\mathcal{O}_j(t)$ is $\delta\mathcal{O}_j = (\delta q_j(t) + i\delta p_j(t))/\sqrt{2}$ where the Hermitian and anti-Hermitian parts of $\delta\mathcal{O}_j(t)$ are, respectively, interpreted as the the amplitude and phase fluctuation operators. Now, if any two operators are classically synchronized, i.e., the phase of say $\langle \mathcal{O}_1(t)\rangle$ and $\langle \mathcal{O}_2(t)\rangle$ are locked, then one can define the phase shift operator with respect to the locking condition as $\delta p_- = [\delta p_1(t) - \delta p_2(t)]/\sqrt{2}$. Hence, a figure of merit for quantum phase synchronization could be given by

$$S_p(t) = \frac{1}{2}\langle \delta p_-(t)\rangle^{-1}. \tag{6.5}$$

A feasible way to gauze the degree of phase synchronization is to solve for the correlation matrix $C_{i,l}(t)$, given in terms of the bosonic fluctuation operators $C_{i,l}(t) = \langle R_i(t)R_l(t)^\dagger + R_l(t)^\dagger\rangle$, where $R(t) = \Big(\delta a_1(t), \delta a_1^\dagger(t), \delta b_1(t), \delta b_1^\dagger(t), \delta a_2(t), \delta a_2^\dagger(t), \delta b_2(t), \delta b_2^\dagger(t)\Big)$. Then, from Eq. (6.3) and (6.4), one can construct a dynamical equation corresponding to the correlation matrix $C_{i,l}(t)$ and solve it with a given initial condition. However, only finding a solution of $C_{i,l}(t)$ is not sufficient here, as the measure of phase synchronization is defined with respect to a frame rotating with the phases of individual classical trajectories. To incorporate such rotations, we give an unitary transformation on $R \to R' = U(t)R$ where $U(t) = \mathrm{diag}\left[e^{-i\phi_{a_1}(t)}, e^{i\phi_{a_1}(t)}, ...\right]$. With this definition, the rotated correlation matrix reads as $C'(t) = U(t)C(t)U'(t)$, from which one can extract all the second moments of the bosonic fluctuation operators, required to evaluate $S_p(t)$.

6.4 Results and discussions

A simulation of quantum phase synchronization between the two mechanical oscillators is plotted in Fig. 6.2. For both configurations, e.g., bidirectional and unidirectional, it is observed that after an initial transient, the system settles into

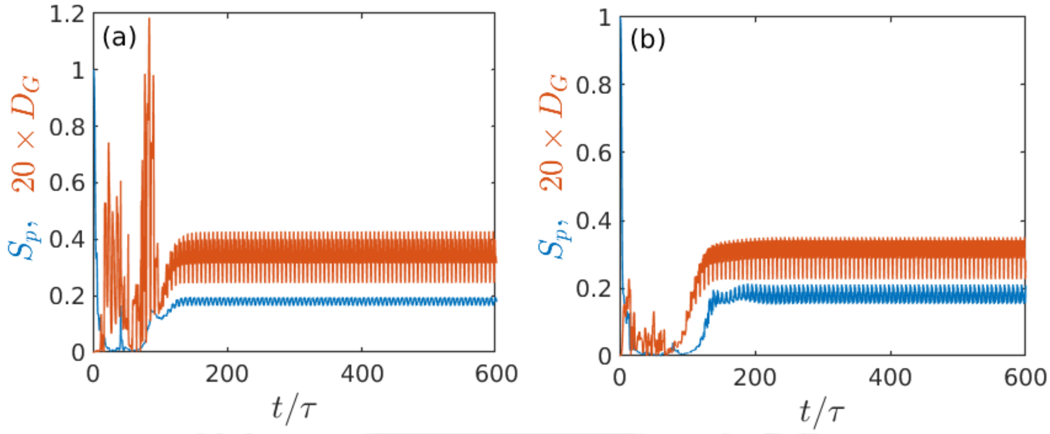

Figure 6.2: Time evolution of quantum phase synchronization (blue solid line) and Gaussian quantum discord (red solid line), between two mechanical oscillators, respectively for bidirectionally (a) and unidirectionally (b) coupled optomechanical oscillators. The parameters (normalized with respect to ω_{mL}) chosen for the simulations are $\omega_{mR} = 1.005$, $\gamma_{mL} = \gamma_{mR} = 0.005$, $\kappa_L = \kappa_R = 0.15$, $g_L = g_R = 0.005$, $E_l = 52$, $\lambda = \kappa/2(\kappa = \kappa_L)$ and $n_{th} = 0$ and $\tau = 1/\omega_{mL}$.

a periodic steady-state with a significant degree of synchronization $S_p(t)$, implying a quantum phase locked state between these two mechanical oscillators. Notably, we find that this quantum phase synchronous motion is also associated with a finite degree of Gaussian quantum discord D_G (2.18). This indicates at a possible relation between the onset of quantum synchronization and the generation of quantum correlation. However, it is worth mentioning that even though the system is quantum mechanically correlated ($D_G > 0$), we could not find any regime with non-zero logarithmic negativity (2.14).

Now, following these observations, a natural question that arises is whether the Gaussian quantum discord is a sufficient order parameter to map the essential traits of quantum (phase) synchronization. To test such hypothesis, in Fig. 6.3 we respectively plot the time-averaged measures of quantum phase synchronization (Fig. 6.3(a)) and the Gaussian quantum discord (Fig. 6.3(b)), as a function of the normalized coupling strength λ/κ and the frequency detuning between these two mechanical oscillators δ/ω_{mL}. It is observed that when the two optomechanical cells interact in a bidirectional manner, both synchronization and quantum discord exhibit a tongue like pattern, which is the quantum analogue of the classic "Arnold tongue". Such an appearance essentially yields a range of frequency detunings and their corresponding coupling strengths for which synchronization and non-classical correlation occur. Not surprisingly, here one finds both the maximum degrees of synchronization and quantum discord around the resonance condition $\delta = 0$, i.e., strictly for a pair identical mechanical oscillators $\omega_{mL} = \omega_{mR}$.

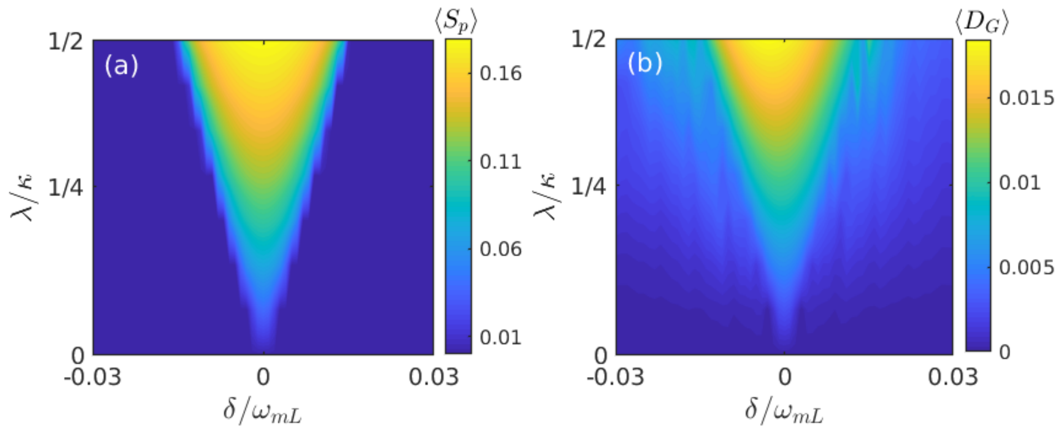

Figure 6.3: Time-averaged measures ($\langle X \rangle = \lim_{T\to\infty} \frac{1}{T}\int_0^T X(t)dt$) of quantum phase synchronization $\langle S_p \rangle$ (a) and Gaussian quantum discord $\langle D_G \rangle$ (b), as a function of frequency detuning δ/ω_{mL} and coupling strengths λ/κ.

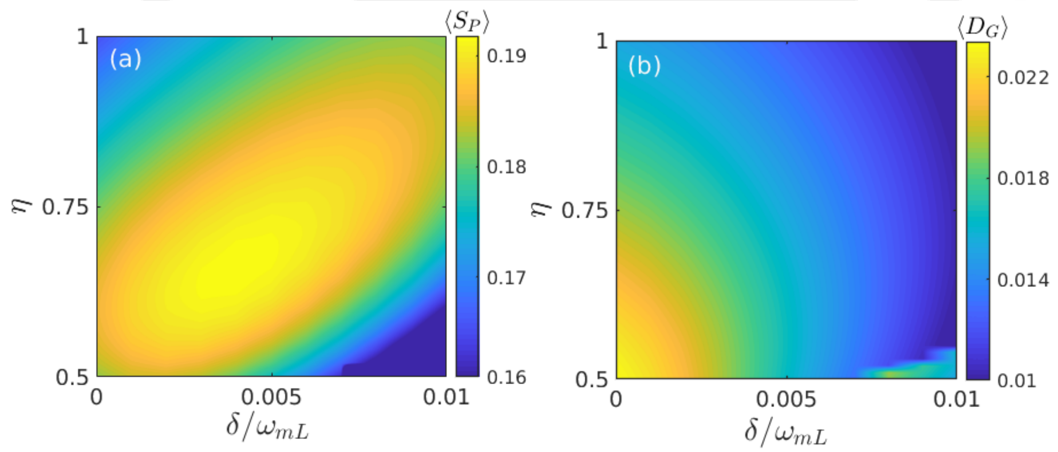

Figure 6.4: Time-averaged measures of quantum phase synchronization $\langle S_p \rangle$ (a) and Gaussian quantum discord $\langle D_G \rangle$ (b), as a function of frequency detuning δ/ω_{mL} and transmission losses η.

However, a similar investigation on the unidirectional configuration reveals a very intriguing outcome. Plotting $\langle S_p \rangle$ with respect to transmission losses η and the frequency detunings δ/ω_{mL} (see Fig. 6.4(a)), we find that the degree of quantum synchronization $\langle S_p \rangle$ is not maximum at the resonance condition, rather, it peaks around finite frequency detunings, depending on the strength of the transmission losses η. Such an anomaly in quantum synchronization has recently observed in

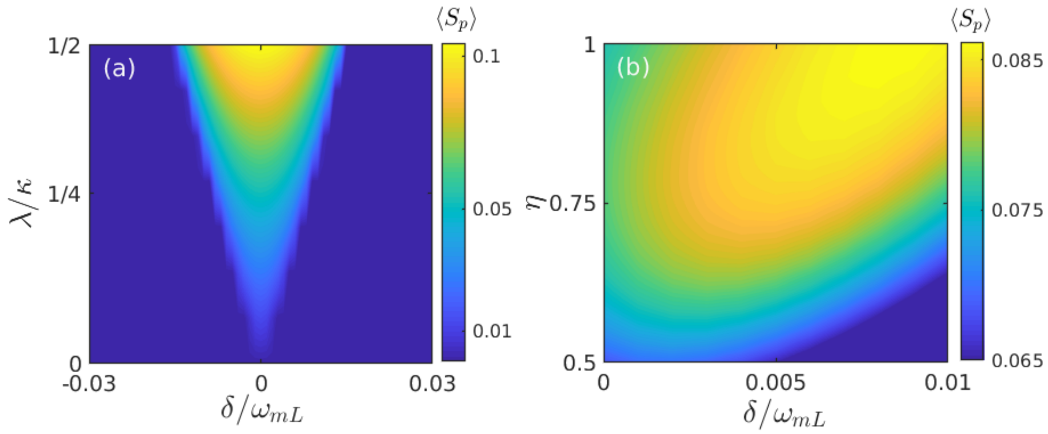

Figure 6.5: Average quantum synchronization, respectively, for bidirectionally (a) and unidirectionally (b) coupled optomechanical oscillators for an initial occupation of $n_{th} = 10$.

Kerr-anharmonic oscillators and coined as quantum synchronization blockade. In Ref. [246] it was well explained in terms of the intrinsic nonlinearity, leading an energy mismatch between the two oscillators. In particular to our system, we note that such occurrence of energy mismatch is inherent here, owing to the intrinsic unidirectionality of the optical coupling. Moreover, as we are specifically focused on $\delta > 0$, i.e., $\omega_{mR} > \omega_{mL}$ the required mismatch condition is always satisfied, leading to a blockade like behavior. However, exercising a similar investigation on the time-averaged Gaussian quantum discord, we find $\langle D_G \rangle$ is unable to reproduce such blockade like behavior. Instead, it retraces a similar a pattern as obtained in Fig. 6.3(b). Hence, one can infer that Gaussian quantum discord is not a conclusive map for quantum synchronization, despite of its strong presence while synchronization generation.

Finally, to investigate whether the appearances of the Arnold tongue and synchronization blockade are exclusive only to the ground states of the mechanical oscillators, we redo the same calculation for an initial occupation $n_{th} = 10$, and, respectively plot $\langle S_p \rangle$ as $f\,(\delta/\omega_{mL}, \lambda/\kappa)$ and $f\,(\delta/\omega_{mL}, \eta)$ (Fig. 6.5). Remarkably, we find that both observation still hold for mechanical oscillators, residing at higher thermal phonon numbers. However, one may notice a lesser degree of synchronization which is quite expected due to the increase in thermal noises.

6.5 Conclusion

In conclusion, we have systematically explored the connection between the onset of quantum phase synchronization and the generation of quantum correlations in two distinct setups of optically coupled optomechanical oscillators. Our results shows that when the two optomechanical cavities exchange photons in a reversible manner, both the measures of phase synchronization and quantum correlation, here Gaussian quantum discord, exhibit a tongue like pattern which is the quantum analogue of the Arnold tongue. Not surprisingly, here we find that the tendency of being synchronized and quantum mechanically correlated become maximum for identical mechanical oscillators. However, when these optomechanical cavities exchange photons in an unidirectional (forward feed) manner, one finds that the synchronization is blocked for identical oscillators. Instead, it becomes maximum for detuned oscillators. Exercising a similar investigation on Gaussian quantum discord, though does not allows one trace such blockade like pattern. Hence, despite of the strong association with quantum synchronization, Gaussian quantum discord fails to provide a conclusive map of quantum phase synchronization. Overall our study provides a further insight into the onset of quantum synchronization and correlation generation in different topological configurations within optomechanical platforms.

Chapter 7

Conclusions

In this thesis, we have explored various types of quantum correlations such as, quantum entanglement, Gaussian quantum discord and quantum synchronization in cavity optomechanical setups. In Chapter 1, we introduced the readers to the basics of cavity optomechanical system, with a brief literature survey. Then, in Chapter 2, we briefly discussed the measures of such quantum correlations (a measure of quantum synchronization has been provided in Chapter 6), that we have throughly used in all the following working chapters.

In Chapter 3, we proposed two schemes to generate and enhance the steady-state optomechanical correlations at a considerably lower coupling strength or external laser driving. In our first scheme, we coupled the mechanical mirror to a single auxiliary qubit, which induces an additional second-order potential term q^2 (q be dimensionless mirror's postion) in the Hamiltonian describing the system. We found that in presence of the mirror-qubit coupling, the system becomes unstable at a lower optomechanical coupling strength, which leads to a significant enhancement of the steady-state entanglement, as well as the Gaussian quantum discord, near the instability threshold. Moreover, we reported that with increasing mirror-qubit coupling strengths, entanglement can be achieved at a lower optomechanical coupling strength, which is also extremely robust with respect to thermal phonon fluctuations. In the second scheme, besides the usual radiation-pressure coupling, we considered an additional cross-Kerr type coupling between the optical and mechanical mode, generated by a two-level system or superconducting charge qubit. We found that invoking the cross-Kerr coupling on a generic optomechanical system not only generates a significant degree of entanglement at a lower external laser driving but also improves the robustness of the generated entanglement against system parameters and mirror's temperature. Furthermore, we considered Gaussian quantum discord (QD) as an additional measure of the quantum correlations. We showed that in presence of the cross-Kerr nonlinearity, QD becomes more robust and survives up to a much higher number thermal phonons as compared to optomechanical entanglement.

In Chapter 4, we studied the entanglement dynamics of two coupled mechanical oscillators, within a modulated optomechanical system. We found that depending on the strength of the mechanical coupling, one could observe either a stationary or a dynamical behavior of the mechanical entanglement, which is also extremely robust against the oscillator temperature. Moreover, we have shown that this entanglement dynamics is strongly related to the stability of the normal modes. Taking the mechanical damping effects into account, an analytical expression corresponding to the critical mechanical coupling strength where the transition from stationary to dynamical entanglement occurs is also reported.

In Chapter 5, we studied the entanglement dynamics in $\mathcal{PT}$ symmetric mechanical oscillators. To realize the mechanical gain and loss into the system, we couple the each of these oscillators to an optomechanical cavity and tune the respective cavity detuning to the Stokes and Anti-Stokes side-bands of the driving lasers. We showed that in binary $\mathcal{PT}$ symmetric system, entanglement (sudden) death ESD can be substantially slowed down, via operating near an exceptional point. We then carried out a similar investigation on the ternary $\mathcal{PT}$ symmetric system by taking a more complicated tripartite entanglement measure into account.

In Chapter 6, we investigated the phenomena of quantum synchronization and quantum correlations in two optically coupled optomechanical oscillators with two different topologies. In one case the oscillators are coupled with optical photons in a reversible manner, termed as bidirectional coupling, while in the other photons are allowed to enter to the other oscillator but not allowed to exchanged back in the opposite direction, termed as unidirectional coupling. It has been found that irrespective of these configurations, when synchronization builds up, the two oscillators also become quantum mechanically correlated with a finite degree of Gaussian quantum discord. However, we have found that depending on these topologies, both synchronization and quantum discord behave in a very distinctive manner. For instance, in bidirectionally coupled optomechanical oscillators, we find both quantum synchronization and quantum discord exhibit a tongue like pattern which is the quantum analogue of an Arnold tongue. Whereas, in the unidirectionally coupled oscillators, we observe a novel blockade like behavior for quantum phase synchronization, also known as the quantum synchronization blockade, quantum discord on the other hand fails to map such an anomalous behavior.

Scopes of Future Work

In this thesis, we have explored the linearized regime of single cavity optomechanical oscillators, or at most two of such coupled oscillators. However, one may recall that going over to the strong coupling limit, one can exploit the intrinsic nonlinearity of an optomechanical interactions. Here, the study of photon and phonon antibunching is of utmost relevance. While incorporating $\mathcal{PT}$ symmetry, we have restricted ourselves only into the $\mathcal{PT}$ symmetric phase. However, one may also look into the broken $\mathcal{PT}$ symmetric phase to investigate quantum correlation dynamics. One could also consider a more extended version of optomechanical oscillators, namely the optomechanical arrays. This facilitates us to explore the quantum many body dynamics over such integrated platforms. Another important aspect would be to study quantum synchronization and correlations in hybrid optomechanical systems. One may even explore the role of $\mathcal{PT}$ symmetry with regard to quantum synchronization. To the best of our knowledge, it is a highly open area of research.

Appendix

A. Generation of additional q^2 potential

Here, we provide a brief discussion on the generation of the additional second-order term, introduced in the system Hamiltonian. As prescribed in Ref. [88], we couple the mechanical mirror to a single auxiliary qubit with the Hamiltonian $H_q = (\Delta_q/2)\sigma_x$, via a linear interaction $H_{int} = \mu_q q \sigma_z$. Here, μ_q is the interaction strength between the mechanical mirror and auxiliary qubit, and, q be the dimensionless position operator of the mechanical mirror. Then, under the condition $\Delta_q \gg \mu_q$, we use the standard time-independent perturbation theory to diagonalize the auxiliary Hamiltonian: $H_{aux} = H_q + H_{int}$, which gives the eigenvalues of H_{aux}, as a power series in $\mu_q q$. Now, by placing the qubit in the eigenstate of σ_x, we can engineer an additional second-order term $H_{mq} = -2\Delta_q(\mu_q/\Delta_q)^2 q^2$ ($\frac{\eta}{2} = 2\Delta_q(\mu_q/\Delta_q)^2$). It should be noted that in the perturbation expansion all the higher order nonlinear terms are neglected, in the limit of $\Delta_q \gg \mu_q$.

Appendix

B. Matheu's Equation

The canonical form of Matheu's equation for the parameters δ and ϵ is given by [255, 256]

$$\ddot{y} + (\delta - 2\epsilon\cos(2t))\, y = 0. \tag{B.1}$$

This equation is a linear second order differential equation, with periodic coefficients. In general, the solution of such equation varies depending on the choice of δ and ϵ. However, it should be noted that to maintain the periodicity of the solution, δ and ϵ must be interrelated. Therefore, one has a set of eigenvalues $\alpha_n(\epsilon)$ $(n = 0, 1, 2, 3, ...)$ and $\beta_n(\epsilon)$ $(n = 0, 1, 2, 3, ...)$ necessary to yield solution of Eq. (B.1). For small ϵ, the first three $\alpha_n(\epsilon)$ and $\beta_n(\epsilon)$ could be written as follows [255]

$$\alpha_o = -\frac{1}{2}\epsilon^2 + \frac{7}{128}\epsilon^4 + O(\epsilon^6), \tag{B.2a}$$

$$\alpha_1 = 1 + \epsilon - \frac{1}{8}\epsilon^2 - \frac{1}{64}\epsilon^3 + O(\epsilon^4), \tag{B.2b}$$

$$\beta_1 = 1 - \epsilon - \frac{1}{8}\epsilon^2 + \frac{1}{64}\epsilon^3 + O(\epsilon^4). \tag{B.2c}$$

Bibliography

[1] M. Aspelmeyer, T. J. Kippenberg, and F. Marquardt, Rev. Mod. Phys. **86**, 1391 (2014).

[2] V. B. Braginski and A. Manukin, Sov. Phys. JETP, **25**, 653 (1967).

[3] V. B. Braginski and A. Manukin, *Measurement of weak forces in Physics experiments*, (University of Chicago Press, Chicago 1977).

[4] C. M. Caves, Phys. Rev. Lett. **45**, 75 (1980).

[5] A. F. Pace, M. J. Collett, and D. F. Walls, Phys. Rev. A **47**, 3173 (1993).

[6] C. Fabre, M. Pinard, S. Bourzeix, A. Heidmann, E. Giacobino, and S. Reynaud, Phys. Rev. A **49**, 1337 (1994).

[7] S. Mancini and P. Tombesi, Phys. Rev. A **49**, 4055 (1994).

[8] K. Jacobs, P. Tombesi, M. J. Collett, and D. F. Walls, Phys. Rev. A **49**, 1961 (1994).

[9] S. Mancini, D. Vitali, and P. Tombesi, Phys. Rev. Lett., **80**, 688 (1998).

[10] S. Bose, K. Jacobs, and P. Knight, Phys. Rev. A, **56**, 4175 (1997).

[11] P. F. Cohadon, A. Heidmann, and M. Pinard, Phys. Rev. Lett. **83**, 3174 (1999).

[12] T. J. Kippenberg, H. Rokhsari, T. Carmon, A. Scherer, and K. J. Vahala, Phys. Rev. Lett. **95**, 033901 (2005).

[13] S. Gigan, H. R. Böhm, M. Paternostro, F. Blaser, G. Langer, J. B. Hertzberg, K. C. Schwab, D. Buerle, M. Aspelmeyer and A. Zeilinger, Nature (London) **444**, 67 (2006).

[14] A. Schliesser, R. Riviére, G. Anetsberger, O. Arcizet and T. J. Kippenberg, Nat. Phys. **4**, 415 (2008).

[15] H. Shi and M. Bhattacharya, Phys. Rev. A **87**, 043829 (2013).

[16] S. Liu, Bo Liu, J. Wang, T. Sun, and W. X. Yang, Phys. Rev. A **99**, 033822 (2019).

[17] M. Bhattacharya and P. Meystre, Phys. Rev. A **78**, 041801(R) (2008).

[18] M. Mikkelsen, T. Fogarty, J. Twamley, and Th. Busch, Phys. Rev. A **96**, 043832 (2017).

[19] J. D. Teufel, T. Donner, Dale Li, J. W. Harlow, M. S. Allman, K. Cicak, A. J. Sirois, J. D. Whittaker, K. W. Lehnert and R. W. Simmonds, Nature London **475**, 359 (2011).

[20] J. Chan, T. P. Mayer Alegre, A. H. Safavi-Naeini, J. T. Hill, A. Krause, S. Gröblacher, M. Aspelmeyer and O. Painter, Nature (London) **478** 89 (2011).

[21] K. H. Lee, T. G. McRae, G. I. Harris, J. Knittel, and Warwick P. Bowen, Phys. Rev.

Lett. **104**, 123604 (2010).

[22] D. Vitali, S. Gigan, A. Ferreira, H. R. Bhm, P. Tombesi, A. Guerreiro, V. Vedral, A. Zeilinger, and M. Aspelmeyer, Phys. Rev. Lett. **98**, 030405 (2007).

[23] M. Paternostro, D. Vitali, S. Gigan, M. S. Kim, C. Brukner, J. Eisert, and M. Aspelmeyer, Phys. Rev. Lett. **99**, 250401 (2007).

[24] C. Genes, D. Vitali, and P. Tombesi, Phys. Rev. A **77**, 050307(R) (2008).

[25] B. Rogers, M. Paternostro, G. M. Palma, and G. De Chiara, Phys. Rev. A **86**, 042323 (2012) .

[26] L. Tian, Phys. Rev. Lett. **110**, 233602 (2013).

[27] A A Clerk, F Marquardt and K Jacobs, New J. Phys. **10**, 095010 (2008).

[28] H. Tan, Gaoxiang Li, and P. Meystre, Phys. Rev. A, **87**, 033829 (2013).

[29] E. G. Dalla Torre, J. Otterbach, E. Demler, V. Vuletic, and M. D. Lukin, Phys. Rev. Lett. **110**, 120402 (2013).

[30] D. W. C. Brooks, T. Botter, S. Schreppler, T. P. Purdy, N. Brahms and D. M. Stamper-Kurn, Nature, (London) **488**, 476 (2012).

[31] S. Rips, M. Kiffner, I. Wilson-Rae and M J Hartmann, New J. Phys. **14**, 023042 (2012).

[32] J. Zhang, K. Peng, and S. L. Braunstein, Phys. Rev. A **68**, 013808 (2003).

[33] L. Tian, Phys. Rev. Lett. **108**, 153604 (2012).

[34] T. A. Palomaki, J. W. Harlow, J. D. Teufel, R. W. Simmonds and K. W. Lehnert, Nature (London) **495**, 210 (2013).

[35] C. A. Regal, J. D. Teufel and K. W. Lehnert, Nat. Phys. **4**, 555 (2008).

[36] L.S. Collaboration, *et al.*, Nat. Phys. **7**, 962 (2011).

[37] M. A. Taylor, J. Janousek, V. Daria, J. Knittel, B. Hage, H.-A. Bachor and W. P. Bowen, Nat. Photonics **7**, 229 (2013).

[38] C. K. Law, Phys. Rev. A **51**, 2537 (1995); P. Meystre, Ann. Phys. (Berlin) **525**, 215 (2013).

[39] W. P. Bowen and G. J. Milburn, *Quantum optomechanics* (CRC Press, 2016).

[40] *Cavity optomechanics: nano-and micromechanical resonators interacting with light* (Springer (Berlin) 2014), Edited by M. Aspelmeye, T. J. Kippenberg and F. Marquardt.

[41] D. F. Walls and G. J. Milburn, *Quantum Optics* (Springer, Berlin, 1994).

[42] S. L. Braunstein and P. V. Loock, Rev. Mod. Phys. **77**, 513 (2005).

[43] C. Weedbrook, S. Pirandola, R. García-Patrón, N. J. Cerf, T. C. Ralph, J. H. Shapiro, and S. Lloyd, Rev. Mod. Phys. **84**, 621 (2012).

[44] G. Adesso and F. Illuminati, J. Phys. A **40**, 7821 (2007).

[45] S. Olivares, Eur. Phys. J. Special Topics **203**, 3 (2012).

[46] R. Simon, E. C. G. Sudarshan, and N. Mukunda, Phys. Rev. A **36**, 3868 (1987).

[47] R. F. Werner and M. M. Wolf, Phys. Rev. Lett. **86**, 3658 (2001).

[48] A. Serafini, F. Illuminati, S. D. Siena, J. Phys. B **37** L21(2004).

[49] P. Horodecki, Phys. Lett. A **232**, 333 (1997).

[50] R. Simon, Phys. Rev. Lett. **84**, 2726 (2000).

[51] G. Vidal and R. F. Werner, Phys. Rev. A **65**, 032314 (2002).
[52] G. Adesso, A. Serafini, and F. Illuminati, Phys. Rev. A **70**, 022318 (2004).
[53] H. Ollivier and W. H. Zurek, Phys. Rev. Lett. **88**, 017901 (2002).
[54] P. Giorda and M. G. A. Paris, Phys. Rev. Lett. **105**, 020503 (2010).
[55] G. Adesso and A. Datta, Phys. Rev. Lett. **105**, 030501 (2010).
[56] L. Mazzola and M. Paternostro, Phys. Rev. A **83** 062335 (2011).
[57] L. Mazzola and M. Paternostro, Sci. Rep. **1**, 199 (2011).
[58] A. Farace, F. Ciccarello, R. Fazio, and V. Giovannetti, Phys. Rev. A **89**, 022355 (2014).
[59] G. Adesso, V. D'Ambrosio, E. Nagali, M. Piani, and F. Sciarrino, Phys. Rev. Lett. **112**, 140501 (2014).
[60] E. Schrödinger, Proc. Cambridge Philos. Soc. **31**, 555 (1935).
[61] R. Horodecki, P. Horodecki, M. Horodecki, and K. Horodecki, Rev. Mod. Phys. **81**, 865, (2009).
[62] J. A. Jones and D. Jaksch, *Quantum Information, Computation and Communication,* (Cambridge University Press, Cambridge, UK, 2012).
[63] *Quantum Entanglement and Information Processing,* edited by D. Estev̀e, J.-M Raimond, and J. Dalibard (Elsivier, Amsterdam, 2003).
[64] O. Mandel, M. Greiner, A. Widera, T. Rom, T. W. Hańsh, and I. Bloch, Nature (London) **425**, 937 (2003).
[65] H. Häffner, W. Hänsel, C. F. Roos, J. Benhelm, D. chek-al-ker, M. Chwalla, T. Körber, U. D. Rapol, M. Riebe, P. O. Schmidt, C. Becher, O, Gühne, W. Dür and R. Blatt, Nature (London) **438**, 643 (2005).
[66] C. Genes, A. Mari, P. Tombesi, and D. Vitali, Phys. Rev. A **78**, 032316 (2008).
[67] M. Tsang, Phys. Rev. A **81**, 063837 (2010).
[68] S. Mancicni, V. Giovannetti, P. Tombesi, and D. Vitali, "Entangling Macroscopic Oscillators Exploiting Radiation Pressure," Phys. Rev. Lett. **88**, 120401 (2002).
[69] S. Barzanjeh, D. Vitali, P. Tombesi, and G. J. Milburn, Phys. Rev. A **84**, 042342 (2011).
[70] S. Pirandola, D. Vitali, P. Tombesi, and S. Lloyd, Phys. Rev. Lett. **97**, 150403 (2006).
[71] C. A. Muschik, E. S. Polzik, and J. I. Cirac, Phys. Rev. A **83**, 052312 (2011).
[72] K. Børkje, A. Nunnenkamp, and S. M. Girvin, Phys. Rev. Lett. **107**, 123601 (2011).
[73] H. T. Tan and G. X. Li, Phys. Rev. A **84**, 024301 (2011).
[74] C. Genes, D. Vitali, and P. Tombesi, New. J. Phys. **10**, 095009 (2008).
[75] D. Vitali, P. Tombesi, M. J. Wooley, A. C. Doherty, and G. J. Milburn, Phys. Rev. A **76**, 042336 (2007).
[76] R. Ghobadi, A. R. Bahrampour, and C. Simon, Phys. Rev. A **84**, 063827 (2011).
[77] R. Ghobadi, A. R. Bahrampour, and C. Simon, Phys. Rev. A **84**, 033846 (2011).
[78] M. Abdi, S. Barzanjeh, P. Tombesi, and D. Vitali, Phys. Rev. A **84**, 032325 (2011).
[79] J. Zhang, K. Peng, and S. L. Braunstein, Phys. Rev. A **68**, 013808 (2003).
[80] P. Ehrenfest, Z. Phys. A **45**, 455.(1927)
[81] A.N. Cleland, *Foundation of Nanomechanics From Solid-state Theory to Device Ap-*

plicationa (Springer-Verlag, Berlin Heidelberg, 2003).
[82] Z. L. Xiang, S. Ashhab, J.Q. You, F. Nori , Rev. Modern Phys. **85**, 623 (2013).
[83] L. Tian, Phys. Rev. B **84**, 035417 (2011).
[84] K. Jacobs, Phys. Rev. Lett. **99**, 117203 (2007).
[85] A.D. Armour, M.P. Blencowe, K.C. Schwab, Phys. Rev. Lett. **88**, 148301 (2002).
[86] S. Rips, I. Wilson-Rae, M.J. Hartmann, Phys. Rev. A **89**, 013854 (2014).
[87] P. Djorwé, S. G. Nana Engo, P. Wofao, Phys. Rev. A **90**, 024303 (2014).
[88] K. Jacobs, A. J. Landahl, Phys. Rev. Lett. **103**, 067201 (2009).
[89] X. Y. Lü, J.-Q. Liao, L. Tian, F. Nori, Phys. Rev. A **91**, 013834 (2015).
[90] D.-Y. Wang, C.-H. Bai, H.-F. Wang, A.-D. Zhu, S. Zhang, Sci. Rep. **6**, 24421 (2016).
[91] K. Jacobs, L. Tian, J. Finn, Phys. Rev. Lett. **102**, 057208 (2009).
[92] M.D. LaHaye, J. Suh, P. M. Echternach, K. C. Schwab, M. L. Roukes, Nature (London) **459**, 960 (2009).
[93] A.D. O'Connel, M. Hofheinz, M. Ansmann, R.C. Bialczak, M. Lenander, E. Lucero, M. Neeley, D. Sank, H. Wang, M. Weides, J. Wenner, J. M. Martinis, A. N. Cleland, Nature (London) **464**, 697 (2010) .
[94] M. Poot, H.S.J. Van der Zant. Phys. Reports **511**, 273 (2012).
[95] A. Jöckel, A. Faber, T. Kampschulte, M. Korppi, M.T. Rakher, P. Treutlein, Nat. Nanotechnology **10**, 55 (2015).
[96] J.-M. Pirkkalainen, S.U. Cho, F. Massel, J. Tuorila, T.T. Heikkilä, P.J. Hakonen, M.A. Sillanpää, Nat. Commun. **6**, 6981 (2015).
[97] G. Kurizki, P. Bertet, Y. Kubo, K. Mlmer, D. Petrosyan, P. Rabl, J. Schmiedmayer, Proc. Natl. Acad. Sci. USA **112**, 3866 (2015).
[98] M. Brunelli, M. Paternostro, arXiv:1610.01172 (2016).
[99] V. Giovannetti and D. Vitali, Phys. Rev. A **63**, 023812 (2001).
[100] R. Benguria and M. Kac, Phys. Rev. Lett. **46**, 1 (1981).
[101] E. X. DeJesus and C. Kaufman, Phys. Rev. A **35**, 5288 (1987).
[102] T. T. Heikkilä, F. Masel, J. Tuorila, R. Khan, and M. A. Sillanpää, Phys. Rev. Lett. **112**, 203603 (2014).
[103] J.-M. Pirkkalainen, S. U. Cho, F Massel, J. Tuorlia, T. T. Heikkilä, P. J. Hakonen, and M. A. Sillanpää, Nat. Commun. **6**, 6981 (2015).
[104] W. J. Munro, K. Nemoto, R. G. Beausoleii, and T. P. Spiller, Phys. Rev. A **71**, 033819 (2005).
[105] W. J. Munro, K. Nemoto, and T. P. Spiller, New. J. Phys. **7**, 137 (2005).
[106] Y.-B. Sheng, L. Zhou, S.-M. Zhao, and B.-Y. Zheng, Phys. Rev. A **85**, 012307 (2012).
[107] D. Menzies and N. Korolkova, Phys. Rev. A **74**, 042315 (2006).
[108] J. Fiurášek, L. Mišta, Jr., and R. Flipp, Phys. Rev. **67**, 022304 (2003).
[109] T. Wang, H. W. Lau, H. Kaviani, R. Ghobadi, and C. Simon, Phys. Rev. A **92**,012316 (2015).
[110] L. Mandel and E. Wolf, *Optical Coherence and Quantum Optics* (Cambridge University Press, Cambridge, 1995).
[111] K. Koshino, Phys. Rev. A **74**, 053818 (2006).

[112] R. Khan, F. Massel, and T. T. Heikkilä, Phys. Rev. A. **91**, 043822 (2015).
[113] R. Sarala and F. Massel, Nanoscale Syst: Math. Model. Theory Appl. **4**, 18 (2015).
[114] W. Xiong, D.-Y. Jin, Y. Qiu, C.-H. Lam, and J. Q. You, Phys. Rev. A **93**, 023844 (2016).
[115] J. El. Qars, M. Daoud and Ahl Laamara, Int. J. Quantum Inform. **13**, 1550041 (2015).
[116] T. A. Palomaki, J. D. Teufel, R. W. Simmonds, and K. W. Lehnert, Science **342** 710 (2013).
[117] M. C. Kuzyk, S. J. Van Enk, H. Wang, Phys. Rev. A **88**, 062341 (2013).
[118] S. G. Hofer, W. Wieczorek, M. Aspelmeyer, and K. Hammerer, Phys. Rev. A **84**, 052327 (2011).
[119] G. Wang, L. Huang, Y.-C. Lai, and C. Grebogi, Phys. Rev. Lett. **112**, 110406 (2014).
[120] A. A. Rakhubovsky and R. Flipp, Phys. Rev. A **91**, 062317 (2015).
[121] V. Vedral, Nature **468**, 769 (2010).
[122] A. Mari and J. Eisert, Phys. Rev. Lett. **103**, 213603 (2009).
[123] A. Farace and V. Giovannetti, Phys. Rev. A **86**, 013820 (2012).
[124] M. Schmidt, M. Ludwig, and F. Marquardt, New J. Phys. **14**, 125005 (2012).
[125] R.-X. Chen, L.-T. Shen, Z.-B. Yang, H.-Z. Wu and S.-B. Zheng, Phys. Rev. A **89**, 023843 (2014).
[126] F. Galve, L. A. Pachón, and D. Zueco, Phys. Rev. Lett. **105** 180501 (2010).
[127] T. F. Roque and J. A. Roversi, Phys. Rev. A **88**, 032114 (2013).
[128] R.-X. Chen, L.-T. Shen, Z.-B. Yang, and H.-Z. Wu, Phys. Rev. A **91**, 012312 (2015).
[129] E. A. Sete, H. Eleuch, and C. H. Raymond Ooi, J. Opt. Soc. Am. B. **31**, 002821 (2014).
[130] J. Li, I. M. Haghighi, N. Malossi, S. Zippilli, and D. Vital, New. J. Phys. **17**, 103037 (2015).
[131] J. Li, G. Li, S. Zippilli, D. Vitali, and T. Zhang, Phys. Rev. A **95**, 043819 (2017).
[132] H. Tan, G. Li, and P. Meystre, Phys. Rev. A **87**, 033829 (2013).
[133] R.-X. Chen, L.-T. Shen, and S.-B. Zheng, Phys. Rev. A **91**, 022326 (2015).
[134] C.-J. Yang, J.-H. An, W. Yang, and Y. Li, Phys. Rev. A **92**, 062311 (2015).
[135] Y.-D. Wang and A. A. Clerk, Phys. Rev. Lett. **110**, 253601 (2013).
[136] M. J. Woolley and A. A. Clerk, Phys. Rev. A, **89**, 063805 (2014).
[137] M. Asjad, S. Zippilli, and D. Vitali, Phys. Rev. **93**, 062307 (2016).
[138] X.-B. Yan, Phys. Rev. A **96**, 053831 (2017).
[139] R. Riedinger, A. Wallucks, I. Marinković, C. Löschnauer, M. Aspelmeyer, S. Hong, and S. Grblacher, Nature (London) **556**, 473 (2018).
[140] C. F. Ockeloen-Korppi, E. Damaskägg, J.-M. Pirkkalainen, A. A. Clerk, F. Massel, M. J. Woolley, and M. A. Sillanpää, Nature (London) **556**, 478 (2018).
[141] I. Marinković, A. Wallucks, R. Riedinger, S. Hong, M. Aspelmeyer, and S. Gröblacher, Phys. Rev. Lett. **121**, 220404 (2018).
[142] C. M. Bender and S. Boettcher, Phys. Rev. Lett. **80**, 5243 (1998).
[143] C. M. Bender, D. C. Brody, and H. F. Jones, Phys. Rev. Lett. **89**, 270401 (2002).

[144] R. El-Ganainy, K.G. Makris, M. Khajavikhan, Z.H. Musslimani, S. Rotter, and D.N. Christodoulides, Nat. Phys. **14**, 11 (2018).
[145] W.D. Heiss, J. Phys. A **45**, 444016 (2012).
[146] K. G. Markis, R. El-Ganainy, D. N. Christodoulides, and Z. H. Musslimani, Phys. Rev. Lett. **100**, 103904 (2008).
[147] Z. H. Musslimani, K. G. Makris, R. El-Ganainy, and D. N. Christodoulides, Phys. Rev. Lett. **100**, 030402 (2008).
[148] A. Guo, G. J. Salamo, D. Duchesne, R. Morandotti, M. Volatier-Ravat, V. Aimez, G. A. Siviloglou, and D. N. Christodoulides, Phys. Rev. Lett. **103**, 093902 (2009).
[149] C. E. Rüter, K. G. Markis, R. El-Ganainy, D. N. Christodoulides, M. Segev and D. Kip, Nat. Phys. **6**, 192 (2010).
[150] A. Regensburger, C. Bersch, M.-A. Miri, G. Onishchukov, D.N. Christodoulides, and U. Peschel, Nature (London) **488** 167 (2012).
[151] B. Peng, S. K. Oždemir, F. Lei, F. Monifi, M. Gianfreda, G. L. Long, S. Fan, F. Nori, C. M. Bender, and L. Yang, Nat. Phys. **10**, 394 (2014).
[152] L. Feng, Z.J. Wong, R.-M. Ma, Y. Wang, and X. Zhang, Science **346** 972 (2014).
[153] H. Hodaei, M.-A. Miri, M. Heinrich, D.N. Christodoulides, and M. Khajavikhan, Science **346**, 975 (2014).
[154] H. Hodaei, A. U. Hassan, W. E. Hayenga, M. A. Miri, D. N. Christodoulides, and M. Khajavikhan, Opt. Lett. **41**, 3049 (2016).
[155] B. Peng, S. K. Özdemir, M. Liertzer, W. Chen, J. Kramer, H. Yilmaz, J. Wiersig, S. Rotter, and L. Yang, Proc. Natl. Acad. Sci. USA **113**, 6845 (2016).
[156] Z. Lin, H. Ramezani, T. Eichelkraut, T. Kottos, H. Cao, and D. N. Christodoulides, Phys. Rev. Lett. **106**, 213901 (2011).
[157] S. Longhi, J. Phys. A **44**, 485302 (2011).
[158] L. Feng, Y.-L. Xu, W.S. Fegadolli, M.-H. Lu, J.E.B. Oliveira, V.R. Almeida, Y.-F. Chen, and A. Scherer, Nat. Mater. **12**, 108 (2013).
[159] J. Wiersig, Phys. Rev. Lett. **112**, 203901 (2014)
[160] H. Hodaei, A.U. Hassan, S. Wittek, H. Garcia-Gracia, R. El-Ganainy, D.N. Christodoulides, and M. Khajavikhan, Nature (London) **548**, 187 (2017).
[161] W. Chen, . K. Özdemir, G. Zhao, J. Wiersig, and L. Yang, Nature (London) **548**, 192 (2017).
[162] T. Goldzak, A. A. Mailybaev, and N. Moiseyev, Phys. Rev. Lett. **120**, 013901 (2018).
[163] P. Miao, Z. Zhang, J. Sun, W. Walasik, S. Longhi, N. M. Litchinitser, and L. Feng, Science **353**, 464 (2016).
[164] C. Hang, G. Huang, and V. V. Konotop, Phys. Rev. Lett. **110**, 083604 (2013).
[165] D. Haag, D. Dast, A. Löhle, H. Cartarius, J. Main, and G. Wunner, Phys. Rev. A **89**, 023601 (2014).
[166] H. Cartarius and G. Wunner, Phys. Rev. A **86**, 013612 (2012).
[167] H. Jing, S.K. Özdemir, X.-Y. Lü, J. Zhang, L. Yang, and F. Nori, Phys. Rev. Lett. **113**, 053604 (2014).

[168] X.-W. Xu, Y.-x. Liu, C.-P. Sun, and Y. Li, Phys. Rev. A **92**, 013852 (2015).
[169] X.-Y. Lü, H. Jing, J.-Y. Ma, and Y. Wu, Phys. Rev. Lett. **114**, 253601 (2015).
[170] F. Quijandría, U. Naether, S. K. Özdemir, F. Nori, and D. Zueco, Phys. Rev. A **97**, 053846 (2018).
[171] Y. Ashida, S. Furukawa, and M. Ueda, Nat. Commun. **8**, 15791 (2017).
[172] S.-L. Chen, G.-Y. Chen, and Y.-N. Chen, Phys. Rev. A **90**, 054301 (2014).
[173] H. Xu, D. Mason, L. Jiang, and J.G.E. Harris, Nature (London) **537**, 80 (2016).
[174] J. Doppler, A.A. Mailybaev, J. Bhm, U. Kuhl, A. Girschik, F. Libisch, T.J. Milburn, P. Rabl, N. Moiseyev, and S. Rotter, Nature (London) **537**, 76 (2016).
[175] B. Gardas, S. Deffner, and A. Saxena, Phys. Rev. A **94**, 040101 (2016).
[176] K. Kawabata, Y. Ashida, and M. Ueda, Phys. Rev. Lett. **119**, 190401 (2017).
[177] G. S. Agarwal and K. Qu, Phys. Rev. A **85**, 031802 (2012).
[178] K. V. Kepesdis, T. J. Milburn, J. Huber, K. G. Makris, S. Rotter, and P. Rabl, New J. Phys. **18**, 095003 (2016).
[179] H.-K. Lau and A. A. Clerk, Nat. Commun. **9**, 4320 (2018).
[180] M. Zhang, W. Sweeney, C. W. Hsu, L. Yang, A. D. Stone, and L. Jiang, arXiv:1805.12001.
[181] S. Vashahri-Ghamsari, B. He, and M. Xiao, Phys. Rev. A **96**, 033806 (2017).
[182] S. Vashahri-Ghamsari, B. He, and M. Xiao, Phys. Rev. A **99**, 023819 (2019).
[183] T. Yu and J. H. Eberly, Science **323**, 598 (2009).
[184] J. Laurat, K. S. Choi, H. Deng, C. W. Chou, and H. J. Kimble, Phys. Rev. Lett. **99**, 180504 (2007).
[185] M. P. Almeida, *et al.*, Science **316**, 579 (2007).
[186] C. Cormick and J. Pablo Paz, Phys. Rev. A **78**, 012357 (2008).
[187] J. P. Paz, A. J. Roncaglia, Phys. Rev. Lett. **100**, 220401 (2008).
[188] A. S. Coelho, F. A. S. Barbosa1, K. N. Cassemiro, A. S. Villar, M. Martinelli, P. Nussenzveig, Science **326**, 823 (2009).
[189] J. Preskill, Proc. R. Soc. London A **454**, 385 (1998).
[190] P. W. Shor, Phys. Rev. A **52**, 2493 (1995).
[191] A. R. P. Rau, M. Ali, and G. Alber, EPL **82**, 40002 (2008).
[192] A. Sing, S. Pradyumna, A. R. P. Rau, and U. Sinha, J. Opt. Soc. Am. B **34**, 681 (2017).
[193] L. Viola, L. Knill, and S. Lloyd, Phys. Rev. Lett. **82**, 2417 (1999).
[194] M. J. Biercuk, H. Uys, A. P. VanDevender, N. Shiga, W. M. Itano, and J. J. Bollinger, Nature (London) **458**, 996 (2009).
[195] D. A. Lidar, I. Chuang, and K. B. Whaley, Phys. Rev. Lett. **81**, 2594 (1998).
[196] P. G. Kwiat, A. J. Berglund, J. B. Altepeter, and A. G. White, Science **290**, 498 (2000).
[197] P. Facchi, D. A. Lidar, and S. Pascazio, Phys. Rev. A **69**, 032314 (2014).
[198] S. Maniscalco, F. Francica, R. L. Zaffino, N. L. Gullo, and F. Plastina, Phys. Rev. Lett. **100**, 090503 (2008).
[199] J.-C. Lee, H.-T. Lim, K.-H. Hong, Y.-C. Jeong, M. S. Kim, and Y.-H. Kim, Nat.

Commun. **5**, 4522 (2014).
[200] Y. S. Kim, Y. W. Cho, Y.-S. Ra, and Y.-H. Kim, Opt. Express **17**, 11978 (2009).
[201] J. C. Lee, Y. C. Jeong, Y. S. Kim, and Y. H. Kim, Opt. Express **19**, 16309 (2011).
[202] Q. Sun, M. Al-Amri, L. Davidovich, and M. S. Zubairy, Phys. Rev. A **82**, 052323 (2010).
[203] W. Li, C. Li and H. Song, Phys. Rev. A **95**, 023827 (2017).
[204] M. Spletzer, A. Raman, A. Q. Wu, X. F. Xu, and R. Reifenberger, Appl. Phys. Lett. **88**, 254102 (2006).
[205] E. Gil-Santos, D. Ramos, V. Pini, M. Calleja, and J. Tamayo, Appl. Phys. Lett. **98**, 123108 (2011).
[206] P. van Lock and A. Furusawa, Phys. Rev. A **67**, 052315 (2003).
[207] R. Y. Teh and M. D. Reid, Phys. Rev. A **90**, 062337 (2014).
[208] E. A. Rojas González, A. Borne, B. Boulanger, J. A. Levenson, and K. Bencheikh, Phys. Rev. Lett. **120**, 043601 (2018).
[209] A. Pikovsky, M. Rosenblum, and J. Kurths, *Synchronization: A Universal Concept in Nonlinear Sciences* (Cambridge University Press, Cambridge, UK 2003).
[210] C. Huygens, *Œuvres Complétes de Christiaan Huygens* (Martinus Nijhoff, The Hague, 1893), Vol. 15, p. 243; *Œuvres Complétes de Christiaan Huygens* (Martinus Nijhoff, The Hague, 1932), Vol. 17, p. 183
[211] S. H. Strogatz, *Sync: The Emerging Science of Spontaneous Order* (Hyperion, New York, 2003).
[212] S. Bregni, *Synchronization of Digital Telecommunications Networks* (Wiley, Chichester, England, 2002).
[213] E. Ranta, V. Kaitala, and P. Lundberg, Science **285**, 1022 (1999).
[214] T. Womelsdrof, J.-M. Schoffelen, R. Oostenveld, W. Singer, R. Desimone, A. K. Engel, and P. Fries, Science **316**, 1609 (2007).
[215] J. Buck and E. Buck, Science **159** 1319 (1968).
[216] M. Toiya, H. O. Gonzalez-Ochoa, V. K. Vanag, S. Fraden, and I. R. Epstein, J. Phys. Chem. Lett. **1**, 1241 (2010).
[217] D. Antonio, D. H. Zanette, and D. Lopez, Nat. Commun. **3**, 806 (2012).
[218] I. Bargatin, E. Myers, J. Aldridge, C. Marcoux, P. Brianceau, L. Duraffourg, E. Colinet, S. Hentz, P. Andreucci and M. M. Roukes, Nano Lett. **12** 1269 (2012).
[219] K. Makino, Y. Hashimoto, J. Yoshikawa, H. Ohdan, T. Toyama, P. van Loock, and A. Furusawa, Science Adv. **2**, e1501772 (2016).
[220] M. Morelli, C. C. C. J. Kuo, and M. O. Pun, Proc. IEEE **95**, 1394 (2007).
[221] K. Wiesenfeld, P. Colet, and S. H. Strogatz, Phys. Rev. Lett. **76**, 404 (1996).
[222] V. M. Vinokur, T. I. Baturina, M. V. Fistul, A. Y. Mironov, M. R. Baklanov, and C. Strunk, Nature (London) **452**, 613 (2008)
[223] T. E. Lee and H. R. Sadeghpour, Phys. Rev. Lett. **111**, 234101 (2013).
[224] S. Walter, A. Nunnenkamp and C. Bruder, Ann. Phys. (Berlin) **527**, 131 (2014).
[225] T. E. Lee, C.-K. Chan, and S Wang, Phys. Rev. E **89**, 022913 (2014).
[226] N. Lörch, E. Amitai, A. Nunnenkamp, and C. Bruder, Phys. Rev. Lett. **117**, 073601

(2016)

[227] M. Xu, D. A. Tieri, E. C. Fine, J. K. Thompson, and M. J. Holland, Phys. Rev. Lett. **113**, 154101 (2014).

[228] M. R. Hush, W. Li, S. Genway, I. Lesanovsky, and A. D. Armour, Phys. Rev. A **91**, 061401 (2015).

[229] A. Roulet and C. Bruder, Phys. Rev. Lett. **121**, 063601 (2018).

[230] M. Koppenhöfer and A. Roulet, Phys. Rev. A **99**, 043804 (2019).

[231] M. Aspelmeyer, T. J. Kippenberg, and F Marquardt, Rev. Mod. Phys. **86**, 1391 (2014).

[232] G. Heinrich, M. Ludwig, J. Qian, B. Kubala, and F. Marquardt, Phys. Rev. Lett. **107**, 043603 (2011).

[233] C. A. Holmes, C. P. Meaney, and G. J. Milburn, Phys. Rev. E **85**, 066203 (2012).

[234] M. Zhang, G. S. Wiederhecker, S. Manipatruni, A. Barnard, P. McEuen, and M. Lipson, Phys. Rev. Lett. **109**, 233906 (2012).

[235] M. Bagheri, M. Poot, L. Fan, F. Marquardt, and H. X. Tang, Phys. Rev. Lett. **111**, 213902 (2013).

[236] M. Zhang, S. Shah, J. Cardenas, and M. Lipson, Phys. Rev. Lett. 115, 163902 (2015).

[237] M. Ludwig and F. Marquardt, Phys. Rev. Lett. **111**, 073603 (2013).

[238] T. Weiss, A. Kronwald and F. Marquardt, New J. Phys. **18**, 013043 (2016).

[239] S. Sonar, M. Hajdušek, M. Mukherje, R. Fazio, V. Vedral, S. Vinjanampathy, and L.-C. Kwek, Phys. Rev. Lett. **120**, 163601 (2018).

[240] A. Mari, A. Farace, N. Didier, V. Giovannetti, and R. Fazio, Phys. Rev. Lett. **111**, 103605 (2013).

[241] G. L. Giorgi, F. Galve, G. Manzano, P. Colet, and R. Zambrini, Phys. Rev. A **85**, 052101 (2012).

[242] G. Manzano, F. Galve, G. L. Giorgi, E. Hernández-García and R. Zambrini, Sci. Rep. **3**, 1439 (2013).

[243] F. Bemani, A. Motazedifard, R. Roknizadeh, M. H. Naderi, and D. Vitali, Phys. Rev. A **96**, 023805 (2017)

[244] V. Ameri, M. Eghbali-Arani, A. Mari, A. Farace, F. Kheirandish, V. Giovannetti, and R. Fazio, Phys. Rev. A **91**, 012301 (2015).

[245] D. Witthaut, S. Wimberger, R. Burioni and M. Timme, Nat. Commun. **8**, 14829 (2017).

[246] N. Lörch, S. E. Nigg. A. Nunnenkamp, R. P. Tiwari, and C. Bruder, Phys. Rev, Lett. **118**, 243602 (2017).

[247] S. E. Nigg, Phys. Rev. A **97**, 013811 (2018).

[248] C.-G. Liao, R.-X. Chen, H. Xie, M.-Y. He, and X.-M. Lin, Phys. Rev. A **99**, 033818 (2019).

[249] L. Ying, Y.-C. Lai, and C. Grebogi, Phys. Rev. A **90**, 053810 (2014).

[250] T. Li, T. Y. Bao, Y. L. Zhang, C. L. Zou, X. B. Zou, and G.C. Guo, Opt. Express **24**, 12336 (2016).

[251] E. Gil-Santos, M. Labousse, C. Baker, A. Goetschy, W. Hease, C. Gomez, A. Lemaître, G. Leo, C. Ciuti, and I. Favero, Phys. Rev. Lett. **118**, 063605 (2017).

[252] C. W. Gardiner, Phys. Rev. Lett. **70**, 2269 (1993).

[253] J. I. Cirac, P. Zoller, H. J. Kimble and H. Mabuchi, Phys. Rev. Lett. **78**, 3221 (1997).

[254] H. Tan, L. F. Buchmann, H. Seok and G. Li, Phys. Rev. A **87**, 022318 (2013).

[255] *NIST Handbook of Mathematical Functions*, edited by F. W. J. Olver, D. W. Lozier, R. F. Boisvert, and C. W. Clark (Cambridge University Press, New York, 2010).

[256] N. W. McLachlan, *Theorey and Applications of Mathieu Functions* (Dover, New York, 1964).

Vita

Subhadeep Chakraborty was born on 19th January, 1991 in Bhatpara, West Bengal, India. He did his B.Sc. with Physics Honours in 2011 from RKMVC College, under the West Bengal State University and M.Sc. in physics from Indian Institute of Technology Guwahati in 2013. He had enrolled into the Ph.D programme at Indian Institute of Technology Guwahati in 2014. He had qualified Graduate Aptitude Test in Engineering (GATE) and National Eligibility Test (NET) in Physics, respectively, in 2013 and 2017. He has earned the Senior Research Fellowship in 2016 by Indian Institute of Technology Guwahati.